

IMPROVING FIBER BRAGG GRATING STRAIN MEASUREMENTS USING PEAK LOCATION ALGORITHMS AND WAVELENGTH REFERENCES

By

Evangeline Rivera

A Thesis
submitted to the Faculty of Graduate Studies
in partial fulfillment of the requirements
for the degree of

Master of Science

Department of Electrical and Computer Engineering
University of Manitoba
Winnipeg, Manitoba, Canada
© May 2004

THE UNIVERSITY OF MANITOBA
FACULTY OF GRADUATE STUDIES

COPYRIGHT PERMISSION

**Improving Fiber Bragg Grating Strain Measurements Using Peak
Location Algorithms and Wavelength References**

BY

Evangeline Rivera

**A Thesis/Practicum submitted to the Faculty of Graduate Studies of The University of
Manitoba in partial fulfillment of the requirement of the degree
Of
MASTER OF SCIENCE**

Evangeline Rivera © 2004

Permission has been granted to the Library of the University of Manitoba to lend or sell copies of this thesis/practicum, to the National Library of Canada to microfilm this thesis and to lend or sell copies of the film, and to University Microfilms Inc. to publish an abstract of this thesis/practicum.

This reproduction or copy of this thesis has been made available by authority of the copyright owner solely for the purpose of private study and research, and may only be reproduced and copied as permitted by copyright laws or with express written authorization from the copyright owner.

ACKNOWLEDGEMENTS

I would like to express my appreciation and gratitude to my advisor, Dr. D.J. Thomson, for his advice, encouragement and insight throughout my research. The work presented in this thesis would not have been possible without his guidance and support.

I would also like to acknowledge Dr. D. Polyzois for his constant support and for introducing me to the field of structural health monitoring. Furthermore, I would like to thank the ECE technicians, especially Mr. A. McKay, Mr. A. Symmons, and Mr. B. Bourbonnais, for their assistance and guidance.

Finally, I would like to thank my family and friends for their continuous support and understanding.

ABSTRACT

Fiber Bragg grating sensors are one of many fiber optic sensor technologies that are currently being used in structural health monitoring systems. The sensors operate by detecting a shift in the wavelength of reflected maxima due to applied strain. This thesis studies a new fiber Bragg interrogation method that combines a swept wavelength laser in combination with wavelength references. These include a gas cell, which is used as the long term wavelength standard and an etalon used for accurate interpolation of peak wavelengths. A gas cell is a pressurized container filled with a certain type of gas that, when exposed to a range of wavelengths, specific wavelength lines are absorbed while an etalon is essentially a filter that has a periodic response over a broad wavelength range. Its wavelength response spacing is smaller than the gas cell and therefore, can be used to determine the intermediate wavelengths between two gas cell absorption lines. Peak location is a key element of this interrogation method and several detection algorithms are investigated. It was determined that polynomial peak fitting is the most computationally efficient method and yields a resolution of better than 0.5pm with signal to noise ratios of 30:1 or better. With higher signal to noise ratios, polynomial peak fitting can yield a resolution of better than 0.25pm and a resolution of better than 0.25pm. Using a tunable laser, a HCN gas cell and an etalon with maxima every 140pm, static load tests have demonstrated that measurements can be made with accuracy of better than 2pm. It is expected that this accuracy will be maintained over a long period of time as it is based on absorption lines in the gas cell. The results of this study are used to demonstrate that absolute accurate strain measurements can be obtained with the use of wavelength references in conjunction with a suitable peak location algorithm.

TABLE OF CONTENTS

ACKNOWLEDGEMENTS	i
ABSTRACT	ii
LIST OF FIGURES	v
LIST OF TABLES	vii

1 INTRODUCTION	
1.1 Introduction.....	1
2 LITERATURE REVIEW OF FIBER OPTIC SENSORS	
2.1 Introduction.....	5
2.2 Classification of Sensors.....	6
2.3 Fiber Optic Theory.....	9
2.4 Fiber Bragg Grating Sensors.....	14
2.5 Gas Absorption Cells.....	17
2.6 Etalon.....	18
2.7 Past Sensor Systems.....	19
2.8 Conclusion.....	25
3 PEAK LOCATION ALGORITHMS	
3.1 Introduction.....	26
3.2 Peak Location Methods.....	29
3.3 Simulations.....	34
3.4 Discussion of Signal to Noise Ratio in the Peak Location Method.....	41
3.5 Conclusion.....	43
4 IMPLEMENTATION INTO THE FBG UNIT	
4.1 Introduction.....	45
4.2 Modifying the FBG Unit.....	45
4.3 Testing of the Modified FBG Unit.....	48
4.4 Short Term Stability Test.....	50
4.5 Implementation of the Etalon as a Wavelength Reference.....	52
4.6 Conclusion.....	57

Table of Contents

5	EXPERIMENTAL TESTING AND RESULTS FROM THE FBG UNIT	
5.1	Introduction.....	58
5.2	Test Setup.....	58
5.3	Test Procedure	63
5.4	Results and Discussion	64
5.5	Conclusion	67
6	CONCLUSION AND RECOMMENDATIONS	
6.1	Conclusion	68
6.2	Recommendations for Future Work.....	70
	REFERENCES	71
	APPENDIX A – MATLAB PROGRAMS	
	APPENDIX B – ETALON SIMULATION EQUATIONS	

List of Figures

Figure 2.1	Configurations of two different interferometers	8
Figure 2.2	Illustration of an extrinsic and intrinsic sensor	8
Figure 2.3	Light propagation between media with different refractive indices	10
Figure 2.4	Complete internal reflection of light through optical fiber	10
Figure 2.5	Cross section of typical optical fiber	11
Figure 2.6	Attenuation due to fiber loss vs wavelength	13
Figure 2.7	Operating principle of the fiber Bragg grating sensor	15
Figure 2.8	Absorption spectrum of a Hydrogen Cyanide gas cell	18
Figure 2.9	Etalon operating principle	19
Figure 3.1	Configuration of FBG sensor system using a swept laser source	26
Figure 3.2	FBG interrogation system setup	27
Figure 3.3	Plot of Bragg grating signal and output voltage from the tunable laser	28
Figure 3.4	Signal reflected from Bragg grating	29
Figure 3.5	First two peak location algorithms	30
Figure 3.6	Polynomial fit algorithm	31
Figure 3.7	First derivative and zero crossing point algorithm	32
Figure 3.8	Lorentzian and Gaussian distribution curves	34
Figure 3.9	Lorentzian and Gaussian peak fit algorithms.	34
Figure 3.10	Peak location error vs noise-to-signal ratio for the first three methods	36
Figure 3.11	Peak location error vs noise-to-signal ratio for four methods	37
Figure 3.12	Peak location error vs noise-to-signal ratio of polynomial fit algorithm using sub-sampling technique	39
Figure 3.13	Peak location error vs noise-to-signal ratio for the first three methods	40
Figure 3.14	Approximation of a Bragg peak	41
Figure 3.15	Shifting the approximation curve by one wavelength position	41
Figure 3.16	Approximation of the Bragg peak using a triangle signal	43
Figure 4.1	Schematic of FBG interrogation unit	46

List of Figures

Figure 4.2	Schematic of FBG unit with sensor and wavelength references as inputs	47
Figure 4.3	Screenshot of Labview user interface	48
Figure 4.4	Plot of signals from the FBG, gas cell and the laser	49
Figure 4.5	Determining the Bragg peak wavelength using interpolation from the gas cell waveform	50
Figure 4.6	Variation of error over a 1 second scan	51
Figure 4.7	Variation of error over a 10 minute time period	51
Figure 4.8	Etalon response in reflection from 1535 to 1537nm	52
Figure 4.9	Etalon response as temperature varies	53
Figure 4.10	Plot of signals from the FBG, gas cell, etalon and laser	54
Figure 4.11	Variation of error over a 1 second scan with the etalon	55
Figure 4.12	Variation of error over a 10 minute time period with the etalon	56
Figure 4.13	Variation of error over a 10 minute time period with and without the etalon	56
Figure 5.1	Constant stress beam design	59
Figure 5.2	Constant stress beam dimensions	61
Figure 5.3	Finite element mesh plot of beam with applied force and boundary	61
Figure 5.4	Stress plot of beam	62
Figure 5.5	Beam with attached sensors	63
Figure 5.6	Cantilever test fixture	63
Figure 5.7	Wavelength references	64
Figure 5.8	Comparison from the first test of strain readouts from the FBG unit to the strain gauge	65
Figure 5.9	Comparison from the second test of strain readouts from the FBG unit to the strain gauge	66
Figure 5.10	Comparison of strain deviations	67

List of Tables

Table 2.1	Summary of the performance of commercial FBG interrogation units	24
Table 2.2	Summary of the performance of currently researched FBG interrogation techniques	25
Table 3.1	Comparison of peak fitting algorithms with respect to the peak wavelength determined from the Gaussian fit method	35
Table 3.2	Noise to signal ratio required for each peak fitting algorithm to maintain an error below 5 picometers	37

CHAPTER 1

INTRODUCTION

As structural health monitoring continues to grow as a field of increasing interest for civil engineers, fiber optic sensor technology is thought to be the most promising alternative to conventional sensors. Traditionally used in the communications field, optical fibers have garnered interest in other fields due to their numerous advantages such as small size, low loss, and electromagnetic interference (EMI) immunity. Presently, fiber optic sensors are used in a wide range of applications such as strain measurement in civil infrastructure [1], oil well logging [2], oil pipeline monitoring [3], and composite structures [4].

Structural health monitoring of civil engineering infrastructure has been a growing issue over the past few years. As structures continue to age and become damaged by fatigue, it becomes increasingly important to create a reliable monitoring system in order to assess their structural integrity. Thus, to successfully monitor the condition of a structure, the measurement device must be able to provide reliable and accurate data over long periods of time. A suitable interrogation system must meet many requirements including signal stability as well as system insensitivity to changes in the environment, such as temperature and humidity [5]. The measurement technique should allow several sensors to be placed on a structure which will provide a thorough representation of the strain distribution. Also, a portable measurement device would allow several structures

to be monitored on a periodic schedule, thus drastically reducing the overall cost by eliminating the need for data acquisition units on every structure [6].

Fiber optic sensors are classified according to the sensing technique by which they operate. These techniques are based on modulating the intensity, phase, or polarization of the light passing through the sensor. Fiber sensors are now being used to monitor various parameters such as strain, temperature, pressure, chemical composition, deformation and corrosion. One type of sensor used to measure strain is the fiber Bragg grating. This sensor is also known as an optical strain gauge. Fiber Bragg grating sensors measure strain through a shift in a spectral peak with applied strain. By determining the shift in the peak wavelength, one can determine how much strain the fiber experienced. One of the main problems associated with the demodulation of fiber Bragg grating sensors is the presence of drift in the light source and/or the photodetector [7-13]. As a result, absolute measurements of strain are hindered. In this thesis, resolution is defined as the minimum amount of Bragg wavelength shift that can be detected and accuracy is how precise the technique is in determining this change. Therefore, improving the accuracy of this wavelength measurement is the core work of this thesis. The development of a measurement technique and the implementation of this technique into an interrogation unit are also significant contributions of the research work presented in this thesis.

Prior to embarking on a full overhaul of the Bragg grating interrogation unit, technical information was first gathered on the various commercial and research techniques employed. After reviewing details of the performance of the various methods employed, it became clear that there was potential for further improvement in the

accuracy of measuring the Bragg wavelength. It was then decided that the first place to start would be investigating various methods of determining the location of the Bragg wavelength on the optical spectrum. Several algorithms were scrutinized based on their accuracy and computation time. Of those algorithms, one was chosen to be implemented in the interrogation system. Wavelength references were then used in conjunction with the algorithm to provide an absolute frame of reference by which the Bragg wavelength could be determined. This algorithm was implemented into an interrogation system whose performance was evaluated through static load tests of the fiber Bragg grating sensor. The data was analyzed and conclusions were made on the effectiveness of this technique in the monitoring of structural performance. To this end, the investigation and development of the sensor demodulation technique is presented in five chapters.

A review of related literature is presented in Chapter 2, where the advantages and disadvantages of fiber optic sensors are discussed. The classifications of sensors, along with some basics on light transmission in optical fibers, are also presented in Chapter 2. Furthermore, two wavelength references, the gas cell and etalon, along with past sensor systems are discussed.

The development of a suitable peak location algorithm is presented in Chapter 3. The ability to find the correct peak location of the Bragg signal is one of the fundamental issues investigated in this thesis. This is investigated by testing several peak location methods and comparing their accuracy and performance with increasing noise in the signal. In addition, another technique called sub-sampling is introduced and used in conjunction with the best peak location algorithm.

The implementation of the peak location algorithm is explained in Chapter 4. The peak location program was created using Matlab and was then modified to find the Bragg wavelength using two wavelength references. The peak location algorithm is used to find the peaks in all three signals. Tests were performed using one and two wavelength references and the results are discussed in this chapter as well. More detail is provided on the operation of the etalon wavelength reference since the main objective of this thesis is to improve the measurement accuracy with the addition of an etalon.

The load testing of the fiber Bragg grating is discussed in Chapter 5. A laboratory load test was performed to evaluate the performance of the fiber Bragg grating interrogation unit with and without the etalon. Also, a finite element model of the beam was used to confirm that the load induces constant stress over the length of the beam. An explanation of the process of attaching a fiber optic sensor onto a surface is included as well. Results from the test are presented and discussed.

In Chapter 6, a summary of the findings is presented and a number of conclusions as to the use of an etalon to further improve the accuracy of strain measurements are drawn. This chapter concludes with recommendations for future work in this area.

CHAPTER 2

LITERATURE REVIEW OF FIBER OPTIC SENSORS

2.1 Introduction

One of the key elements in a structural health monitoring system is the sensing element and data acquisition system. In the past few years, the focus of research has shifted to fiber optic sensors. One of the main reasons is fiber optic sensor technology offers several advantages over conventional sensing techniques [5]:

- 1) Fiber optic sensors are immune to electromagnetic and radio frequency interference (EMI and RFI). This means that they can operate in electrically noisy environments and thus, there is no need for protective shielding.
- 2) Optical fibers are typically small in diameter ($\sim 250\mu\text{m}$). This allows them to be embedded in a composite structure without affecting the structure's mechanical properties. Since they can undergo up to 5% elongation, they can withstand high tensile loading up to $50000\mu\epsilon$.
- 3) They are resistant to corrosion and experience low creep. They are also electrically passive which means they do not conduct electricity and thus, can be embedded in metal structures.
- 4) Fiber optic sensors have both point and distributed sensing capabilities depending on their sensor length. This provides flexibility in deciding what sensor gauge length would be ideal for a specific structure.
- 5) They also possess multiplexing capabilities that allow several sections of a structure to be monitored and reduce the number of lead wires required.
- 6) Some fiber optic sensors are capable of absolute measurement with a linear response. This helps remove any ambiguity and dependence on taking measurements relative to a certain parameter.
- 7) They also are very sensitive and have a large dynamic range. Fiber optic sensors have good signal stability and are suitable for long term monitoring.

Some disadvantages, however, are the cost and availability of suitable optical sources and instrumentation. Also, the long term stability of these sensors still needs to be investigated and the sensor may need to be isolated from unwanted parameters to avoid erroneous measurements. Finally, steps must be taken to account for the low general awareness of fiber optic sensor technology. Although these sensors do have their disadvantages, most can be overcome and the advantages clearly outweigh the drawbacks. Therefore, with the aforementioned advantages and capabilities, fiber optic sensors are proving their worth in various monitoring applications and environments.

In this chapter, different classifications of fiber optic sensors based on the sensing techniques applied are illustrated. Also, basic fiber optic theory is explained and a description of the components used in this thesis including the fiber Bragg grating sensor, the gas absorption cell and the etalon, is provided. Finally, a review of sensor systems using broadband and laser sources and a description of the future for this technology involving the creation of materials with integrated sensors conclude this chapter.

2.2 Classification of Sensors

Fiber sensor technology can be categorized based on the sensing technique applied. These include intensimetric, polarimetric and interferometric based sensing schemes [14].

Intensimetric fiber optic sensors rely on the modulation of the intensity of light in the fiber. This is due to the fact that this technique does not require monitoring the frequency or the phase of the optical field. As a result, amplitude based sensors are the most simple type of sensor in terms of its operation. However, their main disadvantage is

the lack of measurement sensitivity, which is an important requirement when monitoring the health of a structure.

Polarimetric sensors are typically used in applications where a longer sensor gauge length is required. This sensing technique involves two orthogonal polarization eigenmodes of light in the fiber. This can be created using polarizers at the fiber inputs or directing a polarized light beam at 45° to the principal axis of the single mode fiber. Either method will create two components sometimes referred to as perpendicular and parallel polarizations. When the fiber experiences an external influence, a phase change will be created between the two components and as a result, reduce the intensity at the photodetector. Therefore, by monitoring the state of polarization, the external influences on the fiber can be observed as well. Although, polarimetric sensors are more sensitive than intensimetric sensors, the demodulation system is substantially more expensive and complex.

Interferometric sensors operate by detecting any phase changes in the light as it propagates down the fiber. Typically, light is split into two beams after it enters the fiber. After which, the two beams are then recombined when they reach the photodetector. This technique takes advantage of the constructive and destructive interference patterns between the light waves. The resulting fringe pattern is directly related to the optical phase difference between the two beams and in turn, represents any external force experienced by the fiber. Typical configurations of an interferometer include the Michelson and Mach Zehnder interferometers as shown in figure 2.1.

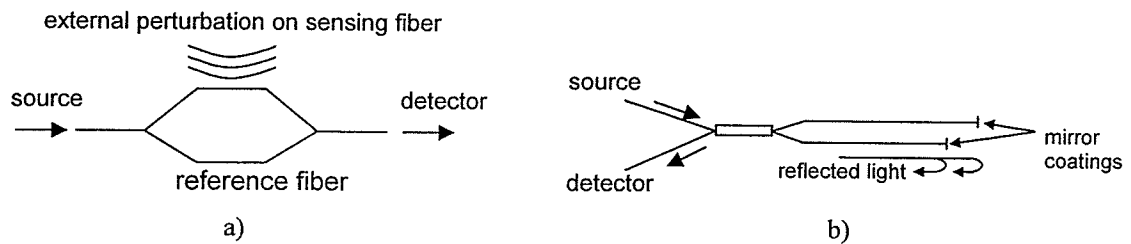


Figure 2.1 Configurations of two different interferometers.
(a) Mach Zehnder (b) Michelson Interferometer.

These sensors have a higher sensitivity than the other types of sensors. However, since most configurations have mechanical moving parts involved, they are not as rugged and adequate for field applications.

Fiber optic sensors can also be classified as extrinsic or intrinsic sensors. An extrinsic sensor uses an external element to sense any perturbations and modulate the light wave accordingly. As a result, an extrinsic sensor merely uses the fiber to transmit and receive light signals. On the other hand, an intrinsic sensor uses the fiber itself as the sensor. Both configurations are shown in figure 2.2.

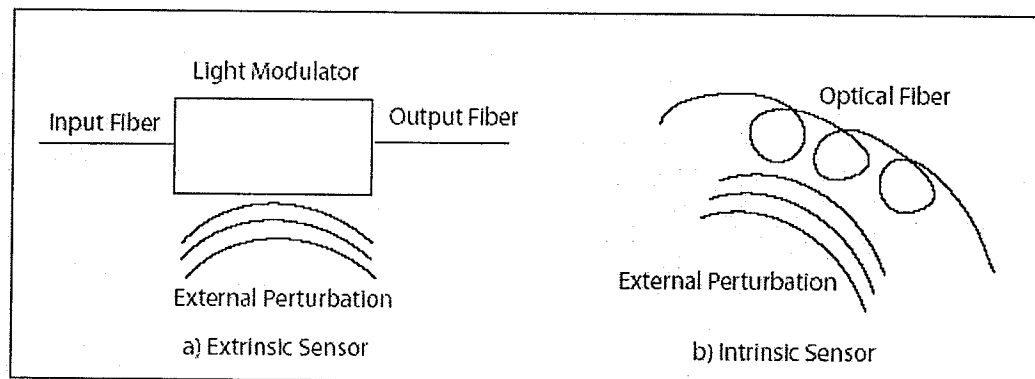


Figure 2.2 Illustration of an extrinsic and intrinsic sensor.

Extrinsic sensors are typically used to measure parameters used in process control operations such as temperature, pressure, liquid level and flow. They can also be used to monitor linear and angular position in aircraft operations. These types of sensors are user

friendly and are easily multiplexed. However, they have less sensitivity and experience problems with connections to the external light modulator.

Intrinsic sensors are used to measure properties such as strain, pressure, vibration, and rotation. These sensors, as shown in figure 2.2, rely on the fiber itself to modulate the light in response to the external forces it experiences. As a result, intrinsic sensors are more sensitive and robust. Also, since the sensor consists of simply optical fiber, it is very versatile for various installation configurations. However, this design does not prevent any unwanted external perturbations from affecting the sensor. For example, a sensor which is being used to measure strain may also be affected by the temperature around it. Therefore, intrinsic sensors require more complicated demodulation schemes. While intrinsic and extrinsic sensors both have their advantages and disadvantages, the choice between using a specific type of sensor ultimately depends on the requirements of the application.

2.3 Fiber Optic Theory

An optical fiber is a cylindrical filament made of transparent material such as glass or plastic [15]. It utilizes the theory of complete internal reflection to guide light along the fiber. As a light ray passes through different media, it bends in accordance to the change in refractive indices between the media. A demonstration of how a light ray bends depending on its approaching angle Θ_1 is shown in figure 2.3.

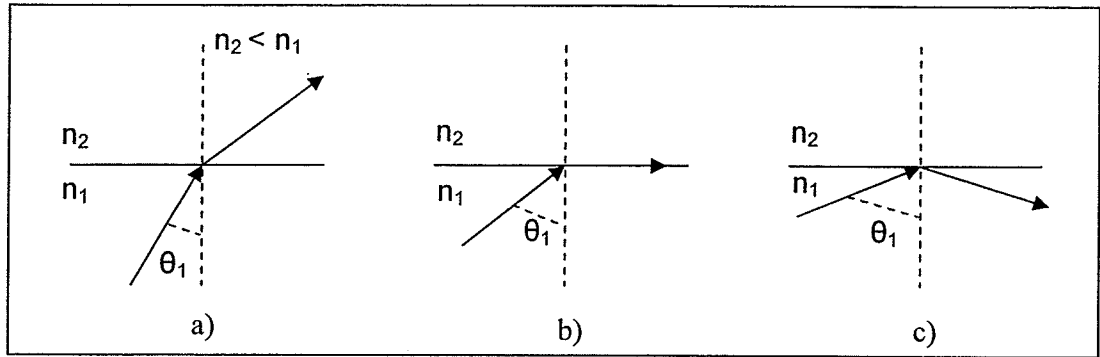


Figure 2.3 Light propagation between media with different refractive indices.

It is important to note that complete internal reflection occurs for incident angles greater than the critical angle Θ_c . The critical angle is expressed as

$$\Theta_c = \arcsin(n_2/n_1) \quad (2.1)$$

where n_1 is the refractive index of the first medium and n_2 is the refractive index of the second medium.

Optical fiber consists of a core made of pure silica which has fewer impurities than regular glass in order to reduce the amount of light absorbed in the fiber. An extra layer of glass called cladding surrounds the core of the fiber. The cladding has a lower refractive index than the core to allow complete internal reflection to occur and create a light guide, as shown in figure 2.4.

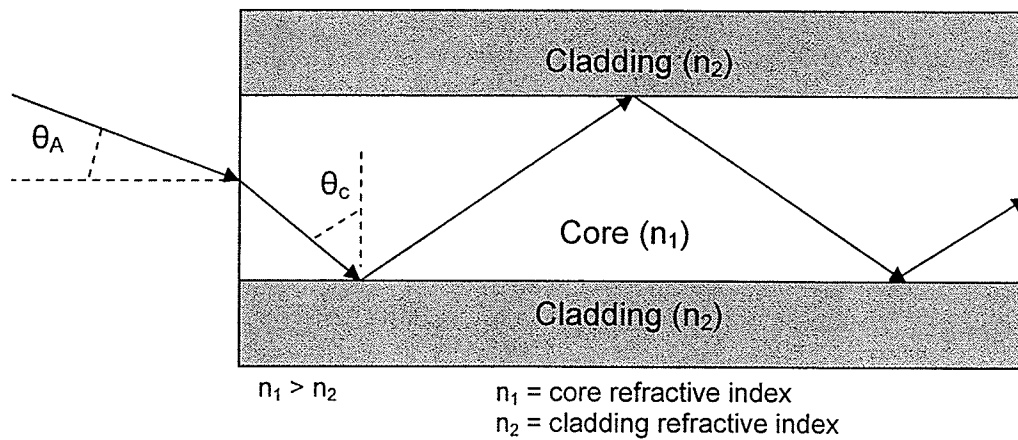


Figure 2.4 Complete internal reflection of light through optical fiber.

The acceptance angle Θ_A determines the conditions in which light can be coupled into the fiber. As shown in figure 2.4, Θ_A is directly related to Θ_c . Therefore, light rays must have an incident angle less than Θ_A in order for the fiber to capture the entire flux from the source. The numerical aperture, NA, of a fiber is determined by the angle of acceptance, both of which are defined by the refractive indices of the core and cladding.

$$\Theta_A = \arcsin(n_1^2 - n_2^2)^{1/2} \quad (2.2)$$

$$NA = \sin(\Theta_A) = (n_1^2 - n_2^2)^{1/2} \quad (2.3)$$

where n_1 is the refractive index of the core and n_2 is the refractive index of cladding. The numerical aperture is an important parameter because it helps define the efficiency in which flux from the source is coupled into the fiber. In other words, the numerical aperture of the source must be less than the numerical aperture of the fiber to maximize the coupling efficiency.

Optical fibers can be created in different sizes to accommodate various applications. However, it is the size of the core that affects the way light travels through it. A typical optical fiber is shown in figure 2.5.

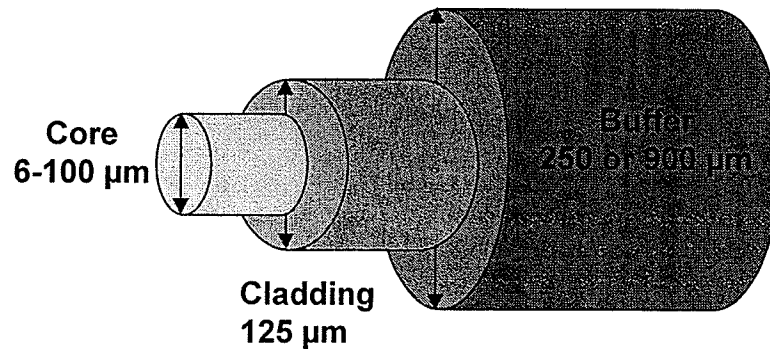


Figure 2.5 Cross section of typical optical fiber.

A coating layer made of polyimide or acrylate material surrounds the cladding to protect the optical fiber and allow for easier handling. The size of the core is small compared to

the cladding and can range from 6 to 100 μm . Light rays can travel different paths in the fiber because the incident angles determine how the rays will propagate. For optical fibers with core sizes in the range of 50 to 100 μm , several ray paths or modes can be supported. These types of fibers are called multimode and since the travel time of different modes can vary, the rays exiting the fiber will become out of sync. Therefore, narrow pulses sent into the fiber start to broaden and exit the fiber wider than the original signal. This effect is called intermodal dispersion and it limits the fiber bandwidth and the maximum pulse rate the fiber can handle.

On the other hand, singlemode fibers have core sizes less than 10 μm which produces a condition in which only a single electromagnetic mode propagates. As a result, singlemode fibers have a broader bandwidth (up to 100GHz*km) than multimode fibers and experience less attenuation as well. Therefore, this type of fiber is better suited for sensor and transmission purposes. The number of modes that can be supported by a fiber is calculated using the fiber's normalized frequency, v . This frequency is expressed as

$$v = (\pi d_{\text{fiber}} \text{NA})/\lambda \quad (2.4)$$

where d_{fiber} is the diameter of the fiber core. For $v < 2.405$, only one mode will propagate down the fiber, which then becomes known as singlemode fiber.

One of the most important aspects of optical fiber is its low attenuation loss. Typical fiber loss is about 0.2dB/km at $\lambda=1.55\mu\text{m}$. The attenuation that still occurs is mainly due to the absorption, Rayleigh scattering, and extrinsic parameters such as impurities in the material. Attenuation due to absorption occurs as a result of interaction of electrons with radiation. This UV absorption has attenuation peaks in the ultraviolet

wavelength region and decreases as the wavelength approaches the infrared. Also, absorption occurs from an interaction with molecular vibration and consequently, this IR absorption has attenuation peaks in the infrared region. Rayleigh scattering is caused by small imperfections in the glass structure which forms the fiber. These imperfections can be trapped gas bubbles, dopants or composition fluctuations which occurred during solidification. This scattering can cause light energy to escape the fiber and attenuation usually occurs at short wavelengths. The combined effect of these fiber losses is shown in figure 2.6.

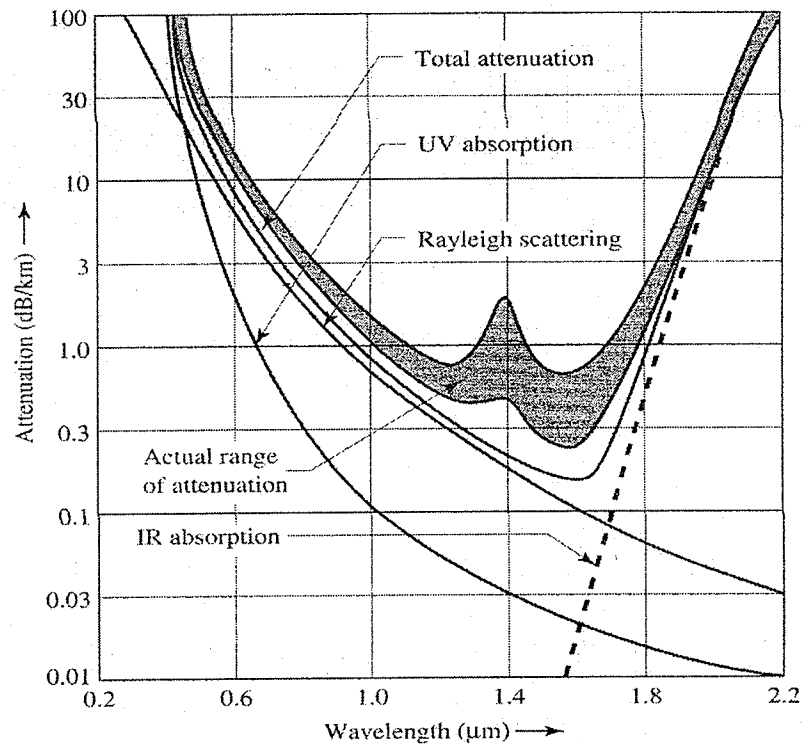


Figure 2.6 Attenuation due to fiber loss vs wavelength [15].

Due to extrinsic factors, the resulting attenuation curve is actually the shaded region in figure 2.6. These factors include impurities in the material, fiber defects caused by the manufacturing process and bends in the fiber due to installation techniques. As a result,

the attenuation curve varies depending on the severity of these extrinsic losses. For example, the most significant impurity is the water radical OH^- which causes an attenuation peak at 1380 nm. From the figure, there are two distinct minima where attenuation is at its lowest. These regions are called transmission windows and optical networks usually operate at one of these wavelengths, 1300 or 1550nm, to achieve the best signal propagation.

There are two types of light sources which can be used with optical fibers, light emitting diodes (LEDs) and laser diodes. The LED is a broadband low power source while a laser diode is a narrowband high power source. Therefore, the decision between which light source to use depends on the requirements of the fiber optic sensor system.

2.4 Fiber Bragg Grating Sensors

A fiber Bragg grating is comprised of periodic changes in the refractive index of the core located in a section of single mode fiber [16]. This modulation creates a sort of filter which causes all wavelengths except one to be transmitted through the grating as shown in figure 2.7. The reflected wavelength is called the Bragg wavelength, λ_B , and is defined by the equation

$$\lambda_B = 2n_{\text{eff}}\Lambda \quad (2.5)$$

where n_{eff} is the effective refractive index in the core and Λ is the spatial period of the refractive index modulation.

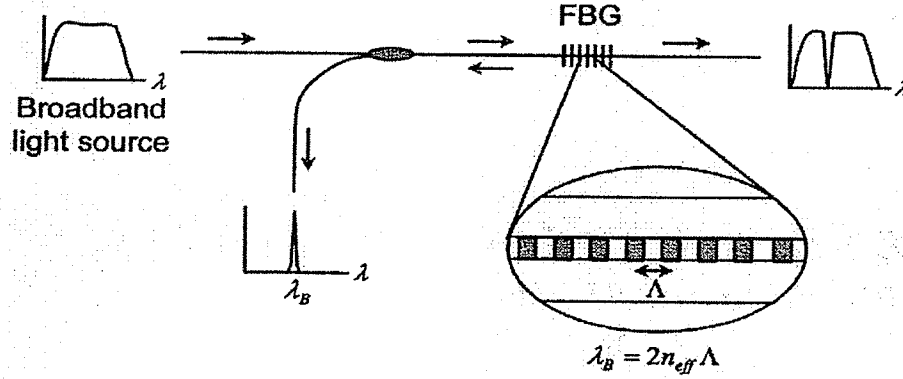


Figure 2.7 Operating principle of the fiber Bragg grating sensor [14].

The grating length is typically 1 to 2cm and the bandwidth of the reflected signal, which is dependent on the grating length, is typically ~ 0.05 to 0.3nm [14].

Bragg gratings are fabricated using different methods. One method involves placing a mask pattern over the optical fiber and shining UV light through it to change the refractive index of the core. The advantage of a Bragg grating is it is very flexible to work with in terms of being able to choose the wavelength range one would want to use. Since the Bragg wavelength depends on the spacing between the gratings, it is possible to create gratings at different wavelengths. The refractive index modulation is on the order of 10^{-4} to 10^{-3} . Therefore, it takes a large number of periods to increase the reflection to over 90% which is usually desired.

The fiber Bragg grating is used for structural health monitoring because it responds to strain through a wavelength shift. This feature is attractive because it does not depend on the amplitude of the signal and as a result, is less susceptible to sensor failure due to signal loss. When it is bonded on or embedded in a material, the reflected wavelength will change when the grating undergoes thermal or mechanical strain. This is a result of a change in length in the grating. The wavelength shift $\Delta\lambda_B$ is defined by

$$\Delta\lambda_B = \lambda_B (\varepsilon(1-\rho_e) + \beta\Delta T) \quad (2.6)$$

where λ_B is the initial peak wavelength, ε is the strain induced, ρ_e is the effective strain optic coefficient, β is the apparent thermal strain and ΔT is the temperature change. The strain optic coefficient is a constant that relates the change in the index of refraction to strain. It is given by

$$\rho_e = n^2/2*[p_{12} - \nu(p_{11} + p_{12})] \quad (2.7)$$

where p_{11} and p_{12} are components of the strain-optic tensor, n is the refractive index and ν is Poisson's ratio. For a silica fiber, the typical values for these parameters are $p_{11} = 0.113$, $p_{12} = 0.252$, $\nu = 0.16$, and $n = 1.444$ [17,18]. This will give a strain optic coefficient of 0.2017. Therefore, assuming $\Delta T \approx 0$ and using equations 2.6 and 2.7, a $1\mu\varepsilon$ strain will cause a 1.22pm wavelength shift at 1550nm.

Since the sensor responds to strain and temperature changes, the wavelength shift in equation 2.6 takes into account both parameters. The strain response is due to a physical change in the length of the grating pitch and the refractive index of the fiber. The temperature response is due to thermal expansion effects from the fiber and changes in the refractive index due to its temperature dependency. A typical fiber grating has a thermal sensitivity of 7 to 10pm/C°. The apparent thermal strain β is defined by

$$\beta = \beta_0 + GF(\alpha_{\text{substrate}} - \alpha_0) \quad (2.8)$$

where β_0 is the thermo-optic response of the grating at fabrication, GF is the gauge factor which expresses a sensor's sensitivity to strain, $\alpha_{\text{substrate}}$ is the thermal expansion coefficient of the substrate and α_0 is the thermal expansion coefficient of the fiber optic material which is approximately $0.5 \times 10^{-6}/\text{C}^\circ$. Using the gauge factor in the strain equation, one can find the wavelength shift by

$$\Delta\lambda_p = \lambda_p (\epsilon(GF) + \beta\Delta T) \quad (2.9)$$

The typical value for the gauge factor at 1550nm is approximately 0.8.

There are several advantages to using a fiber Bragg grating sensor. It is an intrinsic sensor and therefore, it is very sensitive to strain and temperature effects. The strain is determined by measuring wavelength shifts which allows for the absolute measurement of strain changes. They are typically used in point sensing applications; however, they can also be used as a distributed sensor by increasing the grating length. In this configuration, the average strain over the sensor length is determined. Also, Bragg gratings with different center wavelengths can be multiplexed on a single fiber. Therefore, by multiplexing the sensors, a greater amount of sensors can be placed on a structure with less cables and equipment involved. Finally, since these sensors simply rely on absolute wavelength shifts, the system is not severely affected by low source power and losses in the connectors or couplers. This “absolute” nature of the Bragg grating makes it an effective sensor for both static and dynamic strain applications.

2.5 Gas Absorption Cells

Over the past decade, researchers at several research laboratories have investigated the use of gas absorption as a means of providing a wavelength reference that is very stable and directly related to fundamental measurement standards [19]. Gas cells are often used as calibration sources because of their absoluteness and insensitivity to the environment. Thus, they can provide precise wavelength stability and absolute long-term accuracy. For example, a cell 10cm long filled with HCN at a pressure of 100 Torr (~ 0.1 atmospheres) will selectively absorb light at certain wavelengths as shown in

figure 2.8. HCN has absorption lines at 1539.1494, 1539.7855, 1540.4314, 1541.0872nm etc. These lines are spaced approximately 0.65nm apart and are known to an uncertainty of less than 0.3pm [20]. The position of these lines has been shown to drift less than 0.00001nm/°C and will not drift with aging as long as the gas remains uncontaminated. Gas cells provide a wavelength standard that can be used as a fundamental standard that will be stable and interchangeable over long periods of time.

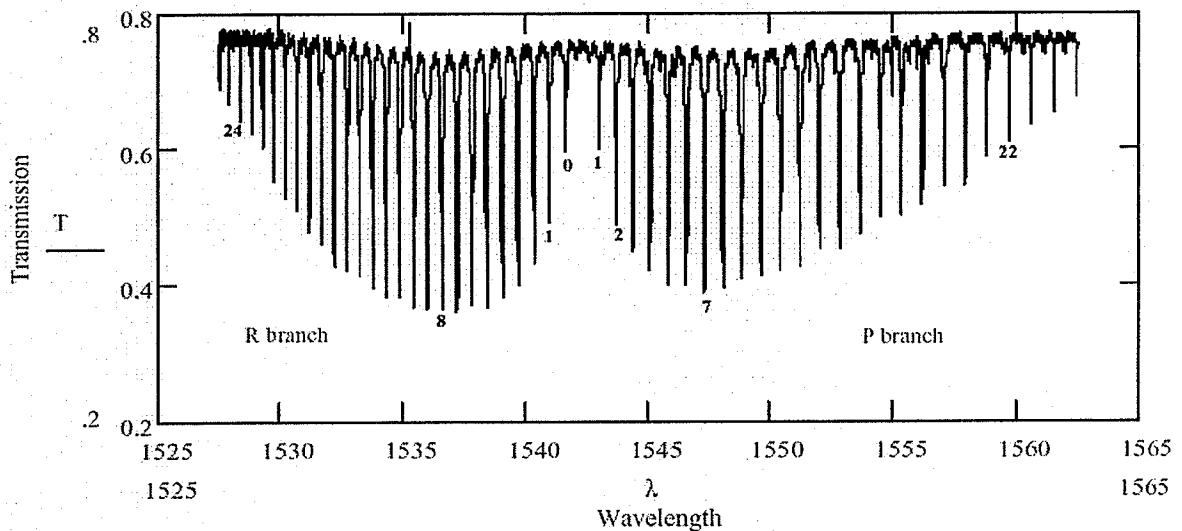


Figure 2.8 Absorption spectrum of a Hydrogen Cyanide gas cell [20].

2.6 Etalon

An etalon is essentially a filter that has a periodic response over a broad wavelength range. It consists of two flat partially reflecting mirrors aligned parallel facing other at a fixed distance apart as shown in figure 2.9a. As light from a point source enters the etalon cavity, light is continually reflected back and forth and since the inner surfaces are not completely reflective, some light is transmitted through the etalon. Therefore, an interference pattern is created on the other side as a result of constructive and destructive interference of the transmitted waves. This is depicted in figure 2.9b.

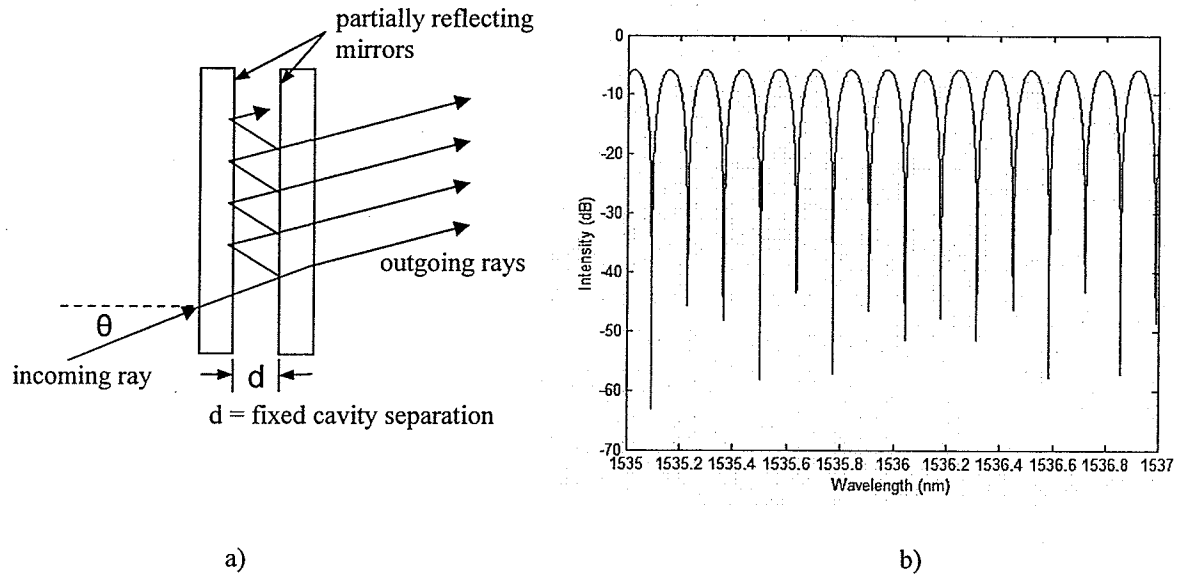


Figure 2.9 Etalon operating principle.
(a) Schematic of etalon (b) Wavelength response

Its wavelength response spacing is smaller than the gas cell and therefore, can be used to determine the intermediate wavelengths between two gas cell absorption lines.

2.7 Past Sensor Systems

Some factors must also be taken into account when considering the implementation of fiber optic sensors in a health monitoring system. The first issue is obviously the cost of the system itself including the sensors, the demodulation system and the installation costs [21]. Fiber optic sensors usually need specific training in order to correctly install them on a structure. For some companies, this may require sending employees to training sessions or contracting out the work to qualified individuals. Although the cost of monitoring the health of a structure may seem expensive, it is fairly small compared to the cost of the structure itself. Also, long term structural health monitoring helps prevent unnecessary maintenance and repair costs by providing real time information on the integrity of the structure. This allows the owner of the structure to determine when a structure actually requires maintenance rather than following a set

schedule. As a result, this will increase the return on investment of the system. Therefore, the initial cost of the implementation of the system is eventually regained over time.

Another issue that must be taken into account is the impact of these sensors on the structure itself and their long term performance. Fiber optic sensors must be capable of being attached to the structure without affecting the structural integrity. For large structures, the sensors are small enough that they will have little effect. However, when working with composite materials, it becomes more difficult. The lead fibers protected with the PVC jacketing cannot be embedded and as a result, the bare fiber sensor is placed in between the composite layers while the rest of the cabling protrudes out of the composite section. For most applications, as long as the cable is not pulling on the embedded fiber, it is not a major problem. Also, the quality of the interface between the sensor and the surface of the structure must be such that the strain experienced by the structure is undergone by the sensor as well. Finally, the sensor must be environmentally resilient and robust with little signal degradation for long term monitoring purposes. After taking these issues into account, fiber optic sensors do prove to have significant advantages for structural health monitoring.

One area that is emerging from structural health monitoring with fiber sensor technology is the creation of materials with integrated sensors or, in other words, smart materials. The advantage of this is the elimination of installing the sensor on site and provides an attractive option for companies who are wary of having to hire someone to install the sensors for them. An example of this is a pultruded FRP reinforcement where the fiber optic sensors and their accompanying fiber leads are embedded during the

pultrusion process [22]. In the research of Kalamkarov et al, the types of sensors used were Fabry-Perot and fiber Bragg gratings. Fatigue testing was performed on the tendons to compare the strain readings from the fiber sensor and externally mounted extensometers. This resulted in excellent conformance between the readings and therefore, extensive loading had no effect on the performance of the embedded sensors. Static loading was also performed on the specimens at 40°C and a maximum discrepancy of 8% occurred between the sensor and extensometer at the peak load of 12.5kN corresponding to 3500 $\mu\epsilon$. Two differently coated optical fibers were immersed in an alkaline solution and filtered sea-water for 3 months to test the degradation of the fibers. Alkaline solution was used because it is typically found in concrete. At the end of the test period, it was determined that there was only mild damage to the surface of the coatings. Therefore, it is plausible to assume that when the fibers are embedded in the composite material, they will be well protected from the environment and are suitable for long term monitoring. From the results of these tests, pultruded FRP reinforcement bars with embedded sensors proved to be quite successful as smart materials.

Another example of this concept is the embedment of sensors in carbon fiber reinforced polymer (CFRP) cables for use in a stay cable bridge in Switzerland [7]. As in the previous instance, the fiber Bragg grating sensors are embedded during the production of the CFRP wires. Each cable consisted of 241 CFRP wires arranged in a hexagonal structure. It was observed that in order to survive high stress applications, the fiber sensors must be embedded during the production of the wire. Static and cyclic testing resulted in good agreement between the fiber sensors and strain gauges. Under a constant strain of 2400 $\mu\epsilon$, the strain readings from the sensors varied $\pm 5\mu\epsilon$ over 5 days

[23]. Reliability assessments have concluded that the sensors on the Storchenbrücke bridge in Switzerland have provided accurate data for over three years. Thus, fiber optic sensors are continuing to prove their long term stability and the use of smart materials demonstrates the ease of installation and feasibility of the commercial potential for structural health monitoring.

A system's performance is limited by its weakest link. In fiber Bragg grating (FBG) measurement systems, the weakest link is in establishing the wavelength at which the peak occurs. There are two common techniques used to determine the peak wavelength. The first technique involves interrogating the FBG with a broadband source and spectrally analyzing the reflected signal to determine the peak wavelength as shown previously in figure 2.7. Although, this is a simple configuration, several issues arise. Since broadband sources typically offer very little power over the peak of the FBG, the output signal at the photodetector has even less power. As a result, the resolution and accuracy of measurement is limited by the intensity of light at the photodetector. In addition, the use of optical spectrum analyzers to determine the peak wavelengths suffers from poor accuracy and drifts that typically greatly exceed 10pm [8,9,10]. Using equation 2.9, this translates to an equivalent strain of greater than $8\mu\epsilon$ at wavelengths of 1550nm and typical gauge factors of 0.8. It is possible to overcome these drifts using gas absorption line references at the expense of sampling rate. Using gas line references, broadband interrogation schemes have achieved sampling rates no greater than 10Hz [7].

A second approach to the interrogation of FBGs makes use of swept wavelength laser sources. In this technique, the peak wavelength can be located by sweeping the output wavelength of the source. This wavelength is typically dependent on the current

applied to the laser. One advantage of using tunable laser sources is they usually have higher power outputs coupled into the fiber than broadband sources. This is important when the power is divided over several channels in the system. The wavelength output by the laser at any particular set of drive conditions is not known and so must be determined by some other technique. For example, commercially available wavelength meters can determine the wavelength of a laser source to approximately 3pm accuracy [11] but are not practical to integrate into a high sampling rate FBG interrogation system and require a significant amount of power as well. Even if a laser source is calibrated using a wavemeter for a particular set of temperatures and drive conditions, the relationship between drive conditions and wavelength will drift uncontrollably over time. This is particularly important in civil infrastructure applications where monitoring is expected to take place over several decades. The best available commercial diode lasers are specified by their manufacturers to drift as much as 80pm/yr [12]. At 1550nm this would correspond to a strain uncertainty of as much as 69 $\mu\epsilon$. These slow frequency drifts may cause falsely interpreted strain measurements. As a result, the precision of strain measurement is dependent on the stability of the laser and the frequency jitter [13]. Arie et al. [24] developed a method of measuring static strain from FBGs using frequency locked lasers. In this technique, the laser frequency is locked to an absorption line in order to eliminate any frequency drifts. For applications which require high resolutions, this method has achieved sensitivities of 1.2 nanostrain/ $\sqrt{\text{Hz}}$ RMS at 1.5Hz and a resolution of 6 nanostrain. This value is limited by the environmental acoustic noise. Consequently, at the cost of sampling rate, high sensitivities are possible using a combination of a laser and wavelength references. Therefore, it is apparent that for civil

infrastructure applications it is necessary to have some form of real time wavelength referencing.

The performance of both commercial and research-based FBG interrogation systems is summarized in the following tables. As one can see, there are a number of commercial units available, each with varying degrees of performance. Often, accuracy is sacrificed for increased scanning frequency, while resolution is approximately the same for most units. As expected, the values for resolution in Table 1 are much better than the commercial units, but the compromises made in the transfer of technology from the research to commercial sector often degrades the initial performance of the system. However, as seen in the Table 2, most of the companies have done an exceptional job of maintaining more than adequate values for resolution and accuracy.

TABLE 2.1 SUMMARY OF THE PERFORMANCE OF COMMERCIAL FBG INTERROGATION UNITS

Company	Model	Resolution (pm)	Accuracy (pm)	Speed (Hz)
Advanced Optics Solutions (AOS) [25]		1.22	± 30.5	500
Insensys [26]		6.1	± 12.2	500
Blue Road Research [27]		2.44	0.24	0.5
SHM Systems [28]	5100a	1.22	± 6.1	100
Micron Optics [29]	si720	0.25	± 1	5
	si425	1	2	244
Systems Planning and Analysis (SPA) [30]	FBG-IS	1	± 10	50
	SL-FOIS	1	± 5	100
Fiberpro [31]	IS7000	1	± 5	200
Intelligent Fiber Optic Systems (IFOS) [32]	I*Sense 14000	1	1.22	200

TABLE 2.2 SUMMARY OF THE PERFORMANCE OF CURRENTLY RESEARCHED FBG INTERROGATION TECHNIQUES

Technique	Resolution	Accuracy (pm)	Speed (Hz)
Broadband source with optical spectrum analyzer [8,9,10]	5pm	± 10	NA
Tunable Laser with Tunable Fabry-Perot Filter [33]	$\pm 0.1\text{pm}$	0.2	NA
Frequency Locked Lasers [24]	$1.2\text{ne}/\sqrt{\text{Hz}}$	NA	1.5
Interferometric Scanning Method [34]	$0.6\text{ne}/\sqrt{\text{Hz}}$	NA	>100
UV induced birefringence of a chirped fiber grating [35]	NA	24.4	300
Acoustooptic Tunable Filter [36]	$150\text{ne}/\sqrt{\text{Hz}}$	NA	200
String Resonator [37]	0.122pm	± 3.66	8
Tunable laser with a gas cell reference [19]	NA	2	NA

2.8 Conclusion

In this chapter, the use of fiber optic sensors in structural health monitoring was reviewed. Also, the background of fiber optic theory and the fiber Bragg grating sensor was discussed. Finally, a review of fiber optic interrogation schemes has provided an adequate introduction to the goal of this thesis. With the use of a swept laser system and wavelength references, the research work presented in this thesis endeavors to improve the accuracy of strain measurements by correctly locating the corresponding Bragg wavelengths.

CHAPTER 3

PEAK LOCATION ALGORITHMS

3.1 Introduction

As previously mentioned, fiber Bragg grating sensors operate by detecting strain through a shift in the reflected wavelength. Therefore, the sensor system's measurement accuracy depends on its ability to detect the peak of the reflected signal. Typically, a wavelength shift measurement error of 100 picometers is equivalent to an error of $100\mu\epsilon$ as found in equation 2.9. In most cases, this is not an acceptable measurement accuracy for monitoring the health of a structure. Therefore, several peak detection algorithms are investigated and their performance when noise is present in the signal is examined. The algorithms evaluated are:

1. 3dB Method
2. Highest Point
3. Polynomial Fitting
4. First Derivative and Zero Crossing Point
5. Lorentzian Fitting
6. Gaussian Fitting

The data used to evaluate the algorithms were obtained by a swept laser configuration as shown in figure 3.1.

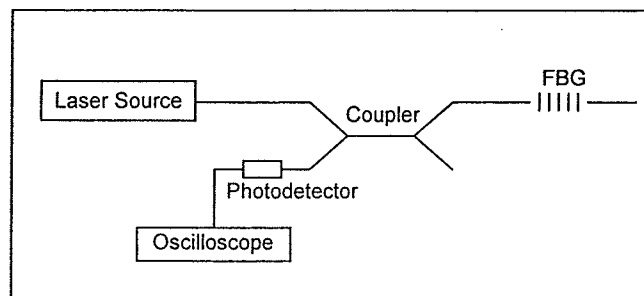


Figure 3.1 Configuration of FBG sensor system using a swept laser source.

The source was a New Focus (model 6262) external cavity tunable diode laser and the photodetector module consisted of an InGaAs PIN photodiode. An oscilloscope was used to view the signal and collect the data.

The light from the free space laser was coupled into the fiber by mounting a lens to the outside of the laser module and aligning the position of the fiber pigtailed collimator in order to capture the light. The setup is shown in figure 3.2a and an overhead view of the entire fiber system is shown in figure 3.2b.

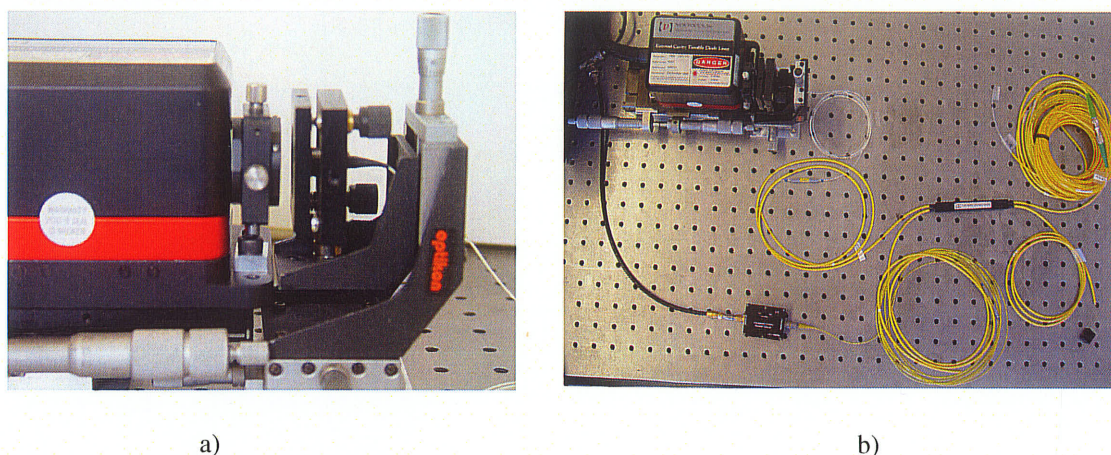


Figure 3.2 FBG interrogation system setup.
(a) Detailed view of light collimation into fiber
(b) Overhead view of entire FBG sensor system

The Bragg grating used for this project had a Bragg wavelength of 1536.214nm as determined by the manufacturer, O/E Land Inc.. The tunable laser source was set to sweep a range of 2nm, from 1535 to 1537nm. The reflected signal from the grating was sent to the photodetector and recorded by the oscilloscope. The wavelength output of the laser source was also sent to the oscilloscope. This signal is a voltage which varies linearly with the output wavelength of the source. The voltage increases with wavelength according to the equation

$$V = f\Delta\lambda \quad (3.1)$$

where $\Delta\lambda$ is in nanometers and f depends on the laser center wavelength and ranges anywhere from 0.2 and 1V/nm. As a result, this was used to determine the start and stop points of the laser sweep. The Bragg grating signal output and the corresponding laser wavelength output is illustrated in the following figure.

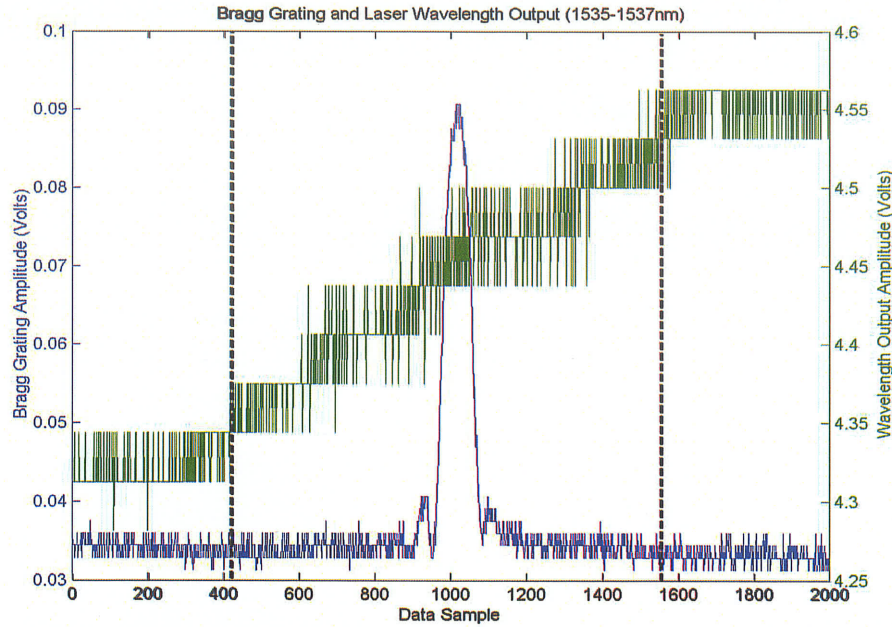


Figure 3.3 Plot of Bragg grating signal and output voltage from the tunable laser.

In the figure, the laser output begins to increase as the wavelength changes and remains constant when the sweep is done. For every file, the oscilloscope saves 2000 data samples. By observation, we can determine the start and stop positions. The start position occurs at data sample = 419 and ends at data sample = 1578. Therefore, there are $1578 - 419 + 1 = 1160$ data samples to represent a 2nm scan. In other words, the data is sampled every 1.72pm.

A graph of the entire Bragg grating signal and a detailed view of the peak of the signal are shown in figures 3.4a and 3.4b, respectively.

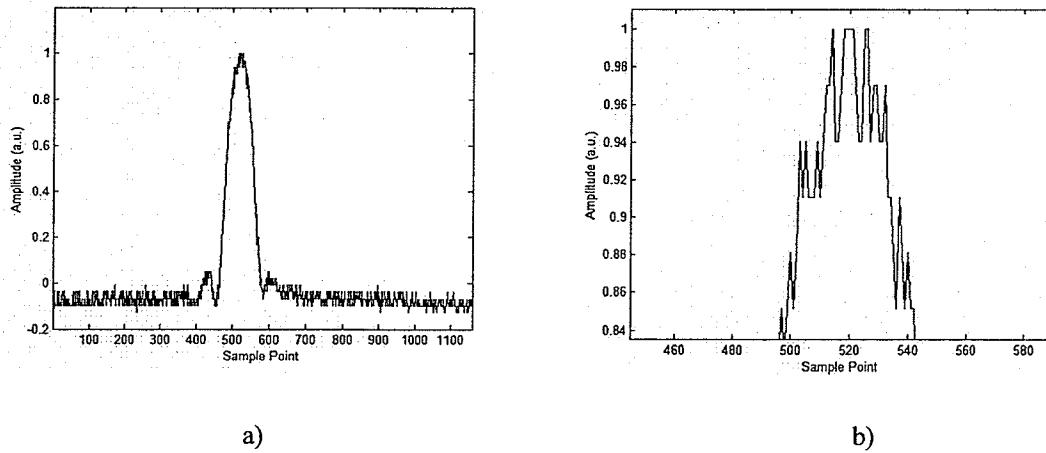


Figure 3.4 Signal reflected from Bragg grating.
(a) entire signal (b) zoomed in view of peak

As shown in the figures, the location of the Bragg peak is not easily located. Also, there is some sampling error due to the oscilloscope but the main source of noise in the system is due to photodetector noise. Although the expected signal in a Bragg sensor system is much smoother than this signal, it was still used to evaluate the algorithms because a noisier signal would be better suited to test performance and reliability of an algorithm.

3.2 Peak Location Methods

As mentioned previously, six peak detection algorithms were evaluated with the signal using the software Matlab. A description of each algorithm follows.

1) 3dB Method

The 3dB method is a common technique used to find the peak in a signal. This method involved finding the 3dB threshold crossing points of the signal and taking the middle value as the peak as demonstrated in figure 3.5a. The 3dB threshold is found using the equation

$$V_t = 0.7079 * \text{max value of the signal} \quad (3.2)$$

and the peak location is found with

$$\text{peak location} = \lambda_p = \frac{(\lambda_1 + \lambda_2)}{2} \quad (3.3)$$

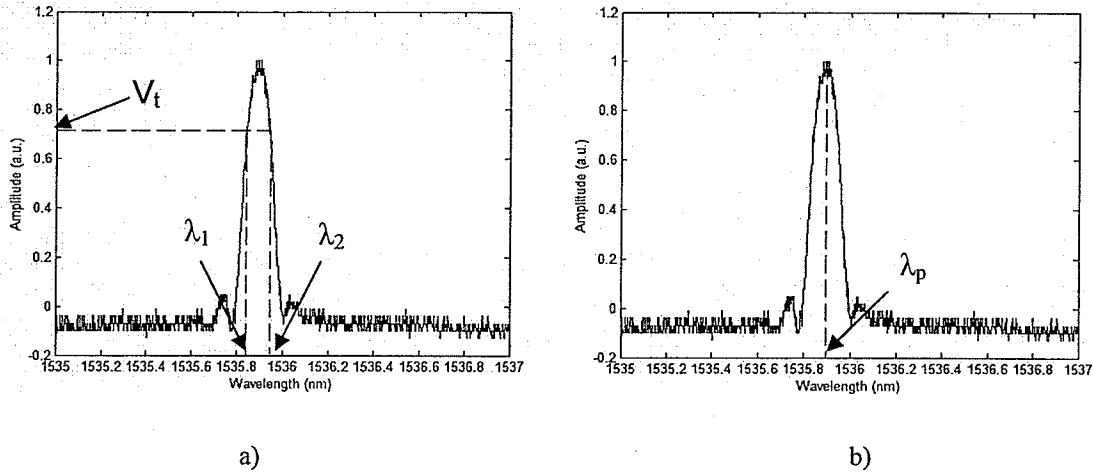


Figure 3.5 First two peak location algorithms.
(a) 3dB method (b) Highest point method

2) Highest Point

This simple yet coarse method involved finding the absolute maximum value of the signal and at what wavelength it occurred. This wavelength was then set as the peak wavelength as shown above in figure 3.5b.

3) Polynomial Curve Fitting

Fitting a polynomial curve to a set of data is a frequently used method in data analysis applications. This method involved creating a threshold and fitting the data points within that threshold to a polynomial curve. For this signal, the polynomial curve used was of 2nd order (ie. Parabola)

$$p(x) = p_1x^2 + p_2x + p_3 \quad (3.4)$$

Polynomial curve fitting involves using a least squares method that minimizes the sum of the squares of the errors between the polynomial curve and the data. Therefore, the

program in Matlab used the least squares method and the x and y values of the signal to find the p coefficients of the optimal polynomial curve. The peak wavelength was then determined to be the location at which the maximum value of the polynomial curve occurs. The original signal and the corresponding polynomial curve fit are shown in figure 3.6.

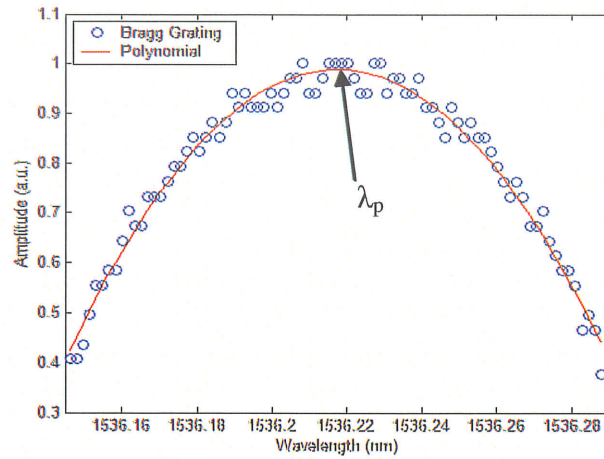


Figure 3.6 Polynomial fit algorithm.

4) First Derivative and Zero Crossing

The first derivative of a signal is used to find the locations of maxima and minima. The zero crossing points of the first derivative define these locations. It is expected that at some point the derivative will change its sign from positive (indicating an increasing function) to negative (indicating a decreasing function). This signifies there is a maxima (ie. Bragg peak) at that critical point.

First, the signal was filtered using a second order Butterworth filter with a cutoff frequency of 100Hz to remove noise. The first derivative was determined using the following forward difference formula:

$$f'(i) = \frac{f(i+1) - f(i)}{x(i+1) - x(i)} \quad (3.5)$$

A smoothing operation was performed on the derivative to reduce the noise in the signal and reduce the amount of intensity variation from one sample point to the next. In this case, Gaussian smoothing was used and it is a 1D convolution operation that uses a kernel that represents the shape of a Gaussian curve. The degree of smoothing depends on the standard deviation of the Gaussian kernel. Gaussian smoothing determines a weighted average around a data point where the average is heavily weighed by the values closer to the data point. As a result, the Gaussian kernel is a gentler smoothing process than the mean filter. After the smoothing is performed, the location of the zero crossing point is determined, as shown in figure 3.7. This location is then assumed to be the peak location as well.

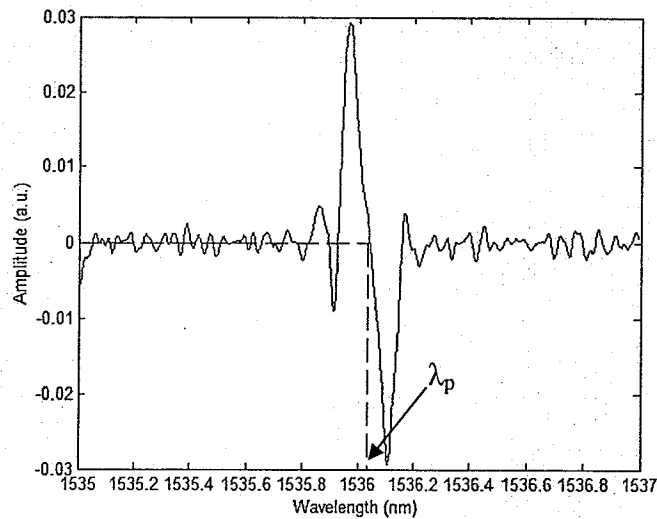


Figure 3.7 First derivative and zero crossing point algorithm.

5) Lorentzian Curve Fitting

This method involved fitting a Lorentzian curve to the data points above a specific threshold. The Lorentzian equation is as follows:

$$f(x) = \frac{1}{\pi} \frac{\Gamma/2}{(x-\mu)^2 + (\Gamma/2)^2} \quad (3.6)$$

where μ = mean and Γ = full width at half maximum. For each data point within the threshold, the Γ was varied. The mean squared error between the original signal and Lorentzian was found for each combination of μ and Γ . The best fit occurred with the combination that produced lowest mean squared error. As a result, the peak wavelength is designated as the μ in that combination.

6) Gaussian Curve Fitting

The same methodology as the Lorentzian method was performed on the signal, except a Gaussian curve was used instead. As before, the data above a designated threshold was fit to a Gaussian function. The Gaussian equation is

$$f(x) = \frac{1}{\sigma\sqrt{2\pi}} \exp \frac{-(x-\mu)^2}{2\sigma^2} \quad (3.7)$$

where μ = mean and σ = standard deviation. In this case, for each data point, the σ was varied. Again, for every combination, the mean squared error between the original signal and Gaussian curve was found. The μ in the combination that resulted with the lowest mean squared error was specified as the location of the peak wavelength.

The difference between the Gaussian and Lorentzian curves is illustrated in figure 3.8. Also, an example of a Lorentzian curve and Gaussian curve fitted to the Bragg grating signal is depicted in figures 3.9a and 3.9b, respectively.

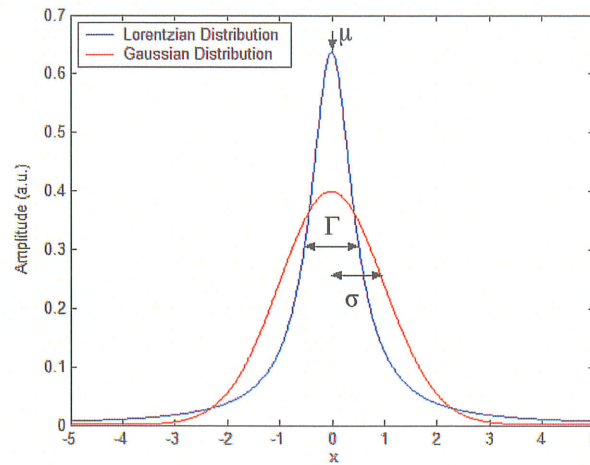
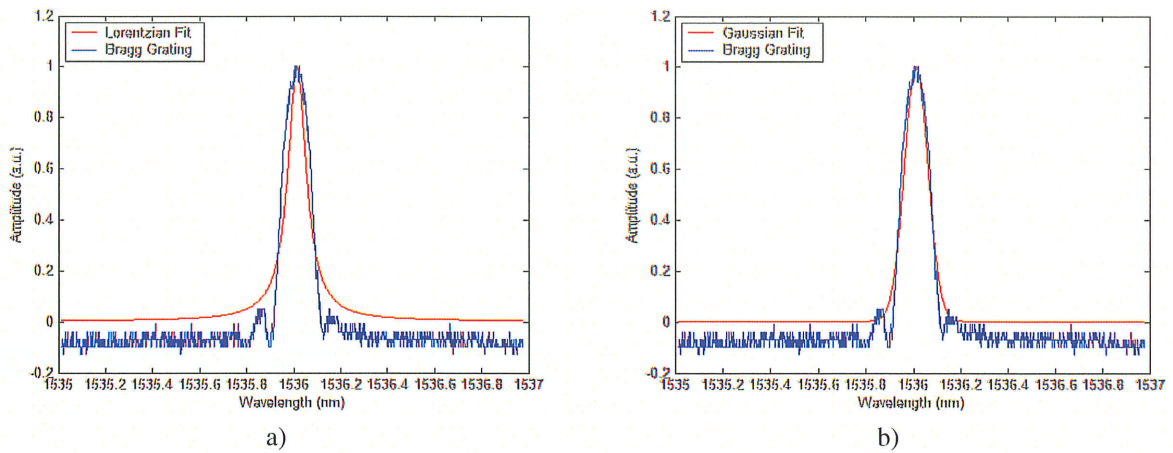


Figure 3.8 Lorentzian and Gaussian distribution curves.

Figure 3.9 Lorentzian and Gaussian peak fit algorithms.
(a) Lorentzian fit (b) Gaussian fit

3.3 Simulations

The signal was first normalized and the peak detection algorithms were performed on it. To provide a reference point, λ_p was determined by fitting a Gaussian peak to the data using the RMS error as a figure of merit. This was used as our baseline for comparison of peak location algorithms. The peaks determined by each algorithm was recorded and the error relative to the “ideal” peak location, λ_p , from the Gaussian fit was calculated for each method. The results of the peak detection algorithms performed on

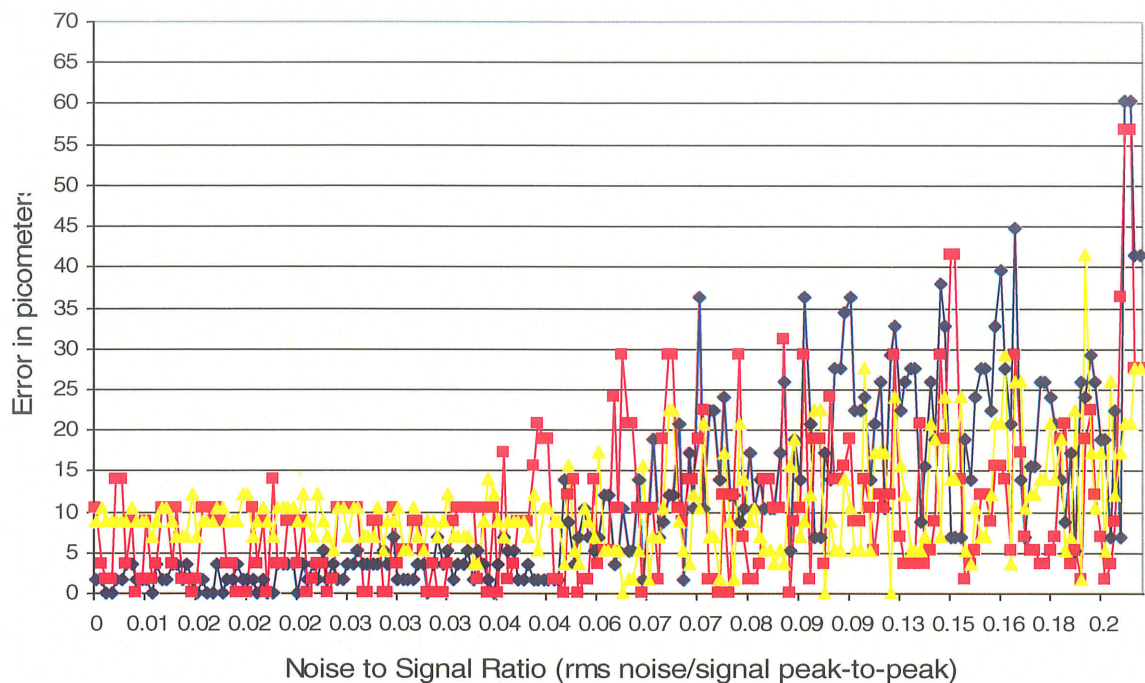
the original signal, with a signal to noise ratio of 80:1 and using a reference wavelength of 1536.214nm, is presented in the following table.

TABLE 3.1 COMPARISON OF PEAK FITTING ALGORITHMS WITH RESPECT TO THE PEAK WAVELENGTH DETERMINED FROM THE GAUSSIAN FIT METHOD

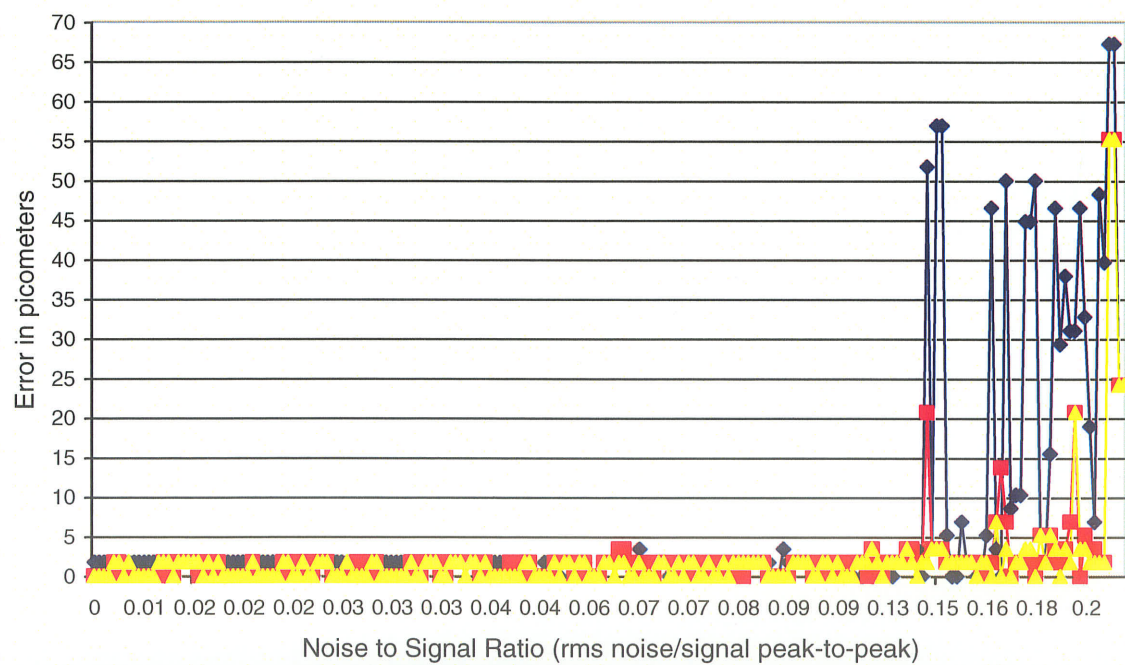
Algorithm	λ_p (nm)	$\Delta\lambda_p$ (ie. $\lambda_p - \lambda_{p \text{ Gaussian}}$) (pm)
3dB Method	1536.2157	1.7
Highest Point	1536.2243	10.3
Polynomial Fitting	1536.2157	1.7
First Derivative	1536.2226	8.6
Lorentzian Fitting	1536.2140	0.0
Gaussian Fitting	1536.2140	0.0

From this, one can see that the highest point and first derivative methods resulted in peak positions which deviated by more than 8pm from the peak position determined by the Gaussian peak fitting. This corresponds to an error of 7 $\mu\epsilon$ and would not be acceptable for many civil infrastructure applications. On the other hand, the 3dB, polynomial, Lorentzian and Gaussian peak fitting methods all produced deviations that were less than 5pm yielding errors of less than 4 $\mu\epsilon$. All these algorithms would produce errors less than those normally considered acceptable for civil infrastructure monitoring applications.

After determining the peaks on the original signal, amplitude noise was then added to it in increasing increments. The peak position was determined for 15 trials at each noise level and the RMS error in determining the peak location is plotted against the noise to signal ratio as shown in figure 3.10a for the first 3 methods, while the results for the last 3 methods is displayed in figure 3.10b. The noise to signal ratio is defined as the RMS noise to the peak signal. The maximum amount of error desired is 5pm. Although from observation only, it is difficult to discern the performance of each algorithm, detailed analysis shows that the polynomial, Lorentzian and Gaussian methods prove to be the most accurate algorithms as shown in figure 3.11.



a)



b)

Figure 3.10 Peak location error vs noise-to-signal ratio for the first three methods.

(a) 3dB, Highest point and First derivative methods

(b) Polynomial, Lorentzian and Gaussian fit methods

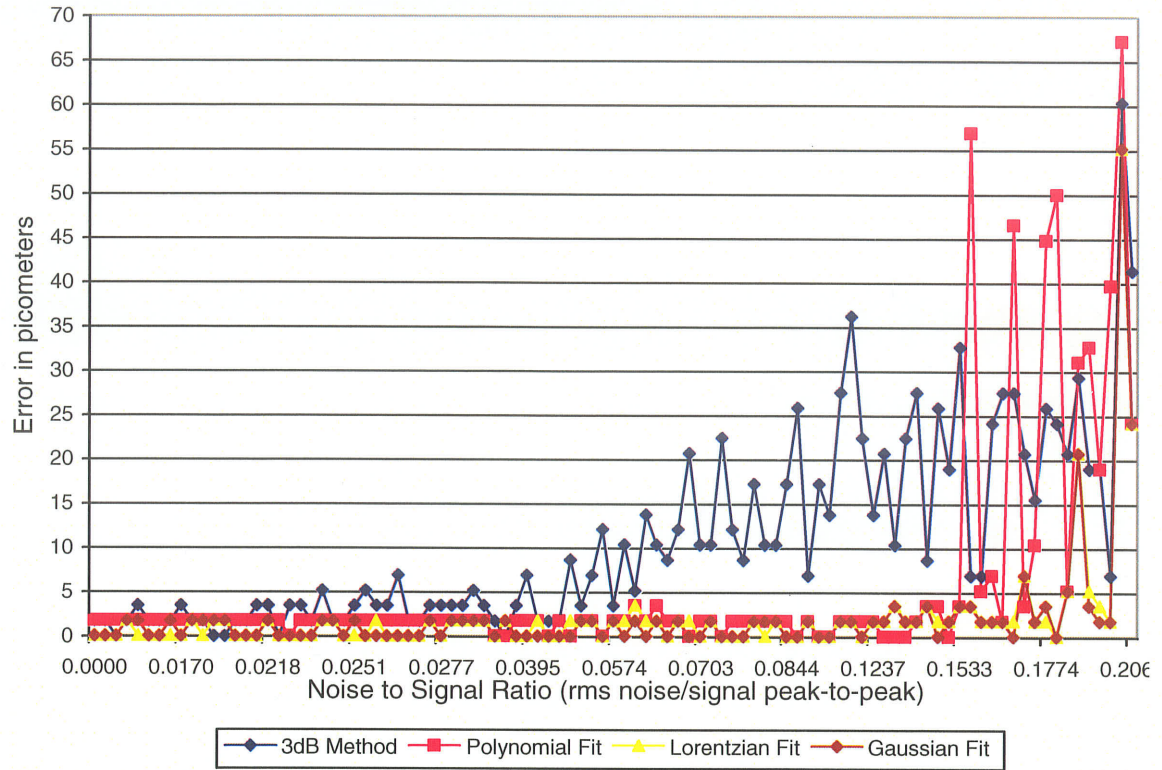


Figure 3.11 Peak location error vs noise-to-signal ratio for four methods.

A summary of the noise to signal ratio required for each peak location algorithm in order to stay under an error of 5pm is found in the following table. It is easily seen that both the highest point and first derivative methods do not achieve errors less than 5pm.

TABLE 3.2 NOISE TO SIGNAL RATIO REQUIRED FOR EACH PEAK FITTING ALGORITHM TO MAINTAIN AN ERROR BELOW 5 PICOMETERS

Algorithm	Noise to Signal Ratio
3dB Method	0.026
Highest Point	NA
Polynomial Fitting	0.154
First Derivative	NA
Lorentzian Fitting	0.175
Gaussian Fitting	0.175

Since optical power comes at a premium in terms of cost and system reliability, it is important to establish the minimum power requirements to perform any particular

measurement. To establish this limit, the original data was modified by adding additional noise and the performance of these peak location algorithms was monitored in the presence of ever increasing levels of noise.

Using the noise to signal ratio established by the simulations, one can estimate the minimum optical power required for these measurements. For example, one first assumes that an optical power of 11.2pW is reflected from the FBG, which corresponds to a photocurrent of 16pA at the photodiode, assuming the quantum efficiency is 0.7. Using the polynomial fit curve in figure 3.11 above, at noise to signal ratios of less than 0.1528 (ie. $S/N \approx 7$), the error in peak position determination was less than 5pm. Assuming shot noise is the dominant source of noise, we use the following equations:

$$I_{SN} = (2 * q * I_{pd} * BW)^{1/2} \quad (3.8)$$

$$\frac{I_{SN}}{I_{pd}} = \frac{(2 * q * BW)^{1/2}}{\sqrt{I_{pd}}} \quad (3.9)$$

where q is the charge of an electron, I_{pd} is the current at the photodetector and BW is the bandwidth. The noise to signal ratio then becomes 0.1415 using a measurement bandwidth of 1MHz, and the noise current would be $I_{SN} = 2nA$. Therefore, for 32 channels at 11.2pW per channel, the total optical power required would be least 400pW. Furthermore, if 1mW of power exits the laser and there are 32 channels in the system, with 80% peak reflection, the power at the photodiode should be about 12.5μW which corresponds to about 12μA, assuming quantum efficiency of 1. As a result, 1mW source is quite sufficient for this measurement system.

Several of the peak location algorithms performed similarly with respect to the signal to noise ratio. These include the polynomial, Lorentzian and Gaussian curve fitting methods. Although the Lorentzian and Gaussian algorithms proved to be the most

accurate, they were also the most computationally time consuming. For most civil structure monitoring purposes, it is desirable to have a system which can measure strains in real time. Therefore, since these methods require extensive amounts of computation, they would not meet the requirements of a strain monitoring system. On the other hand, the polynomial fit method demonstrated to have reasonable accuracies and it was also the most computationally efficient. Therefore, for the remainder of this work, the polynomial fit method was used as the peak location algorithm.

To further extend the resolution of this technique, sub-sampling of the data was performed. This involved adding 32 points between data samples and evaluating the polynomial fit algorithm again with increasing amounts of noise. The result of 10 simulations using the sub-sampling technique is shown in figure 3.12.

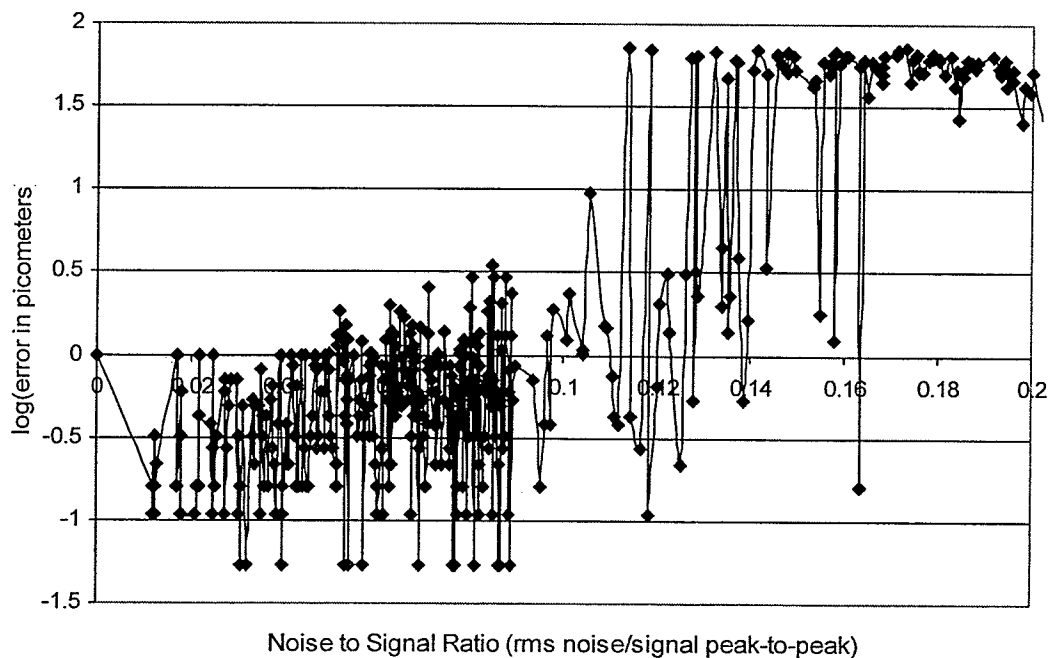
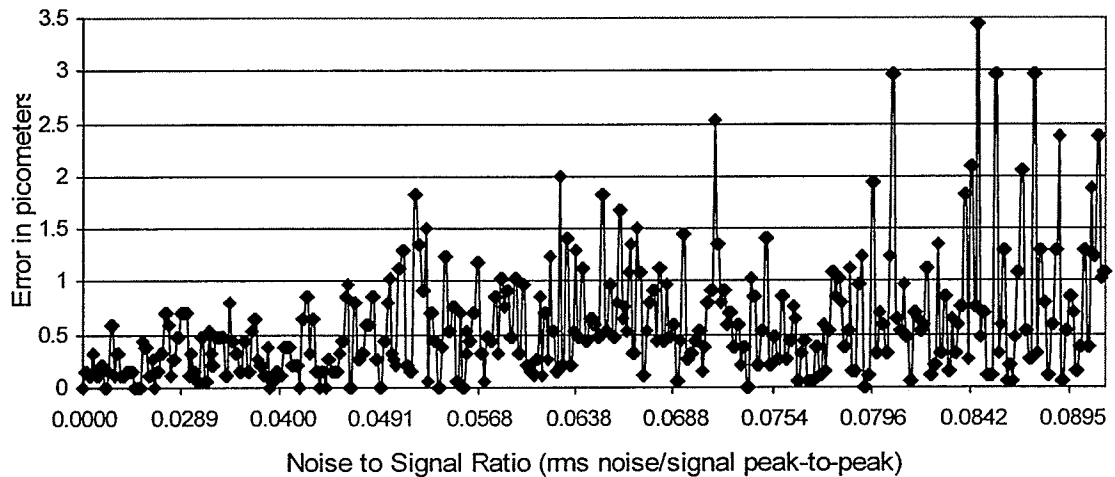


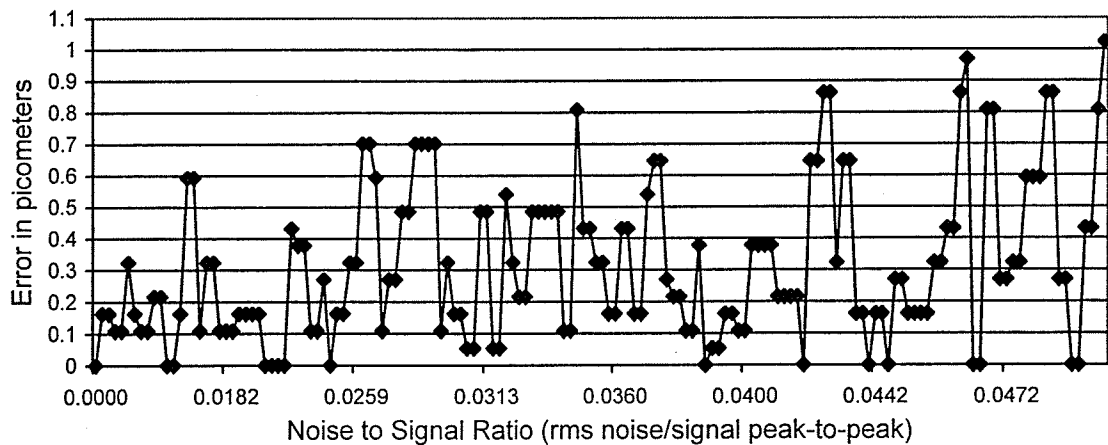
Figure 3.12 Peak location error vs noise-to-signal ratio of polynomial fit algorithm using sub-sampling technique.

Sub-sampling allowed the peak to be placed between data points, thus increasing the resolution. From this technique, the data located below 5pm and 1pm of error is

shown in figures 3.13a and 3.13b, respectively. At noise to signal ratios of 0.104 (ie. $S/N = 9.6$), in figure 3.13a, the RMS error is 0.8185pm and corresponds to a strain resolution of $0.7104\mu\epsilon$. At roughly the same noise to signal ratio, with no sub-sampling, the RMS error was 1.6631pm and the strain resolution was $1.4435\mu\epsilon$. Therefore, this technique improved the resolution by half compared to the results achieved without sub-sampling the data. Also, in figure 3.13b, the 1pm threshold is exceeded at noise to signal ratios of 0.049 (ie. $S/N = 20.4$). This resulted in an RMS error of 0.3987pm which corresponds to a strain resolution of $0.346\mu\epsilon$.



a)



b)

Figure 3.13 Peak location error vs noise-to-signal ratio for the first three methods.
(a) Data below 5pm of error (b) Data below 1pm of error

3.4 Discussion of Signal to Noise Ratio in the Peak Location Method

Peak fitting is a method often used in signal processing applications because it makes better use of more information. When determining a sufficient peak location method, one must take into account the minimum signal to noise ratio required for a specific number of samples. For example, in figure 3.14, the Bragg peak can be approximated with a signal resembling a bandpass filter with a width of $\Delta\lambda$.

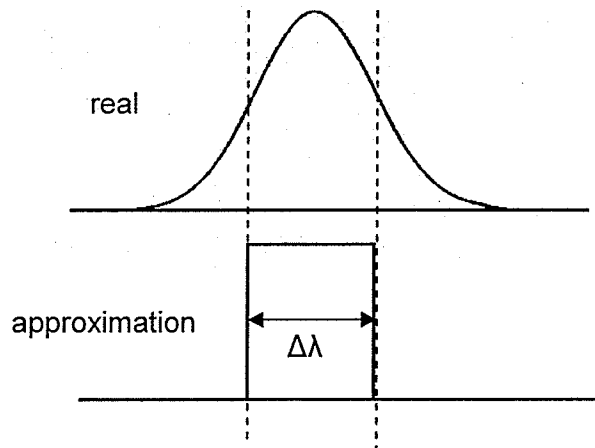


Figure 3.14 Approximation of a Bragg peak.

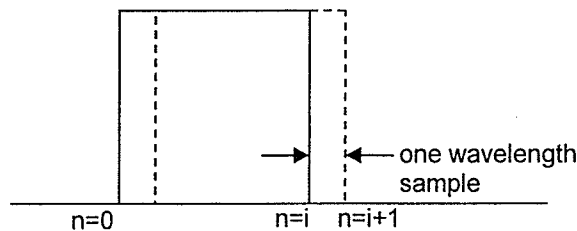


Figure 3.15 Shifting the approximation curve by one wavelength position.

The next step involves determining how large the noise in the signal can be before it becomes impossible to determine when the Bragg peak has shifted one wavelength sample position. For example, if the approximation is located exactly at the peak,

$$S = \sum n \cdot V_i \quad \text{from } n=0 \text{ to } n=i \quad (3.10)$$

where S is the total signal amplitude, i is the total number of samples in the signal, and V_i is the amplitude of the signal at each sample point.

In addition, for each sampling point, the noise will have a certain value, V_n . If the noise is uncorrelated, the total noise will be:

$$N = V_n * \sqrt{i} \quad (3.11)$$

Therefore, in order to determine if the peak has shifted one wavelength sample position, the magnitude of the signal at a certain point would have to be greater than the noise, as shown in the following equations:

$$V_i > V_n * \sqrt{i} \quad (3.12)$$

$$\frac{V_i}{V_n} = \sqrt{i} \quad (3.13)$$

For example, if the Bragg peak is 100 samples wide, where 1 sample corresponds to 1.72pm, then for each sample, the signal to noise ratio would have to be:

$$S/N \geq (100)^{1/2} = 10 \quad (3.14)$$

The noise to signal ratio then becomes 0.1 and it represents the amount of noise required before it becomes impossible to detect a 1.72pm shift in the Bragg peak. As seen in figure 3.13b, the noise to signal ratio of 0.049 is required to exceed the 1pm threshold.

As a comparison, if a triangle signal is used to approximate the Bragg peak, the minimum signal to noise ratio changes significantly. In the following figure, the triangle signal is used to represent the 3dB method.

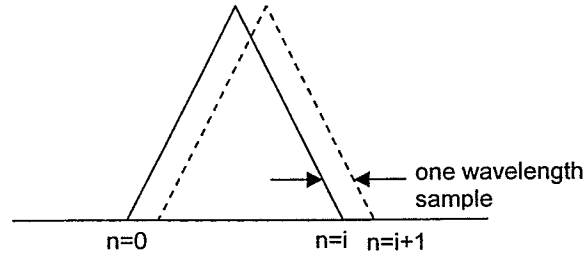


Figure 3.16 Approximation of the Bragg peak using a triangle signal.

In figure 3.16, S is reduced by a factor of 2 and can be compared to the method of finding the center of two threshold crossings. Therefore, the minimum signal to noise ratio also reduces by a factor of 2 as seen in the following equation:

$$\frac{V_i}{V_n} = \frac{i}{2} \quad (3.15)$$

As in the previous example, the S/N required for each point is now 50 and N/S is 0.02. This means that it takes less noise to make it impossible to detect a wavelength shift of 1.72pm. In table 3.2, the 5pm crossing line for the 3dB threshold method occurs at a N/S of 0.026 and 0.154 for the polynomial fit method. This corresponds to a ratio of 1:5.92. If the number of samples in the Bragg peak is 100, using equations 3.13 and 3.15, the ratio of the N/S between the 3dB and polynomial fit is 1:5, which agrees with the ratio acquired for the 5pm crossing line.

To summarize, as the number of samples in increases, the minimum required signal to noise ratio improves as well. Thus, this provides an explanation as to why the polynomial and Gaussian algorithms perform better than the 3dB threshold method.

3.5 Conclusion

In summary, the work involving the evaluation of several peak location algorithms under constraints of maximum RMS error allowed and computation time was

presented. Three methods, specifically the polynomial, Lorentzian, and Gaussian curve fit algorithms, performed well under these constraints. However, due to the long computation times required by the Lorentzian and Gaussian fit methods, the polynomial fit algorithm was determined to be the best method to use in a FBG demodulation unit. Also, the concept of sub-sampling was introduced which demonstrated improvements in the resolution of the polynomial fit algorithm.

CHAPTER 4

IMPLEMENTATION INTO THE FBG UNIT

4.1 Introduction

The goal of this thesis was to develop a method which improved the accuracy of Bragg wavelength measurement. In the previous chapter, several peak detection algorithms were examined based on their performance in finding the peak location under an increasing amount of noise. It was determined that, for the nature of this work, the polynomial curve fit algorithm would be adequate. Therefore, the next step involved implementing this algorithm along with the wavelength references into a fiber Bragg grating readout unit.

4.2 Modifying the FBG Unit

For this project, a FBG readout unit was readily available for modifications and was constructed by a student from the University of Toronto [38]. The readout unit was constructed by modifying a computer tower case with additional parts such as photodetectors, couplers, and a laser diode. The purpose of this was to try to minimize the number of separate modules required for a readout unit and create a compact system design with the potential to become a portable unit in the future. As previously mentioned, it is impractical and cumbersome to bring separate sources and optical spectrum analyzers to monitor Bragg grating sensors. A schematic diagram of this FBG readout system is shown in figure 4.1.

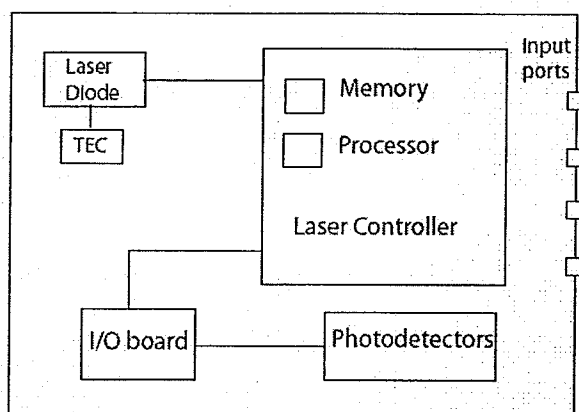


Figure 4.1 Schematic of FBG interrogation unit.

This unit consisted of a laser diode which had a 2nm tuning range in the wavelength ranges of 1535 to 1537nm and 1539 to 1541nm. The wavelength range in which the laser diode operated was controlled using a thermoelectric cooler (TEC). A TEC moves heat from one side of the cooler to the other when a DC voltage is applied to it. As a result, the laser diode is kept at a constant temperature. Therefore, the heat absorption is proportional to the current through the thermoelement. Since the Bragg grating was in the 1536nm range, a 500mA current was applied to the TEC to move the wavelength sweep range to 1535 to 1537nm.

The sensor and the wavelength references were connected to the inputs of the FBG readout unit as shown in figure 4.2. The Bragg grating was placed in input 1, the gas cell input/output ports were connected to inputs 2 and 3 respectively, and the etalon was connected to input 4. For the first trials, the etalon was not used in order to evaluate the performance of the gas cell as a single wavelength reference.

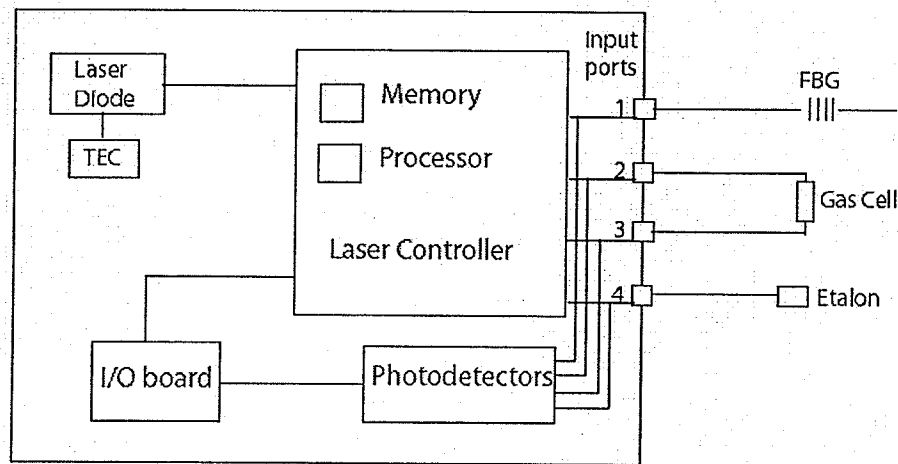


Figure 4.2 Schematic of FBG unit with sensor and wavelength references as inputs.

Data acquisition was performed using the software Labview and signal processing was done in Matlab. The readout unit was modified by replacing the programs in Matlab with ones specific to the use of wavelength references as a means of determining the Bragg peak wavelength. These programs also implemented sub-sampling and polynomial curve fitting techniques and can be found in Appendix A. A screen shot of the Labview user interface is shown in figure 4.3.

This interface allows the user to input the reference Bragg wavelength either from the manufacturer or the value determined during calibration. Also, the user can choose which inputs to monitor, as well as the duration of the scan. For example, the user would choose to highlight input 1 for the Bragg grating and input 3 for the gas cell reference. Inputs 2 or 3 can be used as the gas cell reference since it works in transmission either way. Light is sent down all of the ports each time. Therefore, for a certain scan duration, only the active ports should be highlighted in order for the data acquisition program to determine which outputs from the photodetectors to sample, including the reference signal from the laser itself. The outputs of the interface include the Bragg wavelengths

and strains determined by the Matlab data analysis program using the etalon and gas cell wavelength references or simply just the gas cell alone.

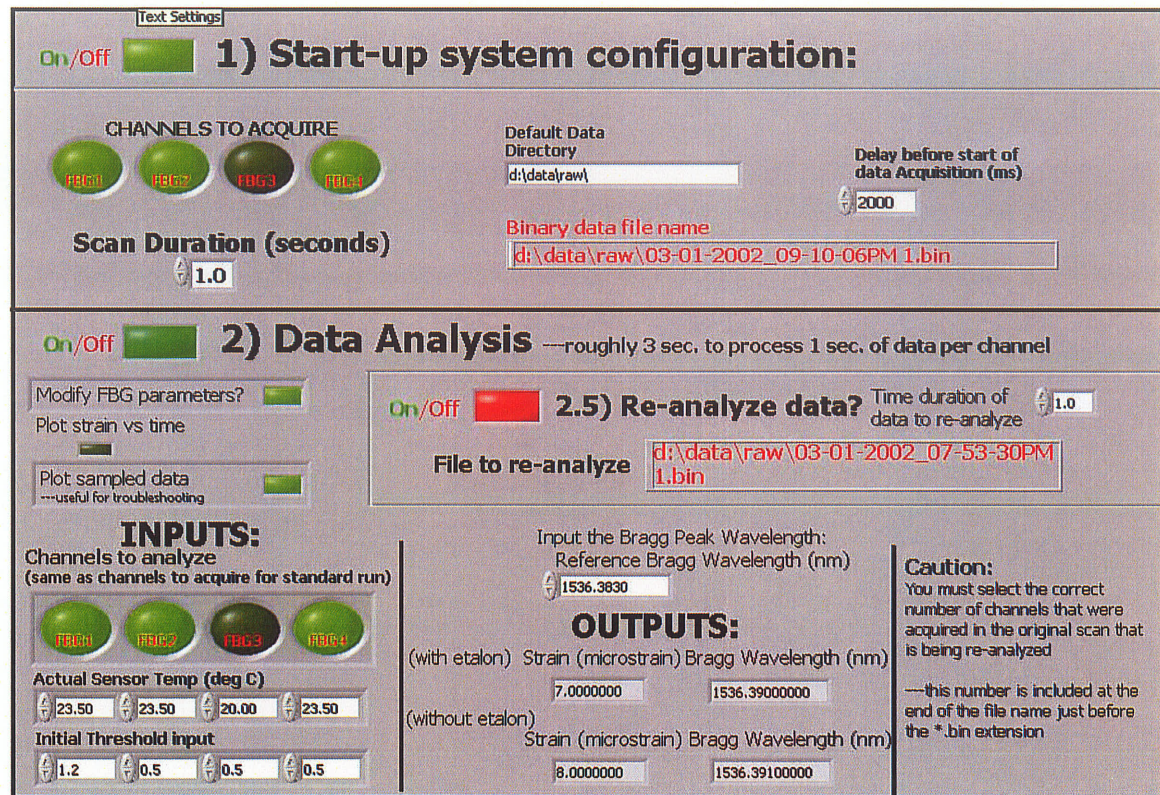


Figure 4.3 Screenshot of Labview user interface.

4.3 Testing of the Modified FBG Unit

For the first test, as mentioned earlier, the Bragg grating and the gas cell reference were used. The Bragg grating was unstrained and placed between two foam cubes for insulation purposes. This was due to the high sensitivity of the Bragg grating to temperature changes. The lab itself was subject to temperature changes of approximately 2°C.

In the system, as the current to the laser is swept, the wavelength will also sweep. As the wavelength of the laser sweeps through a particular gas absorption line, a

minimum in the transmitted power will be observed. Simultaneously, as the wavelength sweeps at a particular wavelength, a peak in the reflected power will occur when λ_p is reached. The reflected Bragg peak, gas cell absorption lines and the reference signal from the laser is shown in figure 4.4. The signals between sample points 1000 and 3600 represent one modulation cycle of the laser sweep from 1535 to 1537nm and back down to 1535nm.

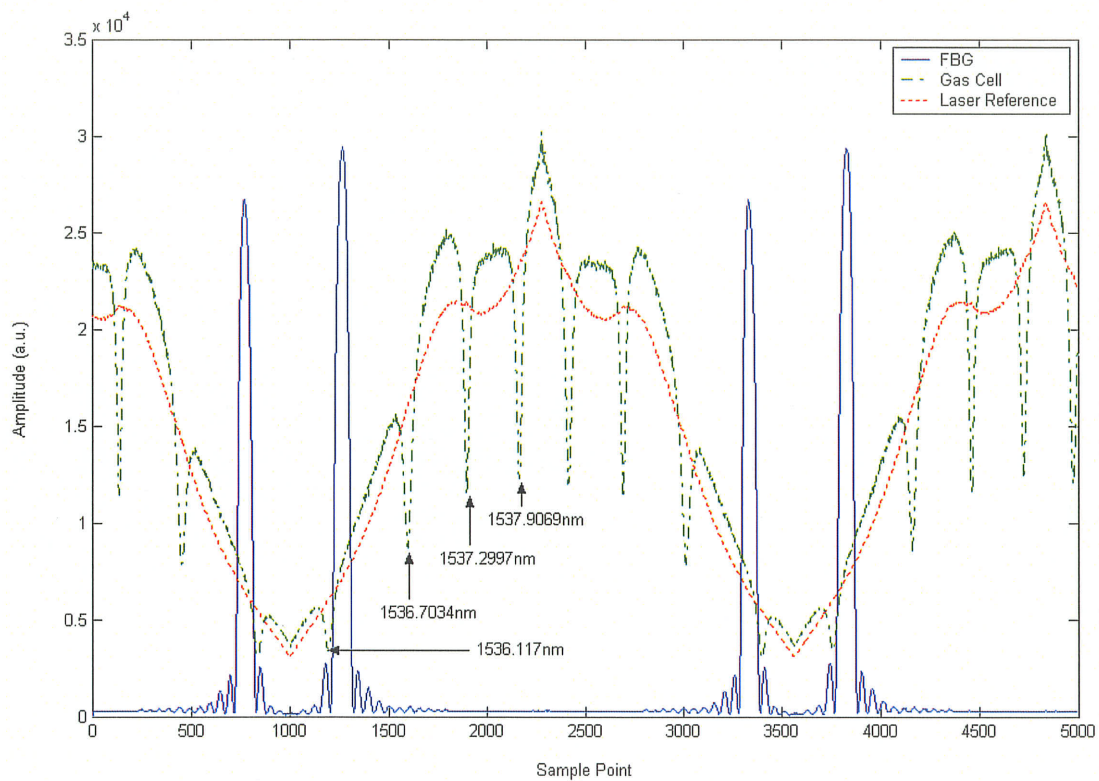


Figure 4.4 Plot of signals from the FBG, gas cell and the laser.

The signals are then normalized using the reference signal from the laser. Using two gas cell absorption lines, the position of a FBG peak λ_p can be estimated by using simple linear interpolation, as shown in figure 4.5.

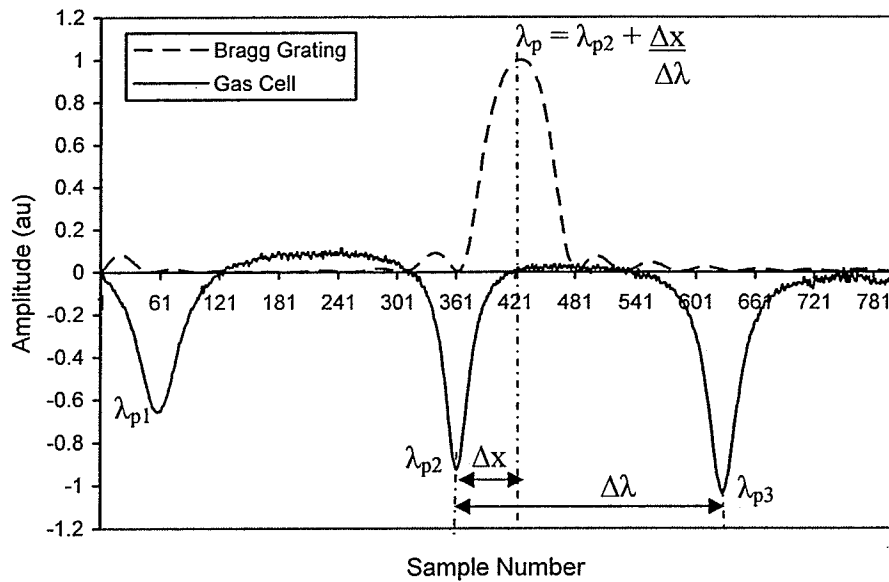


Figure 4.5 Determining the Bragg peak wavelength using interpolation from the gas cell waveform.

Since the laser sweeps through the gas cell absorption minima each cycle, it is possible to interpolate to these peaks on each sweep cycle. As a result, short term and long term drifts in laser wavelength can be corrected for. As a demonstration of this capability, we swept the laser using a triangular current sweep once every 10ms. This allowed the determination of strain in the FBG once every 10ms. However, due to the large amount of computation required, the peak fitting was carried out offline using Matlab. All Matlab programs used in this thesis can be found in Appendix A.

4.4 Short Term Stability Test

As shown in figure 4.6, the peak to peak variation in the measured peak position is less than 0.4pm over this 1 second measurement.

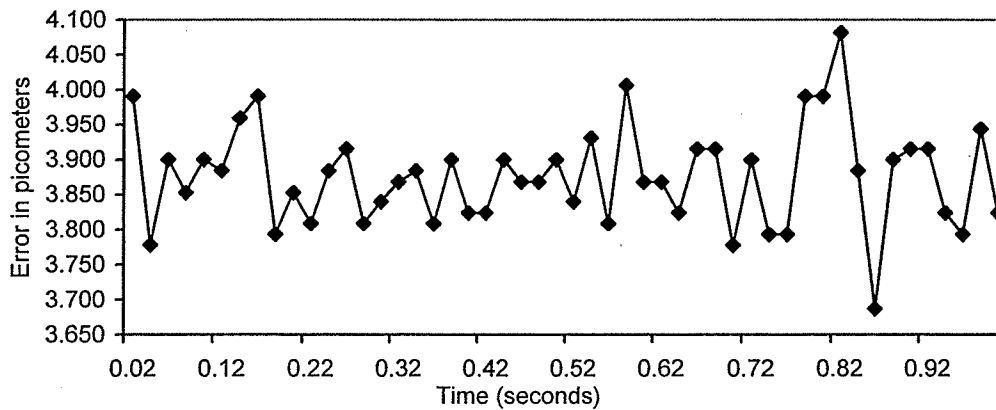


Figure 4.6 Variation of error over a 1 second scan.
RMS=0.071578pm, Peak-to-Peak=0.3948pm

This peak to peak variation, which is approximately $0.39\mu\epsilon$, corresponds to the resolution of the system in short term drifts. This value is much lower than most reported systems which have a resolution of 2pm [19].

In order to test the long term stability of the system, the FBG sensor was insulated again between the foam cubes and readings every 5 seconds were taken over a period of 10 minutes. In this test, the drift was somewhat larger at 1pm as shown in figure 4.7.

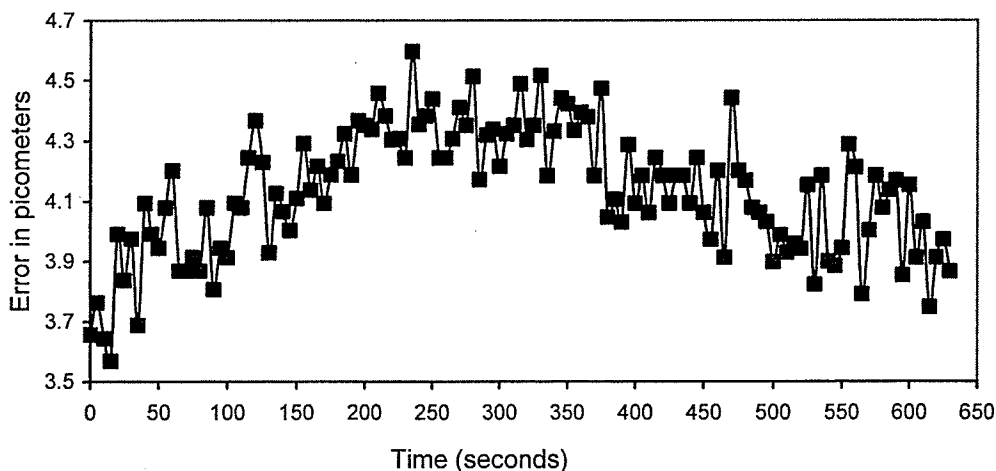


Figure 4.7 Variation of error over a 10 minute time period.
RMS=0.208pm, Peak-to-Peak=1.0281pm

The source of this larger drift has not been identified; however, one possible and likely explanation could be the small (0.1°C) temperature drifts in the FBG as the foam is not a perfect buffer from the environment.

4.5 Implementation of the Etalon as a Wavelength Reference

In the next part of the project, the etalon obtained from Wavelength References Inc. was used for further improvement in the accuracy of the Bragg peak location. As mentioned earlier, an etalon is a comb filter with a large wavelength range and the spacing between the combs is referred to as the free spectral range (FSR). The FSR for this particular etalon was approximately 140pm. It operates in reflection mode because it has a larger dynamic range and is less sensitive to input power variations than in transmission mode. Several simulations using the etalon characteristic equations were performed to observe the etalon signal variations with respect to wavelength and temperature. A simulated etalon waveform in reflection mode in the wavelength range 1535 to 1537nm is shown in figure 4.8.

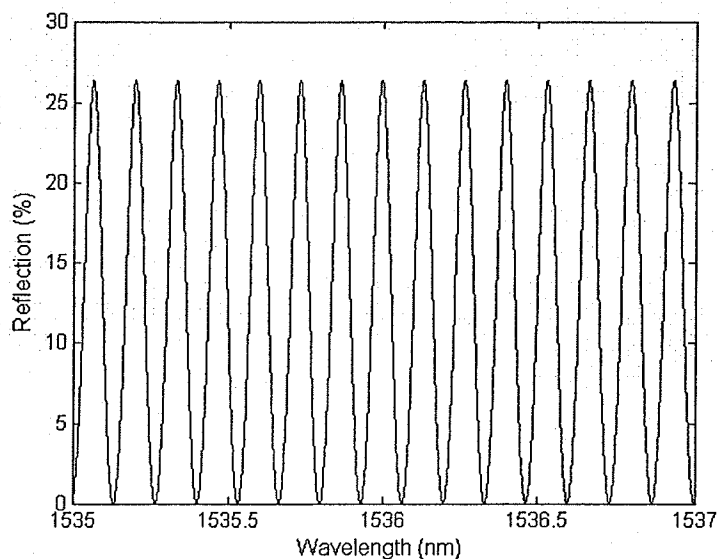


Figure 4.8 Etalon response in reflection from 1535 to 1537nm.

The etalon response also varies with wavelength and temperature, each defined by a specific equation. The Sellmeier dispersion formula, as seen in the following equation, describes the behavior of the etalon waveform as the operating wavelength changes.

$$n^2(\lambda) - 1 = \frac{B_1\lambda^2}{\lambda^2 - C_1} + \frac{B_2\lambda^2}{\lambda^2 - C_2} + \frac{B_3\lambda^3}{\lambda^2 - C_3} \quad (4.1)$$

In the equation above, the B and C coefficients are constants of the dispersion formula and n is the index of refraction with respect to the wavelength. Therefore, the index of refraction changes as the wavelength changes. In addition to this characteristic, the etalon's response to temperature is defined by the Schott formula as shown in the equation below:

$$\Delta n(\lambda, T) = \frac{n_{T0}^2 - 1}{2n_{T0}} (D_0\Delta T + D_1\Delta T^2 + D_2\Delta T^3 + \frac{E_0\Delta T + E_1\Delta T^2}{\lambda^2 - \lambda_{TK}^2}) \quad (4.2)$$

where n_{T0} is the value derived from the Sellmeier formula, and the D, E and λ_{TK} are constants of the formula. Detailed calculations are found in Appendix B. The etalon response to variations in temperature is shown in figure 4.9. As one can see, the temperature has a significant effect as it ranges from -40°C to +80°C.

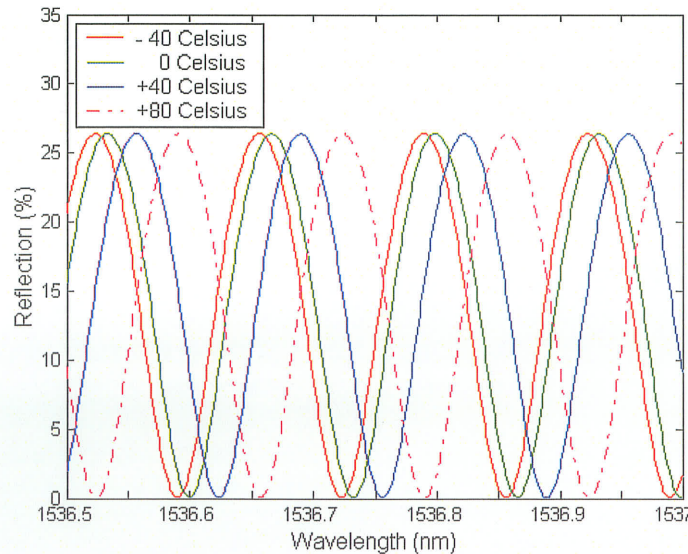


Figure 4.9 Etalon response as temperature varies.

The etalon package contains a temperature sensor which allows for temperature compensation of the response. Also, dispersion is usually an issue for large wavelength ranges. However, it does not have as much effect to the etalon response for a wavelength range of 2nm. Typically, when an etalon is used in conjunction with a gas cell, it is possible to achieve wavelength accuracies of $\pm 1.5\text{pm}$ [39]. As a result, it is expected that the etalon has the potential to further improve the accuracy of locating the Bragg peak.

The etalon was implemented by connecting it to input port 4, as seen in figure 4.2. The reflected Bragg peak, gas cell absorption lines, etalon response and the reference signal from the laser is shown in figure 4.10. One half of the modulation cycle of the laser sweep from 1535 to 1537nm is found between sample points 500 and 1750. The etalon response reveals the nonlinearities in the laser sweep as the spacing between the peaks are not the same. Therefore, the addition of the etalon reduces the error introduced during interpolation from the gas cell alone.

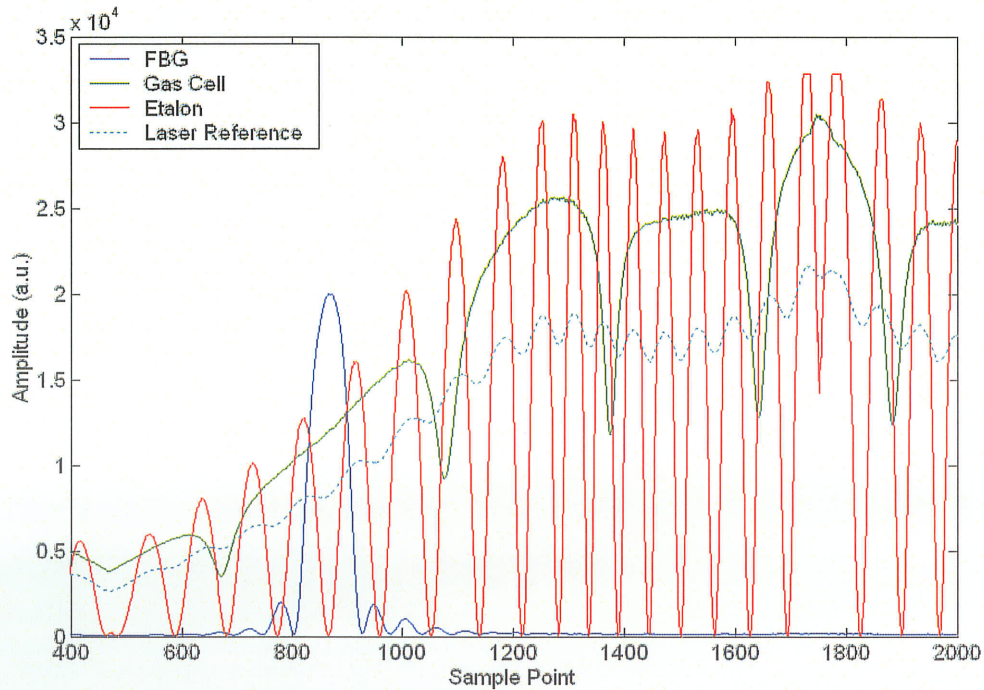


Figure 4.10 Plot of signals from the FBG, gas cell, etalon and laser.

As one can easily observe, the spacing between the etalon peaks is much smaller than the gas cell line separations. After finding each gas cell minima and assigning their specific wavelength found in the NIST standards, the etalon peak locations were determined. The wavelengths of the two etalon peaks nearest to the first gas cell wavelength were found using linear interpolation. These two peaks were then used to determine the constants for the etalon equation which determined the rest of the peak wavelengths. This calculation can be found in Appendix B. The Matlab program then was modified to use linear interpolation from the etalon peaks to determine the Bragg peak wavelength.

Short term and long term stability tests were performed as before; however, this time the etalon was used for interpolation. The results over a one second scan are shown in figure 4.11. This time the peak to peak variation was 0.177pm which was significantly less than the result of 0.3948pm achieved from interpolation from just the gas cell. From this graph, it can be seen that the error was limited by the sampling resolution.

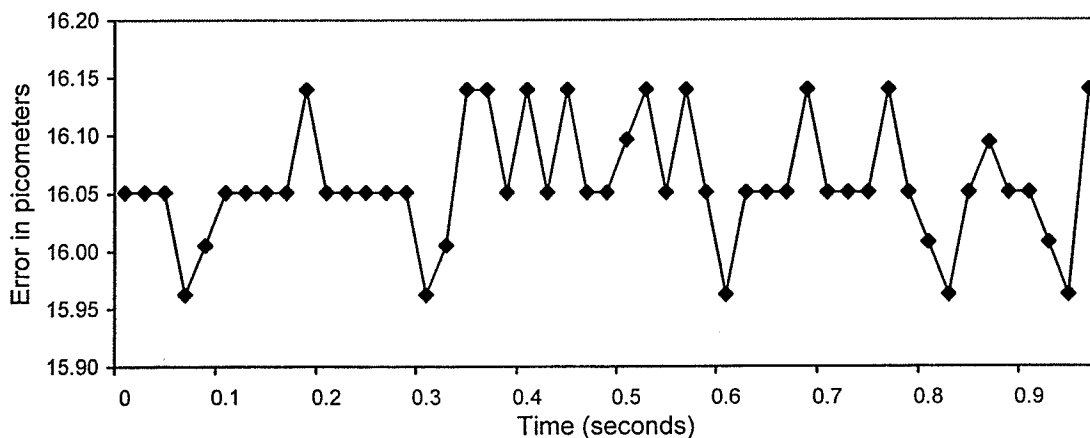


Figure 4.11 Variation of error over a 1 second scan with the etalon.
RMS=0.05089pm, Peak-to-Peak=0.177181pm

The long term stability was then determined by examining the variation of the measurements over a 10 minute time period. This is shown in figure 4.12.

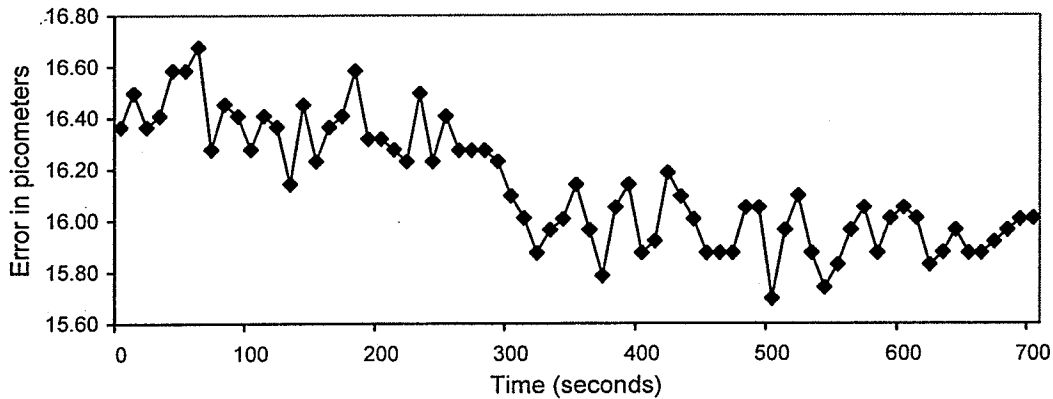


Figure 4.12 Variation of error over a 10 minute time period with the etalon.
 RMS=0.266pm, Peak-to-Peak=0.978054pm

As one can see, there were still some temperature drift effects in the signal. However, in this case, the peak to peak variation was less than 1pm. A comparison of the results from interpolation from the gas cell and from the etalon is illustrated in the following figure. The offset was due to the initial wavelength calculated by each method.

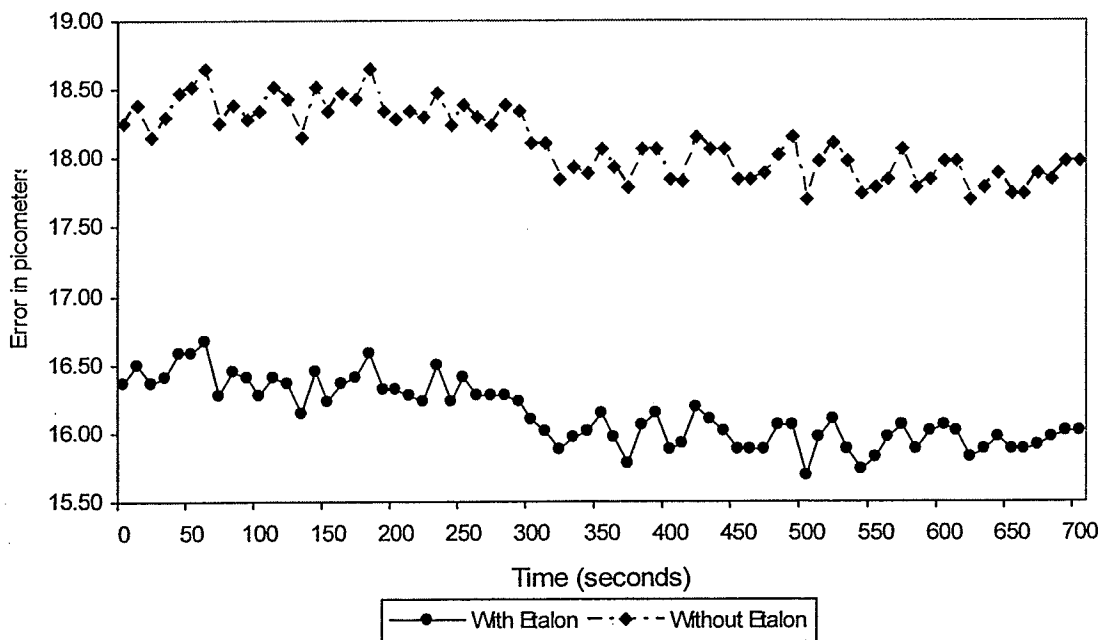


Figure 4.13 Variation of error over a 10 minute time period with and without the etalon.
 With Etalon: RMS=0.266pm, Peak-to-Peak=0.978054pm
 Without Etalon: RMS=0.260pm, Peak-to-Peak=0.952132pm

From the graph, the results from the both the etalon and gas cell interpolations agree well with each other. The difference between the errors may be a result due to the increase in accuracy of measurement with the use of the etalon. As mentioned earlier, it was expected to improve the accuracy of measurements by $\pm 1.5\text{pm}$ and the difference between the two signals is roughly 1.75pm . However, without knowing what the correct value of the Bragg wavelength is, conclusions about the effect of the etalon on the measurement cannot be drawn. Therefore, it is necessary to conduct some experimental tests using the fiber Bragg grating and a metal foil strain gauge in order to conclusively determine whether the etalon does improve strain measurement accuracy.

4.6 Conclusion

In this chapter, the implementation of the polynomial curve fit algorithm in conjunction with two types of wavelength references: a hydrogen cyanide gas absorption cell and an etalon, was discussed. By simply using the gas cell alone, the performance of the FBG unit in strain measurement was found to be sufficient for the requirements of structural health monitoring. However, the goal of this thesis was to explore the possibility of further improving the accuracy in measurement using an etalon. The results shown in this chapter have proved that the etalon does improve the stability of measurements, especially in short term scans. A discussion of the load testing performed and a comparison of the results from the modified FBG unit to a metal foil strain gauge are presented in the following chapter.

CHAPTER 5

EXPERIMENTAL TESTING AND RESULTS FROM THE FBG UNIT

5.1 Introduction

In the previous chapter, the implementation of the wavelength references in the FBG unit was discussed. The results from the unstrained sensor tests proved that the use of the HCN gas cell and/or the etalon increased the accuracy of Bragg peak location thus improving the accuracy of strain measurements. The strain tests carried out on the FBG to evaluate the performance of the FBG unit with the wavelength references are discussed in this chapter.

5.2 Test Setup

An experimental test setup was fabricated in order to test the accuracy of the FBG unit using the wavelength reference. This setup involved designing and manufacturing a constant stress cantilever beam [40] as shown in figure 5.1a. The purpose of creating such a beam was to ensure the Bragg grating experienced constant strain across its entire gauge length. If the strain across the grating was not constant, the grating would experience a strain gradient across its length and thus, result in erroneous strain readings. Also, it was important to reduce any errors between the Bragg grating and the corresponding strain gauge that was mounted right next to it. This way, both sensors would experience the same stress in spite of their different lengths.

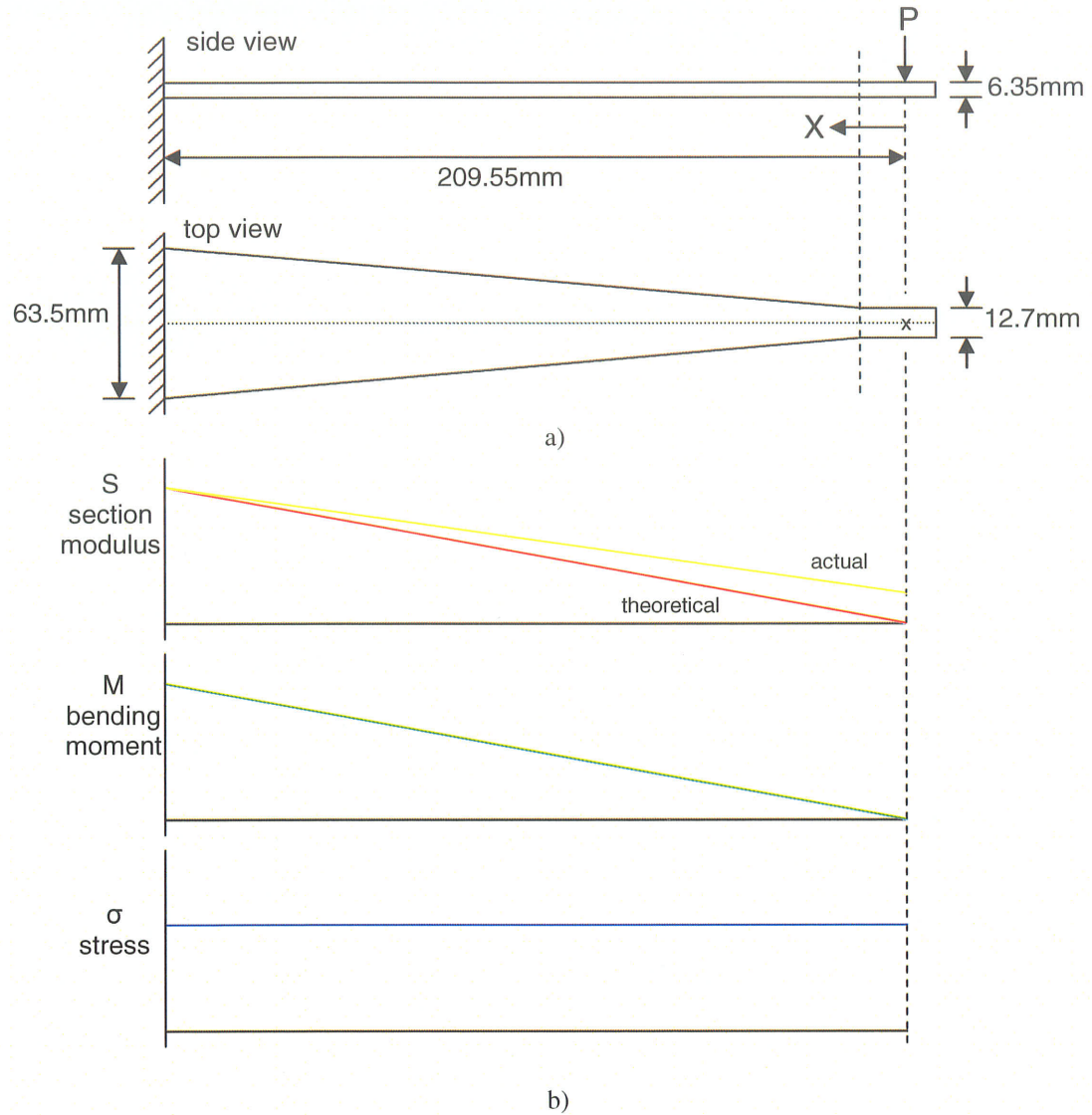


Figure 5.1 Constant stress beam design
(a) Dimensions of the constant stress beam.

(b) Variation of section modulus, bending moment and stress over the beam length with point load P.

The relationship between the bending moment and stress is defined by the following equation:

$$\sigma = \frac{M(x)c}{I(x)} = \frac{Px}{S} \quad (5.1)$$

where σ is the bending stress and M is the bending moment at a distance x from P , the point load. Also, c is equal to half the thickness of the beam and is the distance from the

neutral axis to the beam surface. I is the moment of inertia of the beam cross-section.

Finally, S is the section modulus of the beam and is defined as:

$$S = \frac{b(x)t^2}{6} \quad (5.2)$$

where b is the beam width at a distance x from P , and t is the beam thickness. Strain is linearly proportional to stress and varies with Young's modulus constant, E , as seen in Hooke's law:

$$\varepsilon = \frac{\sigma}{E} = \frac{Px}{ES} \quad (5.3)$$

The calculations for the section modulus, bending moment and stress found in figure 5.1b are as follows:

$$\text{From equation 5.2, } S = \frac{b(x)t^2}{6} \quad \text{where } b(x) = \frac{63.5}{209.55}x$$

$$\text{Therefore, } S = \frac{(63.5 * 6.35^2)}{(209.55 * 6)}x = 2.036x$$

$$\text{Also, } M = Px$$

$$\text{Finally, from equation 5.1, } \sigma = \frac{Px}{S} = \frac{Px}{2.036x} = 0.491P \text{ (N/mm}^2\text{)}$$

Thus, as shown in figure 5.1, the stress is constant along the span of the beam. As shown in figure 5.2, the cantilever was fabricated from Aluminum 6061-T6, which has a Young's modulus, E , of $69 \times 10^9 \text{ N/m}^2$ and a thickness of 6.35 mm ($\frac{1}{4}$ "). The anticipated load, P , which would be applied within the elastic range, was 100 N .

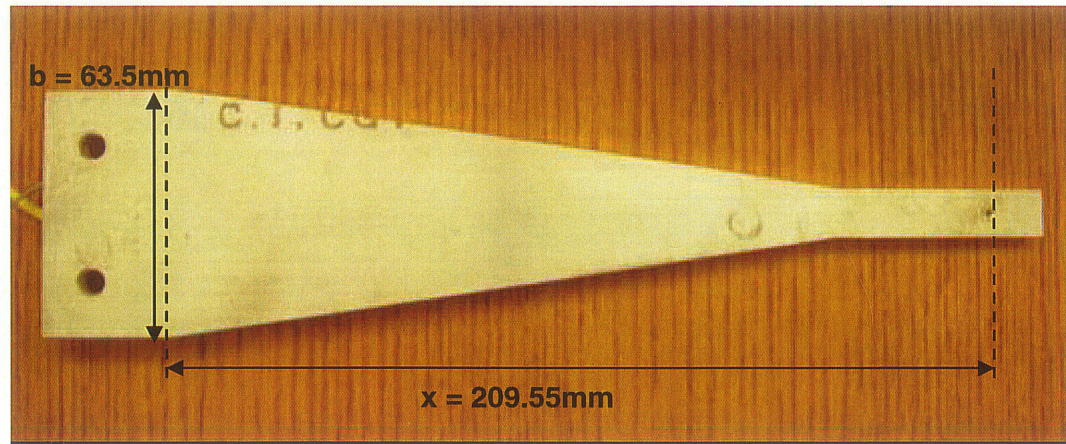


Figure 5.2 Constant stress beam dimensions.

Therefore, the expected stress and strain on the beam was $49.1 \times 10^6 \text{ N/m}^2$, using equation 5.1, and $712 \times 10^{-6} \epsilon$ or $712 \mu\epsilon$, respectively. A finite element model of the cantilever using Adina confirmed that the stress was constant over the span of the beam. The finite element model of the beam is shown in figure 5.3.

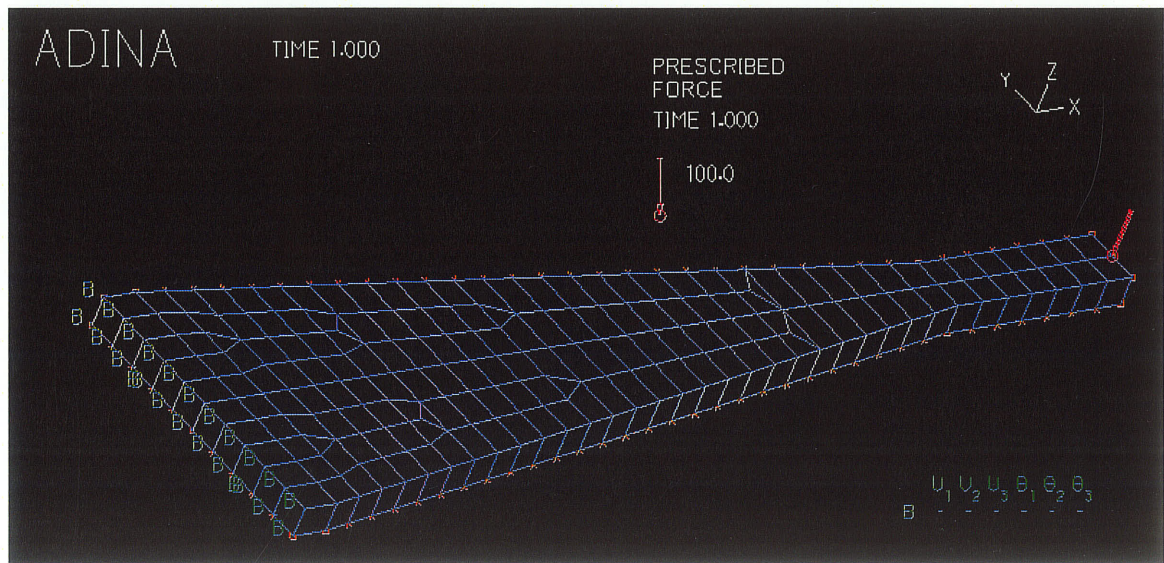


Figure 5.3 Finite element mesh plot of beam with applied force and boundary conditions.

The resulting stress distribution over the length of the beam and the cross section is shown in figures 5.4a and 5.4b, respectively.

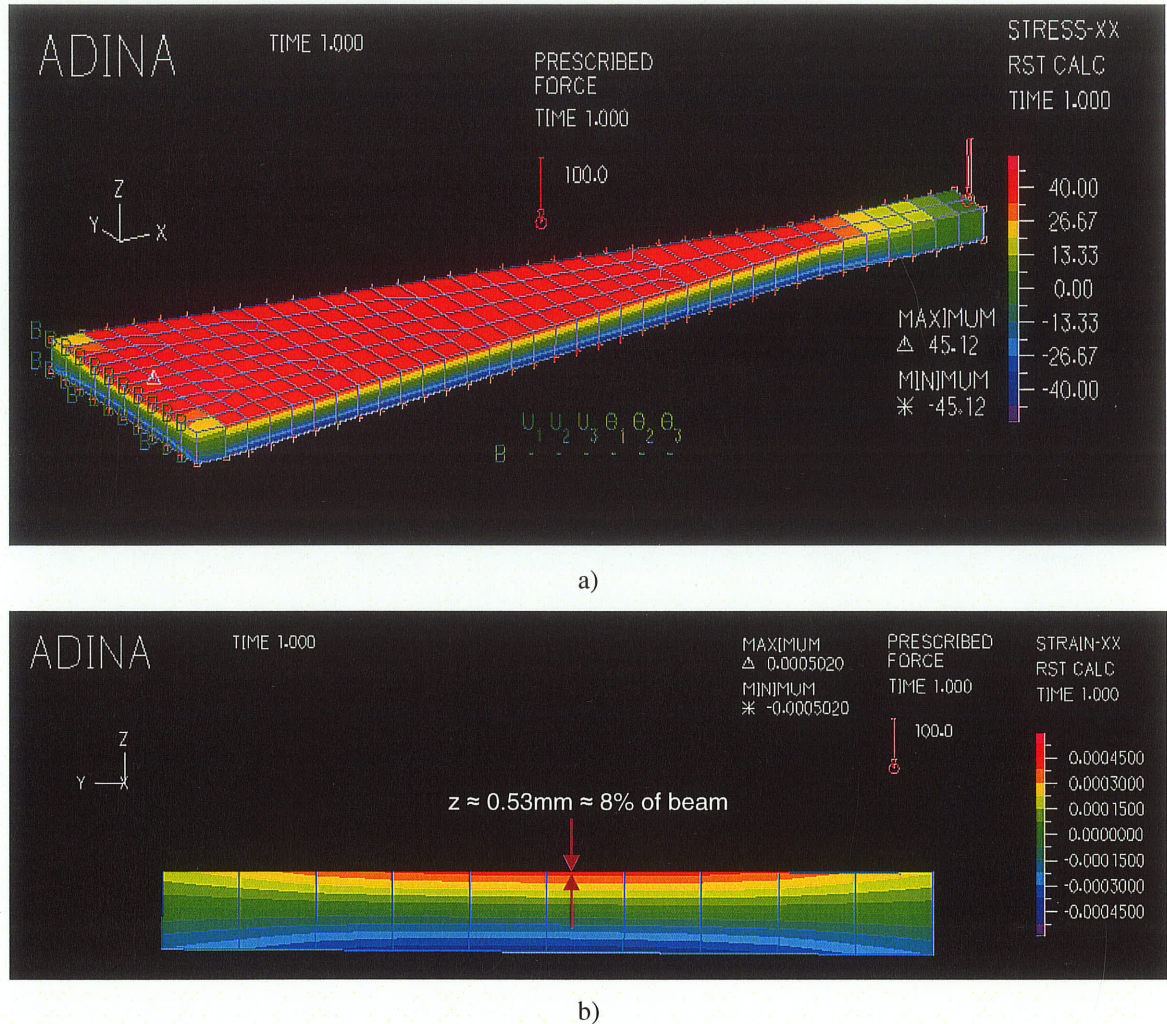


Figure 5.4 Stress plot of beam.

(a) Stress distribution over the length of the beam (b) Cross section view of strain distribution

The color bar in figure 5.4a corresponds to an expected stress of roughly 40kN/m^2 over the top length of the beam which is, approximately, equal to that obtained using equation 5.1. This value of stress then relates to a strain of $580\mu\epsilon$, as seen in the beam cross-section in figure 5.4b. This strain is experienced on the upper 8% ($\sim 0.5\text{mm}$ deep) of the beam thickness.

The fiber optic sensor and strain gauge were attached to the test beam as shown in figure 5.5. The fiber sensor was placed near the center of the beam and the cable and fiber ends were glued on with the fast drying adhesive, Loctite and an accelerator. Epoxy

AE-10, which consists of a mixture of adhesive resin AE and curing agent 10, was mixed in a bottle for 5 minutes before being used to glue the rest of the bare fiber down. After a cure time of 5-6 hours, a final protective coat of nitrile rubber was placed on the fiber. The strain gauge (TML model no. FLA-6-11-5L), which had a measurement error of $\pm 1\%$, was then placed parallel to the fiber sensor and held in place using MBond 200 catalyst and adhesive. A coating was then used to protect the sensor.

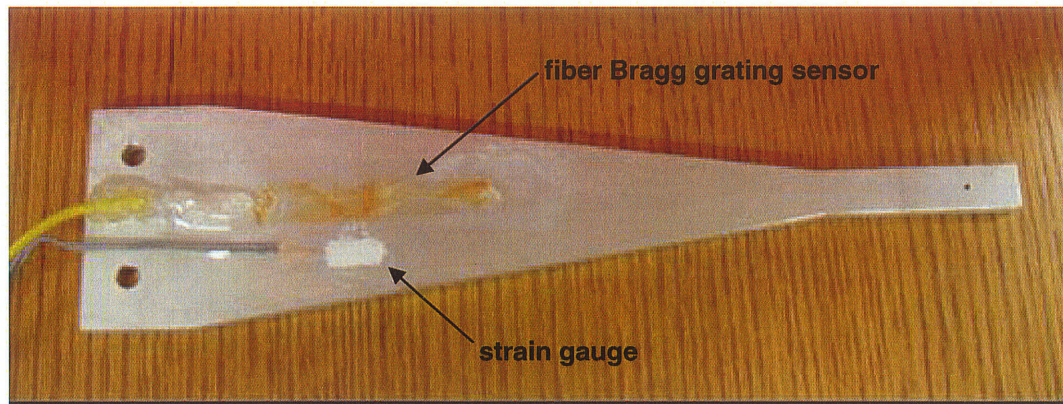


Figure 5.5 Beam with attached sensors.

5.3 Test Procedure

The test beam was then securely attached to the fixture. The strain gauge was hooked up to a data acquisition system while the fiber sensor was connected to the FBG interrogation unit. A screw at the end of the fixture was used to apply the point load to the beam, as shown in figure 5.6.

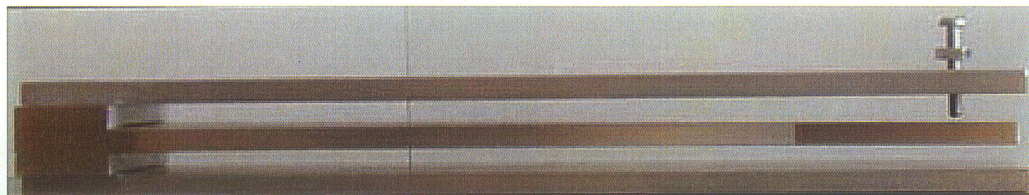
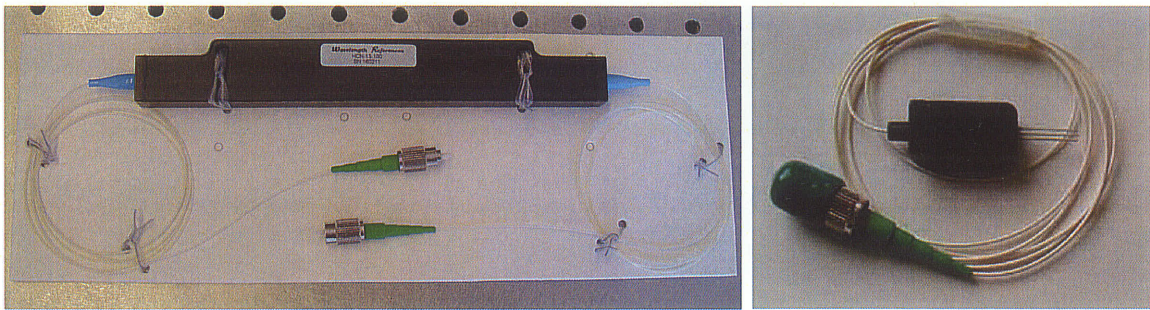


Figure 5.6 Cantilever test fixture.

The gas cell and etalon, which were also connected to the FBG unit, are shown in figures 5.7a and 5.7b. Both devices were obtained from Wavelength References Inc. The gas absorption cell was connected to two ports because it operates in transmission, while the etalon works in reflection.



a) b)
Figure 5.7 Wavelength references.
(a) HCN gas absorption cell (b) etalon

By turning the screw, the load at the end of the beam was increased. This caused an increase in strain in the strain gauge of $5\mu\epsilon$ increments up to a maximum of $200\mu\epsilon$. At each increment, a reading was taken from the FBG unit. After which, these files were later processed offline. The anticipated strain of approximately $700\mu\epsilon$ could not be achieved because of the constraints of the fixture design. In order to achieve a strain of that magnitude, the cantilever required a greater displacement range than the fixture could provide. Although it was possible to alter the design of the fixture, it was decided that it was not necessary to achieve a strain of $700\mu\epsilon$ to test the accuracy of the measurement system.

5.4 Results and Discussion

The test data from the first test of the strain gauge and the FBG unit with and without the etalon for interpolation are shown in figure 5.8.

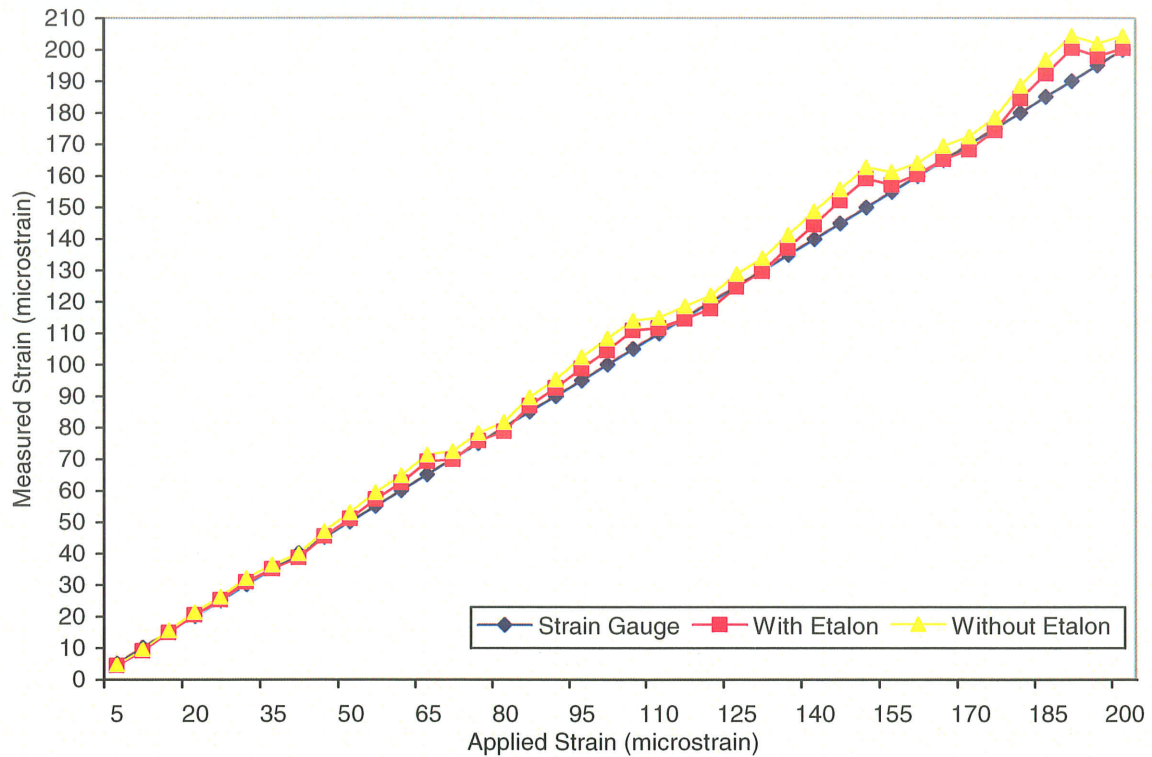


Figure 5.8 Comparison from the first test of strain readouts from the FBG unit to the strain gauge.

The results are relatively good except for some deviations of approximately $10\mu\epsilon$. Through further analysis, it was observed that the tip of the screw used to apply the load was not completely smooth which, in turn, created a large amount of friction between the screw and beam surface. Therefore, this was causing torque on the cantilever and as a result, more strain was applied on the Bragg sensor. To address this problem the screw was rounded smooth using extremely fine sandpaper. The test was then repeated and the results are shown in figure 5.9.

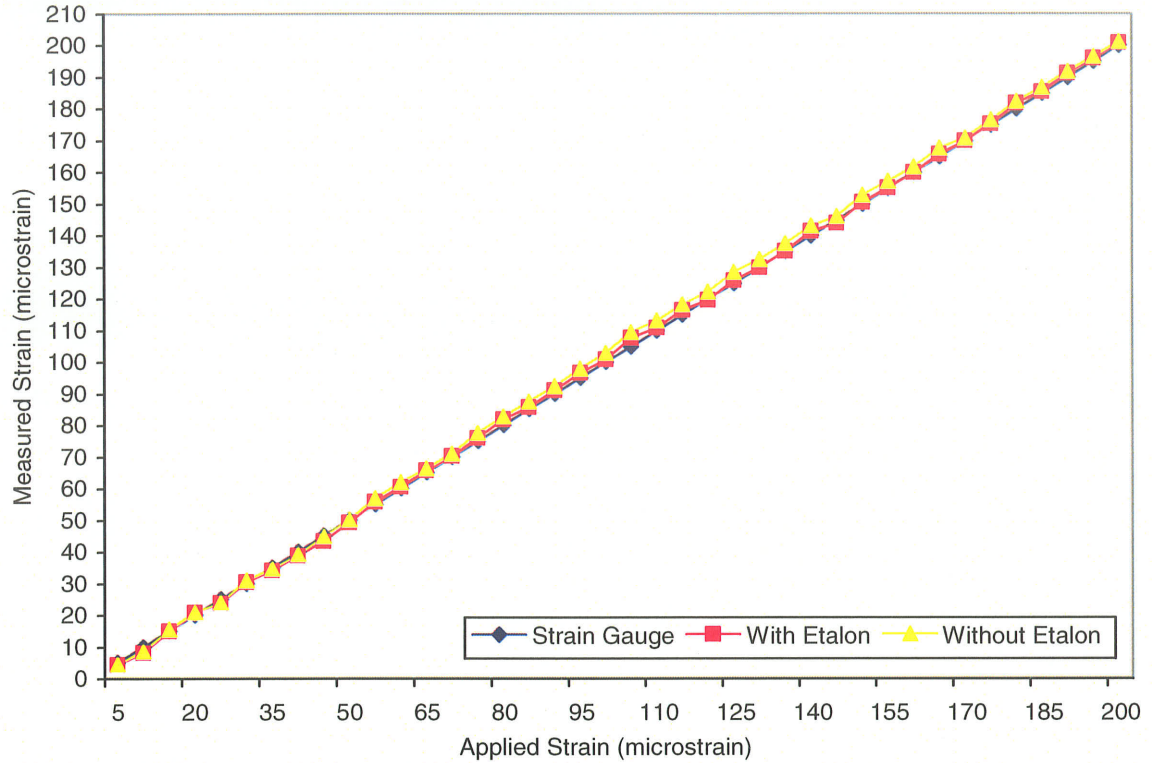


Figure 5.9 Comparison from the second test of strain readouts from the FBG unit to the strain gauge.

The results from the second test are excellent as the difference in readings from the strain gauge and the fiber optic sensor is negligible. The accuracy of the measurement technique was further investigated by regarding the deviations in strain with respect to the strain gauge from the signals obtained with and without the etalon, as shown in figure 5.10. The gauge factor used was 0.8, which corresponds to the $GF = 1 - \rho_e = 1 - 0.2017 = 0.7983$, as calculated in equations 2.7 and 2.9. Using interpolation with the etalon, the average deviation from the strain gauge was $0.264\mu\epsilon$ with a maximum error of $2.598\mu\epsilon$. Without the etalon, or in other words, using interpolation from the gas cell, the average deviation from the strain gauge was $1.478\mu\epsilon$ and the maximum error was $4.236\mu\epsilon$. This demonstrates that the addition of an etalon as a means of interpolation significantly improves the measurement accuracy by about $1.2\mu\epsilon$.

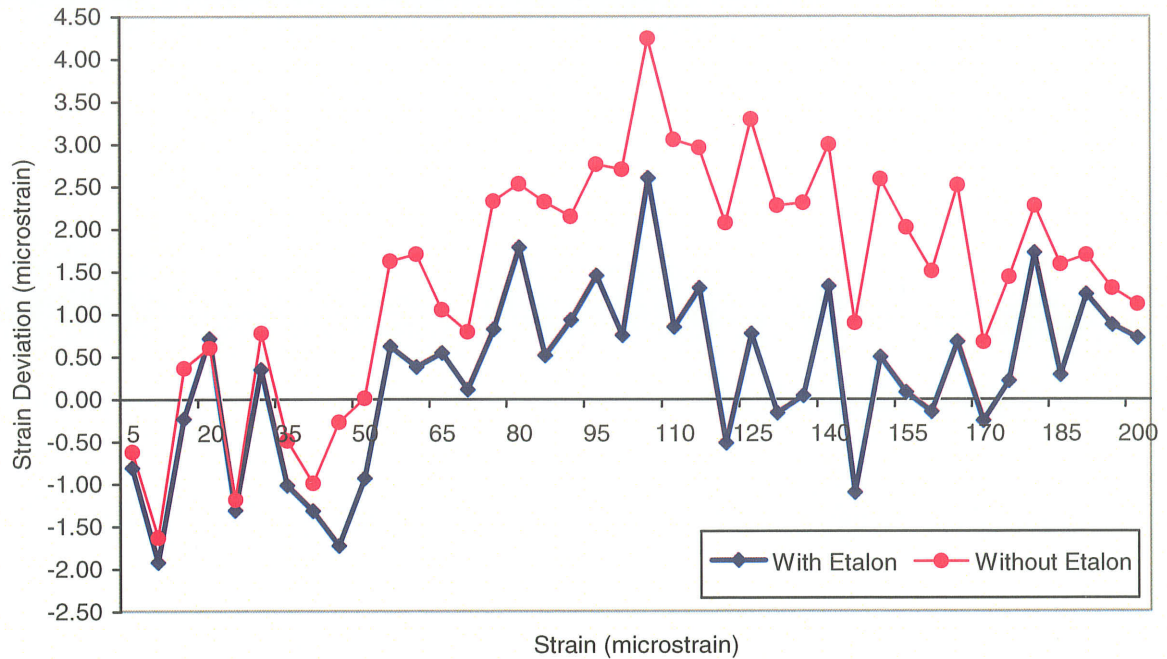


Figure 5.10 Comparison of strain deviations.
 With Etalon: RMS=0.9854 $\mu\epsilon$, Peak-to-Peak=4.5262 $\mu\epsilon$
 Without Etalon: RMS=1.3213 $\mu\epsilon$, Peak-to-Peak=5.8723 $\mu\epsilon$

The RMS error obtained with the etalon was 0.9854 $\mu\epsilon$ while using the gas cell alone resulted in a RMS error of 1.3213 $\mu\epsilon$.

5.4 Conclusion

In this chapter, the design of an experimental test setup and the theoretical modeling carried out using Adina were discussed. Two measurement methods were evaluated: finding the Bragg wavelength using interpolation with and without the etalon. Although both methods performed well in comparison to the strain gauge, it was demonstrated that the use of an etalon does improve the measurement accuracy of determining strain and as a result, is an effective addition as a complementary wavelength reference.

CHAPTER 6

CONCLUSION

6.1 Summary

This thesis has provided a comprehensive study on fiber optic sensors, specifically fiber Bragg gratings, and demonstrated the increased effectiveness of adding an etalon as a complementary wavelength reference. While the gas cell guarantees absolute strain measurements, the etalon further improves the measurement accuracy by providing an additional point of reference.

This thesis began with a comparative study of various peak location algorithms. Using Matlab, six peak location methods were evaluated based on the computation time and the amount of noise required in the signal before the algorithm failed to stay below an error of 5pm. This study concluded that the polynomial, Lorentzian and Gaussian fitting methods were the most stable. However, among those methods, the polynomial peak fitting algorithm had a significantly lower computation time. Therefore, it was decided that polynomial fitting would be used in determining the peak locations in the signals. Also, the method of sub-sampling was introduced and simulations determined that it did slightly improve the performance of the fitting algorithm.

The next step involved writing a program to determine the Bragg wavelength using the wavelength references. This program incorporated the polynomial peak fitting algorithm and the sub-sampling technique. Since the gas cell wavelengths were previously known values, the etalon peaks were found by interpolation and use of the

etalon transmission equations. After the etalon wavelengths were determined, the Bragg wavelength was calculated by interpolation from the etalon peaks. Using simply the gas cell alone, it was found that the measurement error in a one second scan was 0.4pm and 1.03pm in a 10 minute scan. However, the addition of the etalon reduced that error to 0.18pm over a one second scan and 0.98pm over a 10 minute period. These initial simulations helped prove that the addition of an etalon does improve the accuracy of measurements.

Finally, load testing was performed on a constant stress beam with a Bragg sensor and strain gauge to provide a comparison in the readings. After the strain gauge and Bragg sensor were attached to the cantilever, static load testing was performed on the fixture. The strain readouts from both the strain gauge and Bragg sensor were compared. In order to determine the strain on the Bragg sensor, two methods were implemented: the first using interpolation from the etalon and the second using interpolation from the gas cell alone. It was determined that both measurement methods performed favorably. However, the method using interpolation from the etalon was slightly more accurate by 1.2 $\mu\epsilon$ than using gas cell interpolation alone.

In conclusion, this thesis has met the goals set out to be achieved. It has demonstrated that an efficient and accurate peak location algorithm incorporated with a gas cell and etalon can significantly improve the accuracy of strain measurements from a Bragg sensor. Moreover, wavelength references provide numerous benefits, namely, providing an absolute standard by which the strain is determined and ensuring long term monitoring due to their stability. By improving the method in which a Bragg sensor is

interrogated, stable and accurate strain measurements are now possible for fiber sensors in structural health monitoring projects.

6.2 Recommendations for Future Research

The list below features some suggestions for future work in the area of fiber Bragg grating sensor systems.

- Develop a measurement technique to measure Bragg sensors which are multiplexed on a single fiber.
- A more detailed study on better techniques for peak location.

REFERENCES

- [1] Tennyson, R.C., Coroy, T., Duck, G., Manuelpillai, G., Mulvihill, P., Cooper, D., Smith, P.W.E., Mufti, A.A., and Jalali, S.J., (2000) "*Fiber optic sensors in civil engineering structures*," Can. J. Civ. Eng. 27:880-889.
- [2] McCarthy, D.C., (2000) "*Fiber Optic Sensor Greases the Wheels for Oil Production*," Photonics Spectra, October 2000.
www.photonics.com/spectra/applications/XQ/ASP/aoaid.180/QX/read.htm
- [3] Tennyson, R.C., (2002) "*Application of Fox-Tek Fiber Optic Sensors for Monitoring Pipelines*," Fox-Tek Application Note 3 September 2002. www.fox-tek.com
- [4] Seim, J., Udd, E., Schulz, W., and Laylor, H., (1999) "*Composite Strengthening and Instrumentation of the Horsetail Falls Bridge with Long Gauge Length Fiber Bragg Grating Strain Sensors*," SPIE proceedings, vol. 3746, p. 196.
- [5] ISIS Canada Design Manual (2001) "*Installation, Use and Repair of Fiber Optic Sensors*," ISIS Canada Design Manual No. 1, September 2001.
- [6] Inaudi, D., Vurpillot, S., Casanova N. and Kronenberg, P., (1998) "*Structural monitoring by curvature analysis using interferometric fiber optic sensors*," Smart Mater. Struct., 7, pp. 199-204.
- [7] Bronnimann, R., Nellen, Ph.M., and Sennhauser, U., (1998) "*Application and reliability of a fiber optical surveillance system for a stay cable bridge*," Smart Mater. Struct. Vol. 7, No. 2, April 1998.
- [8] Ando Optical Spectrum Analyzer Model AQ6319, www.ando.co.jp/English
- [9] Anritsu Optical Spectrum Analyzer Model MS9710C, www.us.anritsu.com
- [10] Agilent Optical Spectrum Analyzer Model 8614xB, www.agilent.com
- [11] Exfo, *Multi-Wavelength Meter Model No. IQS-5320*, www.exfo.com
- [12] Takaaki, H., Mamoru, H., and Nagayama, H., (2001) "*Wavelength-Stable Laser Diode and Photodiode Array for Laser Interferometer Positioning Systems*," Yokogawa Technical Report English Edition, No. 32, 2001.
www.yokogawa.com/TR/pdf/English/No32/P01_04.pdf
- [13] Measures, R.M., Alavie, A.T., Maaskant, R., Ohn, M., Karr, S., and Huang, S., (1995) "*A structurally integrated Bragg grating laser sensing system for a carbon fiber prestressed concrete highway bridge*," Smart Mater. Struct. Vol. 4, No. 1, pp.20-30, March 1995.

[14] Yu, Shizhuo, and Yu, Francis T.S., (2002) "*Fiber Optic Sensors*," New York; Marcel Dekker, 2002.

[15] Uiga, E., (1995) "*Optoelectronics*," Prentice Hall, 21 February, 1995.

[16] Hill, K.O., Fujii, Y., Johnson, D.C., and Kawasak, B.S., (1978) "*Photosensitivity in optical fiber waveguides: application to reflection filter fabrication*," Appl. Phys. Lett. Vol. 7, pp. 647-649, (1978).

[17] Moses, A.J., (1971) "*Optical Materials Properties*," Handbook of Electronic Materials, Volume 1, pp. 68-69, (1971).

[18] Duan, G., Lyori, V., Myllyla, R., Suopajarvi, P., and Karioja, P., (2001) "*Bragg Grating Fiber Applied in Strain Measurement*," The Second Annual Symposium on Computer Science and Electrical Engineering; Lulea, Sweden, 2001.

[19] Chan, C.C., Jin, W., Ho, H.L., Wang, D.N., and Wang, Y., (2001) "*Improvement of measurement accuracy of fibre Bragg grating sensor systems by use of gas absorption lines as multi-wavelength references*," IEEE Electronics Letters, Vol. 37, No. 12, 7th June 2001.

[20] Gilbert, S.L., Swann, W.C., and Wang, C-M., "*Standard Reference Materials - Hydrogen Cyanide $H^{13}C^{14}N$ Absorption Reference for 1530 to 1640 nm Wavelength Calibration - SRM2519*," NIST Special Publication 260-137 (1998).

[21] Fan, N.Y., (1997) "*Development of Fibre Optic Sensing Techniques for Structural Assessment*," Ph.D. Thesis, University of Toronto, 1997.

[22] Kalamkarov, A.L., Georgiades, A.V., Saha, G.C., and Challagulla, K.S., (2002) "*Smart FRP Reinforcements with Embedded Fiber Optic Sensors*," Proceedings of the First International Workshop on Structural Health Monitoring of Innovative Civil Engineering Structures; Winnipeg, Canada, September 2002.

[23] Bronnimann R., Nellen, Ph.M., and Sennhauser, U., (1999) "*Reliability monitoring of CFRP structural elements in bridges with fiber optic Bragg grating sensors*," J. Intelligent Material Systems and Structures, 10(4), pp. 322-329, 1999.

[24] Arie, A., Lissak, B., and Tur, M., (1999) "*Static Fiber-Bragg Grating Strain Sensing Using Frequency-Locked Lasers*," Journal of Lightwave Technology, Vol. 17, No. 10, October 1999.

[25] Advanced Optics Solutions, www.aos-fiber.com

[26] Insensys, www.insensys.com

- [27] Udd, E., Kunzler, M., Laylor, H.M., Schulz, W., Kreger, S., Corones, J., McMahon, R., Soltesz, S., and Edgar, R., (2001) "*Fiber Grating Systems for Traffic Monitoring*," Proceedings of SPIE, Vol. 4337, p. 510, 2001.
- [28] Structural Health Monitoring (SHM) Systems, www.shmsystems.com
- [29] Micron Optics, www.micronoptics.com
- [30] Systems Planning and Analysis (SPA), www.spa.com/smtproducts.htm
- [31] Fiberpro, www.fiberpro.com
- [32] Intelligent Fiber Optic Systems (IFOS), www.ifos.com
- [33] Rose, A.H., Wang, C.-M., and Dyer, S.D., (2000) "*Round Robin for Optical Fiber Bragg Grating Metrology*," J. Res. Natl. Inst. Stand. Technol. Vol. 105, No. 6, pp. 839-866, 2000.
- [34] Rao, Y.J., (1997) "*In-fibre Bragg grating sensors*," Meas. Sci. Technol., Vol. 8, pp. 355-375, 1997.
- [35] Kim, S., Kim, S., Kwon, J., and Byoungho, L., (2001) "*Fiber Bragg Grating Strain Sensor Demodulator Using a Chirped Fiber Grating*," IEEE Photonics Technology Letters, Vol. 13, No. 8, August 2001.
- [36] Boulet, C., Webb, D.J., Douay, M., and Niay, P., (2001) "*Simultaneous Interrogation of Fiber Bragg Grating Sensors Using an Acoustooptic Tunable Filter*," IEEE Photonics Technology Letters, Vol. 13, No. 11, November 2001.
- [37] Lee, Yeong-Kyoon, Song, In-Cheon, Jeong, Sung-Ho, Lee, Byung-Ha, and Lee, Sun-Kyu, (2001) "*Absolute Strain Measurement For Fiber Bragg Grating Sensor Using A String Resonator With High Accuracy*," Proceedings of the 2001 ASPE Conference, Washington, D.C., pp. 180-183, Nov. 12-15, 2001.
- [38] Darling, G., University of Toronto, 2001.
- [39] Wavelength References Operators Manual for DWDM Wavelength Reference Hydrogen Cyanide Absorption Cell (with 100 Torr carbon 13 cell: HCN-13-C-100) and Etalon with Temperature Sensor (OA-140-R-T)
- [40] Kingsbury, D., (2003) "*Constant Stress Beams*," Integrated Mechanical Testing Laboratory, Fulton School of Engineering, Arizona State University, October 2003.

APPENDIX A

MATLAB PROGRAMS

%This program is the main program used in the Labview interface and determines the Bragg wavelength using the gas cell and etalon wavelength references

```
function process_data_v8(binfile, parameter_array, duration, chan_array, laser_source, raw_plot, peak_wavelength)
```

```
%parameter_array = [0 0 0 1; 1536 1536 1536 1536; 0.5 0.5 0.5 0.5; 6.5e-6 6.5e-6 6.5e-6  
%6.5e-6; 0.80 0.80 0.80 0.80; 23.5 23.5 23.5 23.5; 23.5 23.5 23.5 23.5; 1536.214  
%1536.214 1536.214 1536.214; 0.1e-8 0.1e-8 0.1e-8 0.1e-8; 0.55e-6 0.55e-6 0.55e-6  
%0.55e-6];  
%binfile='C:\Documents and Settings\All Users\Documents\Data 06-10-2003\06-10-  
%2003_08-30-22PM 3.bin';  
%duration=0.5;  
%chan_array=[1 1 0 1];  
%laser_source=1;  
%raw_plot=0;  
%peak_wavelength=1536.430;
```

```
dynamic=0; %scan over 1 second file
```

```
%some variable initialization
```

```
clear REF;  
clear fbg1;  
clear fbg2;  
clear fbg3;  
clear gascell_peak;  
clear bragg_peak;  
clear etalon_peak;
```

```
%Global Variables
```

```
global strain; %strain value for bragg grating  
global braggwavelength; %calculated bragg peak wavelength  
global output_G;  
global strain_gc;  
global braggwavelength1;  
%global gascell_peak; %gascell peaks  
%global bragg_peak; %bragg peaks  
%global etalon_peak; %etalon peaks  
%global fbg1; %channel 1  
%global fbg2; %channel 2  
%global fbg3; %channel 3  
%global REF; %reference signal
```

```
channels = NNZ(chan_array); %finds active channels
```

```
chans_G = channels + 1; %total number of active channels plus the reference signal
```



```

samples = duration*chans_G*258000;
fid = fopen(binfile,'r'); %Here the binary file is opened with read only access
[rawdata,count]=fread(fid,samples,'int16'); % this reads successive 16 bit integers
fclose(fid); % this closes file after reading data
%REF_offset = offset_fixer(rawdata,chans_G);
REF_offset=0;

if dynamic==0
    datalength=6000; %sets data to contain one cycle of a wavelength sweep
else
    if chans_G==3
        datalength=length(rawdata)/3; %entire length of data
    else
        datalength=length(rawdata)/4;
    end;
end;

X = [1:1:datalength];

%%%%%%%%%%%%%%%%%%%%%%%%%%%%%%%%%%%%%%%%%%%%%%%%%%%%%%%%%%%%%%%%%%%%%%%%
%%%%%%%%%%%%%%%%%%%%%%%%%%%%%%%%%%%%%%%%%%%%%%%%%%%%%%%%%%%%%%%%%%%%%%%%

[fbg1,fbg2,fbg3,REF]=channel_assign(rawdata,REF_offset,datalength,chans_G,raw_plot,
X);

%%%%%%%%%%%%%%%%%%%%%%%%%%%%%%%%%%%%%%%%%%%%%%%%%%%%%%%%%%%%%%%%%%%%%%%%
%%%%%%%%%%%%%%%%%%%%%%%%%%%%%%%%%%%%%%%%%%%%%%%%%%%%%%%%%%%%%%%%%%%%%%%%

%sub-sampling of data
signal=X;
wi=1:0.0625:length(X);
ri=interp1(X,REF,wi,'spline');
gi=interp1(X,fbg2,wi,'spline');
bi=interp1(X,fbg1,wi,'spline');
if chans_G==4
    ei=interp1(X,fbg3,wi,'spline');
end;

REF=ri;
fbg2=gi;
fbg1=bi;
if chans_G==4
    fbg3=ei;

```

```
end;  
wavelength=wi;
```

```
if chans_G==3  
etalon=fbg3;  
end;
```

```
[minvr minr]=min(REF);  
[minvg ming]=min(fbg2);  
[minvb minb]=min(fbg1);  
if chans_G==4  
[minve mine]=min(fbg3);  
end;
```

```
ref=REF-minvr;    %remove offset  
gascell=fbg2-minvg;  
bragg=fbg1-minvb;  
if chans_G==4  
etalon=fbg3-minve;  
end;  
ref_norm=ref/max(ref);    %normalizing  
gascell_norm=gascell/max(gascell);  
bragg_norm=bragg/max(bragg);  
if chans_G==4  
etalon_norm=etalon/max(etalon);  
end;
```

```
ref=ref_norm;  
gascell=gascell_norm;  
bragg=bragg_norm;  
if chans_G==4  
etalon=etalon_norm;  
end;
```

```
%figure  
%plot(X,gascell,X,bragg,'r');
```

```
%%%%%%%%%%%%%%%%%%%%%%%%%%%%%%%%%%%%%%%%%%%%%%%%%%%%%%%%  
%%%%%%%%%%%%%%%%%%%%%%%%%%%%%%%%%%%%%%%%%%%%%%%%%%%%%%%%
```

```
[maxref maxr]=max(ref);  
min=0.2*maxref;  
start=0;
```

```

if dynamic==0
    minpoint=start_end_points(min,start,ref,dynamic); %finding start and end points of
one cycle
    start_position=minpoint(1);
    end_position=minpoint(2);
    minx=start_position;
    numsignal=channels;
    if chans_G==4

[gascell_peak,bragg_peak,etalon_peak]=peak_finder_interp8(gascell,bragg,etalon,wavele
ngth,start_position,end_position,numsignal);

[braggwavelength1,braggwavelength2,braggwithetalon1]=wavelength_calc_interp8(gasc
ell_peak,bragg_peak,etalon_peak,wavelength);
    %braggwavelength=braggwavelength1;
    braggwavelength=braggwithetalon1;
    else

[gascell_peak,bragg_peak,etalon_peak]=peak_finder_interp(gascell,bragg,etalon,wavelen
gth,start_position,end_position,numsignal);

[braggwavelength1,braggwavelength2]=wavelength_calc_interp(gascell_peak,bragg_pea
k,wavelength);
    braggwavelength=braggwavelength1;
    end;
    strain_et=strain_calc(parameter_array,peak_wavelength,braggwavelength);
    strain_gc=strain_calc(parameter_array,peak_wavelength,braggwavelength1);
    else
    minpoint=start_end_points(min,start,ref,dynamic);
    numsignal=channels;
    format long;
    for i=1:length(minpoint)-1
        start_position=minpoint(i);
        end_position=minpoint(i+1);
        if chans_G==4

[gascell_peak,bragg_peak,etalon_peak]=peak_finder_interp8(gascell,bragg,etalon,wavele
ngth,start_position,end_position,numsignal);

[braggwavelength1,braggwavelength2,braggwithetalon1]=wavelength_calc_interp8(gasc
ell_peak,bragg_peak,etalon_peak,wavelength);
        %bragg_wavelength1(i)=braggwavelength1;
        %bragg_wavelength2(i)=braggwavelength2;
        %braggwavelength=braggwavelength1;
        bragg_wavelength1(i)=braggwithetalon1;
        %bragg_wavelength2(i)=braggwithetalon2;

```

```

        braggwavelength=braggwithetalon1;
        braggwithgc1(i)=braggwavelength1;
        braggwithgc2(i)=braggwavelength2;
    else

[gascell_peak,bragg_peak,etalon_peak]=peak_finder_interp(gascell,bragg,etalon,wavelength,start_position,end_position,numsignal);

[braggwavelength1,braggwavelength2]=wavelength_calc_interp(gascell_peak,bragg_peak,wavelength);
        bragg_wavelength1(i)=braggwavelength1;
        bragg_wavelength2(i)=braggwavelength2;
        braggwavelength=braggwavelength1;
    end;
    strain_et=strain_calc(parameter_array,peak_wavelength,braggwavelength);
    strain_gc=strain_calc(parameter_array,peak_wavelength,braggwavelength1);
    bragg_strain(i)=strain_et;
    bragg_gc_strain(i)=strain_gc;
end;
end;

if dynamic==1
data(1:length(bragg_wavelength1),1)=bragg_wavelength1';
%data(1:length(bragg_wavelength2),2)=bragg_wavelength2';
data(1:length(bragg_strain),3)=bragg_strain';
data(1:length(braggwithgc1),4)=braggwithgc1';
data(1:length(braggwithgc2),5)=braggwithgc2';
data(1:length(bragg_gc_strain),6)=bragg_gc_strain';

%dlmwrite('temp.out',data);

save temp.out data -ASCII -double -tabs
end;

braggwavelength
strain_et
braggwavelength1
strain_gc

```

%This function assigns the correct data to each channel from the raw data

```
function  
[fbg1,fbg2,fbg3,REF]=channel_assign(rawdata,REF_offset,datalength,chans_G,raw_plot,  
X)
```

```
%global fbg1;  
%global fbg2;  
%global fbg3;  
%global REF;
```

```
if chans_G == 4  
for i = 4:chans_G:4*datalength  
    fbg1(i/4) = abs(rawdata(i-3));  
    fbg2(i/4) = abs(rawdata(i-2));  
    fbg3(i/4) = abs(rawdata(i-1));  
    REF(i/4) = rawdata(i) - REF_offset;  
end  
if raw_plot==1  
figure(1)  
plot(X,fbg1,X,fbg2,X,fbg3,X,REF,'.');  
title('Reflected signals from FBG sensors and laser REF sampled at 250 kS/s each');  
legend('FBG','Gas Cell','Etalon','Laser REF');  
end  
end
```

```
if chans_G == 3  
for i = 3:chans_G:3*datalength  
    fbg1(i/3) = abs(rawdata(i-2));  
    fbg2(i/3) = abs(rawdata(i-1));  
    REF(i/3) = rawdata(i) - REF_offset;  
end  
if raw_plot==1  
figure(1)  
plot(X,fbg1,'-',X,fbg2,'-',X,REF,'.');  
title('Reflected signals from FBG sensors and laser REF sampled at 250 kS/s each');  
legend('FBG','Gas Cell','Laser REF');  
end  
fbg3=0;  
end
```

```
if chans_G == 2  
for i = 2:chans_G:2*datalength  
    fbg1(i/2) = abs(rawdata(i-1));  
    REF(i/2) = rawdata(i) - REF_offset;
```

```
end
if raw_plot==1
figure(1)
plot(X,fbg1,X,REF,':');
title('Normalized FBG signal sampled at 250 kS/s each');
legend('FBG','Laser REF');
end
end
```

%This function finds the start and end points of one modulation cycle

function minpoint=start_end_points(min,start,ref,dynamic)

[maxref maxr]=max(ref);

min=0.01*maxref;

count=1;

minimum_found = 0;

%this will turn off loop once minimum is found

flag1=0;

flag2=0;

if dynamic==0

cycles=2;

for w=1:cycles

while minimum_found == 0

while flag1 == 0

if ref(count) < min;

position1 = count;

flag1 =1;

end

count=count+1;

end;

count=count+30;

while flag2==0

if ref(count)>min

position2=count;

flag2=1;

end;

count=count+1;

end;

array=ref(position1:position2);

[value,minpos]=min(array);

minimum_found=1;

end

xarray=position1:position2;

minpoint(w)=xarray(minpos);

count=count+60;

minimum_found=0;

flag1=0;

flag2=0;

end;

else

allminfound=0;

w=1;

```

while allminfound==0
    while minimum_found == 0
        while flag1 == 0
            if count>=length(ref),break,end
            if ref(count) < min
                position1 = count;
                flag1 =1;
            end
            count=count+1;
        end;
        count=count+20;
        while flag2==0
            if count>=length(ref),break,end
            if ref(count)>min
                position2=count;
                flag2=1;
            end;
            count=count+1;
        end;
        if count>=length(ref),break,end
        array=ref(position1:position2);
        [value,minpos]=min(array);
        minimum_found=1;

    end

    if (allminfound==0)&(count<length(ref))
        xarray=position1:position2;
        minpoint(w)=xarray(minpos);
        end;
        count=count+20;
        flag1=0;
        flag2=0;
        w=w+1;
        if count>=length(ref)
            minimum_found=1;
        else
            minimum_found=0;
        end;
        if count>=length(ref)
            allminfound=1;
        end;
        if allminfound==1,break,end
    end;
end;

```



```
end;
```

```
t=length(minpoint);
```

```
if minpoint(t)==minpoint(t-1)
```

```
    minpoint=minpoint(1:t-1);
```

```
end;
```

**%This function determines the locations of the peaks for the bragg grating,
%gas cell, and etalon using the polynomial fit algorithm**

```
function  
[gascell_peak,bragg_peak,etalon_peak]=peak_finder_interp8(gascell,bragg,etalon,wavele  
ngth,start_position,end_position,numsignal)
```

```
n=numsignal;  
for phase=1:n  
    if phase==1  
        signal=gascell;  
        threshold=0.05;  
        limit=8;  
    elseif phase==2  
        signal=bragg;  
        limit=2;  
        maxbragg=bragg(start_position);  
        for i=start_position:end_position  
            if bragg(i)>maxbragg  
                maxbragg=bragg(i);  
            end;  
        end;  
        threshold=0.75;  
    elseif phase==3  
        signal=etalon;  
        limit=33;  
        threshold=0.12;  
    end;  
    start=start_position+1920;  
    flag_1=0;  
    num_peaks=0;  
    flag_2=0;  
    peaknum=1;  
    if phase==2  
        start=start_position+3520;  
    end;  
    if phase==3  
        start=start_position+100;  
    end;  
  
    while num_peaks == 0  
        count=start;  
        flag_1=0;  
        while flag_1 == 0           %finding threshold crossing points  
            if phase==1
```

```

        if (signal(count)<threshold)&(signal(count+5)<threshold)
            point1=count;
            flag_1=1;
        end;
    else
        if signal(count) > threshold;
            point1 = count;
            flag_1 = 1;
        end;
    end;
    count=count+5;
end;
count=count+5;
flag_2=0;
while flag_2==0
    if phase==1
        if (signal(count)>threshold)&(signal(count+5)>threshold)
            point2=count;
            flag_2=1;
        end;
    else
        if signal(count)<threshold
            point2=count;
            flag_2=1;
        end;
    end;
    count=count+5;
end;

x=wavelength(point1:point2);
y=signal(point1:point2);
p=polyfit(x,y,2);      %polynomial fit algorithm
f=polyval(p,x);
if phase==1
    [minpol,z]=min(f);
else
    [maxpol,z]=max(f);
end;

if phase==1
    gascell_peak(peaknum)=x(z);    %gas cell wavelength peaks
elseif phase==2
    bragg_peak(peaknum)=x(z);      %bragg wavelength peaks
elseif phase==3
    etalon_peak(peaknum)=x(z);     %etalon wavelength peaks
end;

```

```

peaknum=peaknum+1;
start=point2+60;
if phase==1           %moving threshold closer to the next peak
    if length(gascell_peak)<limit
        num_peaks=0;
        if length(gascell_peak)<2
            threshold=0.35;
            start=start+3550;
        elseif (length(gascell_peak)>=2)&(length(gascell_peak)<5)
            threshold=0.6;
            start=start+700;
        elseif (length(gascell_peak)>=5)&(length(gascell_peak)<6)
            start=start+3900;
            threshold=0.6;
        elseif (length(gascell_peak)>=6)&(length(gascell_peak)<7)
            start=start+4375;
            threshold=0.35;
        else
            start=start+300;
            threshold=0.05;
        end;
    else
        num_peaks=1;
    end;
elseif phase==2
    if length(bragg_peak)<limit
        num_peaks=0;
    else
        num_peaks=1;
    end;
elseif phase==3
    if length(etalon_peak)<limit
        num_peaks=0;
        if length(etalon_peak)<=6
            threshold=threshold+0.06;
        elseif (length(etalon_peak)>=7)&(length(etalon_peak)<=15)
            threshold=0.7;
        elseif length(etalon_peak)==16
            threshold=0.9;
        elseif (length(etalon_peak)>=17)&(length(etalon_peak)<=24)
            threshold=0.7;
        elseif (length(etalon_peak)>=25)&(length(etalon_peak)<=26)
            start=start+1000;
            threshold=0.55;
        elseif (length(etalon_peak)>=27)&(length(etalon_peak)<=29)
            start=start+900;

```

```
        threshold=threshold-0.1;
    else
        start=start+670;
        threshold=0.12;
    end;
else
    num_peaks=1;
end;
end;
end;
end;
```

**%This function finds the corresponding wavelengths to the gas cell and
%etalon peaks and determines the bragg wavelength using interpolation**

function

[braggwavelength1,braggwavelength2,braggwithetalon1]=wavelength_calc_interp8(gascell_peak,bragg_peak,etalon_peak,wavelength)

gcpeak1=1536.1170; %known value of gas cell minima

gcpeak2=1536.7034;

gcpeak3=1537.2997;

gcpeak4=1537.9069;

gcpeaks=[gcpeak1;gcpeak2;gcpeak3;gcpeak4];

peaks=gascell_peak;

for n=1:8

z=peaks(n)/0.0625;

p1=z-40;

p2=z+40;

for r=p1:p2

if wavelength(r)==peaks(n)

data_peaks(n)=r;

end;

end;

end;

for n=1:2

z=bragg_peak(n)/0.0625;

p1=z-40;

p2=z+40;

for r=p1:p2

if wavelength(r)==bragg_peak(n)

b_peaks(n)=r;

end;

end;

end;

for n=1:33

z=etalon_peak(n)/0.0625;

p1=z-40;

p2=z+40;

for r=p1:p2

if wavelength(r)==etalon_peak(n)

eta_peaks(n)=r;

```
end;  
end;  
end;
```

```
waveperdiv1=(gcpeak2-gcpeak1)/(data_peaks(2)-data_peaks(1));  
waveperdiv2=(gcpeak3-gcpeak2)/(data_peaks(3)-data_peaks(2));  
waveperdiv3=(gcpeak4-gcpeak3)/(data_peaks(4)-data_peaks(3));  
waveperdiv4=(gcpeak2-gcpeak1)/(data_peaks(8)-data_peaks(7));  
waveperdiv5=(gcpeak3-gcpeak2)/(data_peaks(7)-data_peaks(6));  
waveperdiv6=(gcpeak4-gcpeak3)/(data_peaks(6)-data_peaks(5));  
waveperdiv=[waveperdiv1;waveperdiv2;waveperdiv3;waveperdiv4;waveperdiv5;waveperdiv6];
```

```
gascell_peaks=peaks;
```

```
%%%%%%%%%%%%%%%%%%%%%%%%%%%%%%%%%%%%%%%%%%%%%%%%%%%%%%%%%%%%  
%%%%%%%%%%%%%%%%%%%%%%%%%%%%%%%%%%%%%%%%%%%%%%%%%%%%%%%%%%%%
```

```
%Etalon Simulation  
%Assuming n varies with temperature  
%Applying Schott Formula  
format long;
```

```
%Nominal Temperature  
t0=20; %degrees celsius  
temp=20;  
deltatemp=temp-t0;
```

```
%Schott constants  
d0=-4.93e-6;  
d1=7.94e-9;  
d2=-6.32e-11;  
e0=9.79e-7;  
e1=14.7e-10;  
lamdatk=0.296e-6;
```

```
%Assuming n varies with wavelength  
%Applying Sellmeier dispersion formula
```

```
%Sellmeier Coefficients  
b1=1.78922056;  
b2=3.28427448e-1;  
b3=2.01639441;  
c1=1.35163537e-2;  
c2=6.22729599e-2;
```

```
c3=1.68014713e2;
```

```
%Wavelength Range
```

```
min=1536.1e-9;
```

```
max=1537.9e-9;
```

```
lamda=min:1e-12:max;
```

```
%Find n using Sellmeier Formula
```

```
term1=(b1*(lamda.*1e6).^2)/((lamda.*1e6).^2-c1);
```

```
term2=(b2*(lamda.*1e6).^2)/((lamda.*1e6).^2-c2);
```

```
term3=(b3*(lamda.*1e6).^2)/((lamda.*1e6).^2-c3);
```

```
n=sqrt(term1+term2+term3+1);
```

```
%find dn/dT using Schott formula
```

```
termone=(n.^2-1)/(2*n);
```

```
termtwo=(d0*deltatemp)+(d1*deltatemp.^2)+(d2*deltatemp.^3);
```

```
termthree=((e0*deltatemp)+(e1*deltatemp.^2))/((lamda*1e9).^2-(lamdatk*1e9)^2);
```

```
dn=termone.*(termtwo+termthree);
```

```
nrev=n+dn;
```

```
n=nrev;
```

```
%Finding l using raw data
```

```
peak1=gcpeak1+(eta_peaks(3)-data_peaks(1))*waveperdiv1;
```

```
peak2=gcpeak1+(eta_peaks(4)-data_peaks(1))*waveperdiv1;
```

```
m_est=peak1/(peak2-peak1);
```

```
m=round(m_est);
```

```
nl=m*peak2/2;
```

```
lam=peak2*1e-3;
```

```
term1=(b1*(lam).^2)/((lam).^2-c1);
```

```
term2=(b2*(lam).^2)/((lam).^2-c2);
```

```
term3=(b3*(lam).^2)/((lam).^2-c3);
```

```
n_est=sqrt(term1+term2+term3+1);
```

```
l=nl/n_est*1e-9;
```

```
%Solving for Etalon Transmission
```

```
%l=0.00493777618254; %l=nl/n @ 1550.0nm l=8.704025e-3/1.76274190612355
```

```
delta=(4*pi*n*l)/lamda;
```

```
r=((n-1).^2)/((n+1).^2);
```

```
t=((1-r).^2)/((1-r).^2+4*r.*(0.5-0.5*cos(delta)));
```

```
%sig=1-t;
```

```
%t=sig;
```

```
t=t-0.7367;
```



```

%figure
%plot(lamda*1e9,10*log10(1-t),'r');
%title('Simulated Etalon Spectrum using Sellmeier Dispersion Formula');
%xlabel('Wavelength (nm)');
%ylabel('Intensity (dB)');
%grid on;
%figure
%plot(lamda*1e9,(t),'r');
%axis([min*1e9 max*1e9 0 0.27]);
%grid
%title('Simulated Etalon Spectrum using Sellmeier Dispersion Formula');
%xlabel('Wavelength (nm)');
%ylabel('Intensity');
%grid on;
flag_1=0;
num_peaks=0;
flag_2=0;
peaknum=1;
start=50;
%threshold=0.95;
threshold=0.262;
limit=13;
while num_peaks == 0
    count=start;
    flag_1=0;
    while flag_1 == 0
        if t(count) > threshold;
            point1 = count;
            flag_1 =1;
        end
        count=count+1;
    end;
    count=count+5;
    flag_2=0;
    while flag_2==0
        if t(count)<threshold
            point2=count;
            flag_2=1;
        end;
        count=count+1;
    end;

    x=lamda(point1:point2);
    y=t(point1:point2);
    p=polyfit(x,y,2);

```

```

f=polyval(p,x);
[maxpol,z]=max(f);
eta_sim(peaknum)=x(z);
peaknum=peaknum+1;
start=point2+20;
if length(eta_sim)<limit
    num_peaks=0;
else
    num_peaks=1;
end;
end;
eta_sim=eta_sim*1e9;    %etalon peaks from simulation equation

%%%%%%%%%%%%%%%%%%%%%%%%%%%%%%%%%%%%%%%%%%%%%%%%%%%%%%%%%%%%%%%%%%%%%%%%%%%%%%
%%%%%%%%%%%%%%%%%%%%%%%%%%%%%%%%%%%%%%%%%%%%%%%%%%%%%%%%%%%%%%%%%%%%%%%%%%%%%%
%Determining which etalon peaks are located between each set of gas cell peaks
bgloop=1;
for count=1:length(eta_peaks)
    if (eta_peaks(count)>data_peaks(bgloop))&(eta_peaks(count)<data_peaks(bgloop+1))
        index(count)=count;
    end;
end;
k = find(index);
f=k(1);
mainindx(bgloop)=f;
clear index;
bgloop=2;
for count=1:length(eta_peaks)
    if (eta_peaks(count)>data_peaks(bgloop))&(eta_peaks(count)<data_peaks(bgloop+1))
        index(count)=count;
    end;
end;
k = find(index);
f=k(1);
mainindx(bgloop)=f;
clear index;
bgloop=3;
for count=1:length(eta_peaks)
    if (eta_peaks(count)>data_peaks(bgloop))&(eta_peaks(count)<data_peaks(bgloop+1))
        index(count)=count;
    end;
end;
k = find(index);
f=k(1);
mainindx(bgloop)=f;

```

```

clear index;
bgloop=4;
for count=1:length(eta_peaks)
    if (eta_peaks(count)>data_peaks(bgloop))&(eta_peaks(count)<data_peaks(bgloop+1))
        index(count)=count;
    end;
end;
k = find(index);
f=k(1);
mainindx(bgloop)=f;
clear index;

```

```

%ndx=1;
%for jx=1:length(mainindx)-1
%    n=mainindx(jx);
%    m=mainindx(jx+1)-1;
%    for b=n:m
%        epeak(b)=gcpeaks(ndx)+(eta_peaks(b)-data_peaks(ndx))*waveperdiv(ndx);
%    end;
%    ndx=ndx+1;
%end;

```

```

sim_etalonpeak=eta_sim;
meas_etalonpeak=eta_peaks(mainindx(1):mainindx(4)-1);

```

%determining the Bragg wavelength using interpolation from the etalon

```

for dx=1:length(meas_etalonpeak)
    if (b_peaks(1)>=meas_etalonpeak(dx))&(b_peaks(1)<meas_etalonpeak(dx+1))
        braggwithetalon1=sim_etalonpeak(dx)+(b_peaks(1)-
meas_etalonpeak(dx))*(sim_etalonpeak(dx+1)-
sim_etalonpeak(dx))/(meas_etalonpeak(dx+1)-meas_etalonpeak(dx));
    end;
end;

```

%determining the Bragg wavelength using interpolation from the gas cell

```

if (bragg_peak(1)>=gascell_peak(1))&(bragg_peak(1)<gascell_peak(2))
    braggwavelength1=gcpeak1+(b_peaks(1)-data_peaks(1))*waveperdiv1;
elseif (bragg_peak(1)>=gascell_peak(2))&(bragg_peak(1)<gascell_peak(3))
    braggwavelength1=gcpeak2+(b_peaks(1)-data_peaks(2))*waveperdiv2;
elseif (bragg_peak(1)>=gascell_peak(3))&(bragg_peak(1)<gascell_peak(4))
    braggwavelength1=gcpeak3+(b_peaks(1)-data_peaks(3))*waveperdiv3;
end;;

```

```
if (bragg_peak(2)>=gascell_peak(7))&(bragg_peak(2)<gascell_peak(8))
    braggwavelength2=gcpeak1+(data_peaks(8)-b_peaks(2))*waveperdiv4;
elseif (bragg_peak(2)>=gascell_peak(6))&(bragg_peak(2)<gascell_peak(7))
    braggwavelength2=gcpeak2+(data_peaks(7)-b_peaks(2))*waveperdiv5;
elseif (bragg_peak(2)>=gascell_peak(5))&(bragg_peak(2)<gascell_peak(6))
    braggwavelength2=gcpeak3+(data_peaks(6)-b_peaks(2))*waveperdiv6;
end;;
```

%This function calculates the strain corresponding to the bragg wavelength

```
function calcstrain=strain_calc(parameter_array,peak_wavelength,braggwavelength)

global strain;

format long;
channel_info=parameter_array;
column_number=1;

%calibration coefficients
baseline = channel_info(2,column_number);
beta_nought = channel_info(4,column_number); %thermo-optic response of grating at
fabrication
GF = channel_info(5,column_number); %gauge factor ~0.5
lambda=peak_wavelength; %baseline
wavelength as defined by user
alpha_sub = channel_info(9,column_number); %thermal expansion coefficient of
substrate
alpha_fiber = channel_info(10,column_number); %thermal expansion coefficient of
fiber ~0.55e-6 per degree K (fused silica)

ref_temp = channel_info(6,column_number); %reference temp of sensor at
calibration
act_temp = channel_info(7,column_number); %actual temp at measurement

%calculate beta
BETA = ( beta_nought + GF * abs(alpha_sub - alpha_fiber) ); %apparent thermal
strain

%per degree celsius
%temperature shift
delta_T = (act_temp - ref_temp);

%wavelength shift
delta_lambda=braggwavelength-lambda;

%strain calculation
strain= (1/GF)*( delta_lambda/lambda - BETA*delta_T )*1e6;

calcstrain=strain;
```

**%This is the Main Peak Location Program which compares the various methods
%used to find the Bragg peak**

```
%Obtains signal from excel spreadsheet
clear all;
a=xlsread('C:\Documents and Settings\Evangeline\My Documents\Thesis\laser
data\Signals\bragg.xls');
signal=a(:,2);
signal=signal(419:1578);
y=length(signal);
wavelength=1:y;
avg=sum(signal)/y;
signal=signal-avg;
signal=(signal)/max(signal);
orig_signal=signal;
[imin imin]=min(signal);
[imax imax]=max(signal);
totalsig=abs(max-min);
rmssignal=sqrt(sum(signal.^2)/y);
deviation=[0 0.0002 0.0004 0.0006 0.0008 0.001 0.002 0.004 0.006 0.008 0.01 0.02 0.03
0.04 0.05];
t=length(deviation);
orig_signal=signal;

for count=1:t
    stddev=deviation(count);
    sumnoise=0;
    if stddev~=0
        for i=1:y
            noise=sqrt(stddev)*randn(1);
            new_signal(i)=orig_signal(i)+noise;
            sumnoise=sumnoise+(noise)^2;
        end;
    else
        new_signal=orig_signal;
    end;
    if stddev==0
        sumnoise=0;
    end;
    rmsnoise=sqrt((sumnoise)/y);
    rmsnoise2=sqrt(sum(new_signal.^2)/y);
    %signal=(signal)/max(signal);
    minerror=4e6;
    signal=new_signal;
    format long;
    figure,
```

```

subplot(3,2,1);
plot(wavelength,signal);
ylabel('Normalized Amplitude');
%xlabel('Data Point');
title(['Original Signal with Noise standard deviation ',num2str(stddev)]);

%Method 1
%Threshold and Middle Value
peak1=middlevalue(signal,wavelength);

%Method 2
%Highest point/Lowest Point
peak2=highlow(signal,wavelength);

%Method 3
%Fitting a polynomial
[peak3,xvalues,ysignal,polysignal]=polynomial(signal,wavelength);
subplot(3,2,2);
plot(xvalues,ysignal,'o',xvalues,polysignal,'-');
ylabel('Normalized Amplitude');
%xlabel('Data Point');
title('Polynomial Fit to Signal');

%Method 4
%Take the Derivative and find the Zero Crossing
[peak4,filtersig,derivsig,xderiv]=derivative(signal,wavelength);
subplot(3,2,3);
plot(wavelength,filtersig);
ylabel('Normalized Amplitude');
%xlabel('Data Point');
title('Filtered Signal');
subplot(3,2,4);
plot(xderiv,derivsig);
ylabel('Normalized Amplitude');
%xlabel('Data Point');
title('Derivative of Filtered Signal');

%Method 5
%Fitting a Lorentzian Curve
[peak5,lorentz,newsig,xrange]=lorentzian(signal,wavelength,minerror,y);
subplot(3,2,5);
plot(xrange,lorentz,'r',xrange,newsig);
ylabel('Normalized Amplitude');
xlabel('Data Point');
title('Lorentzian Fit to Signal');

```

%Method 6

%Fitting a Gaussian Curve

```
[peak6,gauss,newsignal,xaxis]=gaussian(signal,wavelength,minerror,y);  
subplot(3,2,6)  
plot(xaxis,gauss,'r',xaxis,newsignal);  
ylabel('Normalized Amplitude');  
xlabel('Data Point');  
title('Gaussian Fit to Signal');
```

%Peaks from Different Methods

```
peak(count,:)= [peak1 peak2 peak3 peak4 peak5 peak6];  
ideal=peak(1,6);  
difference(count,:)=abs(peak(count,:)-ideal);
```

%Noise to Signal Ratio

```
noisesig(count,:)=rmsnoise/rmssignal;  
logofnoisesig(count,:)=log(rmsnoise/rmssignal);  
noisedev(count,:)=stddev;  
noisetosigratio(count,:)=rmsnoise/totalsig;  
logofntosratio(count,:)=log(rmsnoise/totalsig);  
end;
```

%Noise to Signal Ratio

```
noise=ones(t,3);  
noise(:,1)=noisedev;  
noise(:,2)=noisetosigratio;  
noise(:,3)=logofntosratio;
```

```
rmsnoise=ones(t,2);  
rmsnoise(:,1)=noisesig;  
rmsnoise(:,2)=logofnoisesig;
```

%data

```
data=zeros(t,17);  
data(:,1:3)=noise;  
format;  
data(:,5:10)=peak;  
data(:,12:17)=difference;
```

```
%write to temporary file temp.out in C:\MatlabR12\work  
dlmwrite('temp.out',data,',');
```


**%This function takes the 3dB threshold crossings and assigns the middle value as
%the peak location**

```
function peak=middlevalue(signal,wavelength)

threshold=0.7079*max(signal); %3db threshold
i=1;
while signal(i)<threshold
    i=i+1;
end;
point1=signal(i);
[maxsig n]=max(signal);
j=n;
while signal(j)>threshold
    j=j+1;
end;
point2=signal(j);
k=i+j;
if mod(k,2)==0
    n=k/2;
else
    n=(k-1)/2;
end;
peak=wavelength(n);
```

**%This function takes the point where the highest value occurs and assigns that as
%the peak location**

function peak=highlow(signal,wavelength)

**x=max(signal);
for i=1:length(signal)
 if signal(i)==x;
 peak=wavelength(i);
 end;
end;**

**%This function fits a second order polynomial signal to the raw data and assigns
%the point where the maximum value of the polynomial occurs as the peak location**

```
function [peak,x,y,f]=polynomial(signal,wavelength)
```

```
threshold=0.4*max(signal);
```

```
i=1;
```

```
while signal(i)<threshold
```

```
    i=i+1;
```

```
end;
```

```
point1=signal(i);
```

```
[maxsig n]=max(signal);
```

```
j=n;
```

```
while signal(j)>threshold
```

```
    j=j+1;
```

```
end;
```

```
point2=signal(j);
```

```
x=wavelength(i:j);
```

```
y=signal(i:j);
```

```
p=polyfit(x,y',3);
```

```
f=polyval(p,x);
```

```
%figure
```

```
%plot(x,y,'o',x,f,'-');
```

```
[maxpol,z]=max(f);
```

```
peak=x(z);
```

**%This function take the first derivative of the signal and assigns the zero crossing
%point as the peak location**

```
function [peak,filtsig,sy,x]=derivative(signal,wavelength)
```

```
[thresh tmax]=max(signal);  
threshold=0.8*thresh;
```

```
%figure  
%plot(wavelength,signal);
```

```
[b,s]=butter(2,0.1); %2nd order filter with wn=0.1  
w=filter(b,s,signal);  
filtsig=w;
```

```
%figure  
%plot(wavelength,filtsig);
```

```
n=length(filtsig);  
z=1;  
for j=1:n-1;  
    deriv2(j)=(filtsig(j+1)-filtsig(j))/(wavelength(j+1)-wavelength(j));  
    z=z+1;  
end;  
k=length(deriv2);
```

```
x = 1:k; % for discrete plots  
fineness = 1/100;  
finex = 1:fineness:k; % for continuous plots
```

```
% make and plot random data  
y = deriv2;  
% parameters for Gaussian kernel  
FWHM = 10;  
sig = FWHM/sqrt(8*log(2));  
% do the smooth  
sy = zeros(size(y));  
for xi = x  
    kerny_i = (1/(sqrt(2*pi)*sig))*exp(-(x-xi).^2/(2*sig^2));  
% kerny_i = kerny_i / sum(kerny_i);  
    sy(xi) = sum(y.*kerny_i);  
end
```

```
%plot of data  
%figure  
%plot(x,sy);
```

```
%hold on;
%q=(1/(sqrt(2*pi)*sig))*exp(-(x).^2/(2*sig^2));
%w=conv(y,q); %use convolution command
%plot(x,w(1:length(sy)), 'r');
```

```
%[b,a]=butter(1,0.8);
%sy=filter(b,a,sy);
```

```
% plot of smoothed data
%figure
%plot(x,sy);
deriv2=sy;
```

```
%[m i]=max(deriv);
%q=length(deriv);
%deriv2=deriv(i+1:q);
```

```
[min imin]=min(deriv2);
[max imax]=max(deriv2);
```

```
g=1;
h=1;
zerofound=0;
if imax<imin
    for i=imax:imin;
        if (deriv2(i)>0)&(deriv2(i+1)<0)
            zerofound=zerofound+1;
            peak(g)=wavelength(i+1);
            g=g+1;
        elseif (deriv2(i)<0)&(deriv2(i+1)>0)
            zerofound=zerofound+1;
            valley(h)=wavelength(i+1);
            h=h+1;
        end;
    end;
elseif imax>imin
    while imax>imin
        deriv2(imax)=0;
        [max imax]=max(deriv2);
    end;
    for i=imin:imax;
        if (deriv2(i)>0)&(deriv2(i+1)<0)
            zerofound=zerofound+1;
            peak(g)=wavelength(i+1);
            g=g+1;
        elseif (deriv2(i)<0)&(deriv2(i+1)>0)
```

```
        zerofound=zerofound+1;
        valley(h)=wavelength(i+1);
        h=h+1;
    end;
end;
end;

if g>1
    peak=peak(g-1);
elseif g==1
    peak=peak(1);
end;
```

**%This function fits a Lorentzian curve to the raw data and assigns the maximum
%value of the curve as the peak location**

```
function [minmu,fmin,signalmin,xrange]=lorentzian(signal,wavelength,minerror,y)
```

```
threshold=0.5*max(signal);
```

```
i=1;
```

```
while signal(i)<threshold
```

```
    i=i+1;
```

```
end;
```

```
point1=signal(i);
```

```
[maxsig n]=max(signal);
```

```
j=n;
```

```
while signal(j)>threshold
```

```
    j=j+1;
```

```
end;
```

```
point2=signal(j);
```

```
for mu=wavelength(i):wavelength(j)
```

```
    xmin=mu-(y/2);
```

```
    xmax=mu+(y/2)-1;
```

```
    if xmin<1
```

```
        xmin=1;
```

```
    end;
```

```
    if xmax>y
```

```
        xmax=y;
```

```
    end;
```

```
    sigmamin=1;
```

```
    sigmamax=150;
```

```
    count=1;
```

```
    for sigma=sigmamin:1:sigmamax
```

```
        x=xmin:xmax;
```

```
        signalnew=signal(xmin:xmax);
```

```
        f=(1/pi).*((sigma/2)./((x-mu).^2+(sigma/2)^2));
```

```
        maxf=max(f);
```

```
        f=f/maxf;
```

```
        f=f';
```

```
        error=0;
```

```
        for k=1:length(f)
```

```
            error=error+(signalnew(k)-f(k)).^2;
```

```
        end;
```

```
        lse(count)=error/length(f);
```

```
        count=count+1;
```

```
    end;
```

```
    sigma=sigmamin:1:sigmamax;
```

```
    [minlse z]=min(lse);
```

```

if minlse<minerror
    minerror=minlse;
    minsig=sigma(z);
    minmu=mu;
    minx=minmu-(y/2);
    maxx=minmu+(y/2)-1;
    if minx<1
        minx=1;
    end;
    if maxx>y
        maxx=y;
    end;
    xrange=minx:maxx;
    signalmin=signal(minx:maxx);
    fmin=(1/pi).*((minsig/2)./((xrange-minmu).^2+(minsig/2)^2));
    maxf=max(fmin);
    fmin=fmin/maxf;
    fmin=fmin';
end;
end;

%figure,
%plot(xrange,fmin,'r',xrange,signalmin);

```


**%This function fits a Gaussian curve to the raw data and assigns the maximum
%value of the curve as the peak location**

```
function [minmu,fmin,signalmin,xrange]=gaussian(signal,wavelength,minerror,y)
```

```
threshold=0.4*max(signal);
```

```
i=1;
```

```
while signal(i)<threshold
```

```
    i=i+1;
```

```
end;
```

```
point1=signal(i);
```

```
[maxsignal]=max(signal);
```

```
j=n;
```

```
while signal(j)>threshold
```

```
    j=j+1;
```

```
end;
```

```
point2=signal(j);
```

```
for mu=wavelength(i):wavelength(j)
```

```
    xmin=mu-(y/2);
```

```
    xmax=mu+(y/2)-1;
```

```
    if xmin<1
```

```
        xmin=1;
```

```
    end;
```

```
    if xmax>y
```

```
        xmax=y;
```

```
    end;
```

```
    sigmamin=1;
```

```
    sigmamax=70;
```

```
    count=1;
```

```
    for sigma=sigmamin:1:sigmamax
```

```
        x=xmin:xmax;
```

```
        signalnew=signal(xmin:xmax);
```

```
        f=(1/(sigma*sqrt(2*pi))).*exp((-1*(x-mu).^2)./(2*sigma^2));
```

```
        maxf=max(f);
```

```
        f=f/maxf;
```

```
        f=f;
```

```
        error=0;
```

```
        for k=1:length(f)
```

```
            error=error+(signalnew(k)-f(k)).^2;
```

```
        end;
```

```
        lse(count)=error/length(f);
```

```
        count=count+1;
```

```
    end;
```

```
    sigma=sigmamin:1:sigmamax;
```

```
    [minlse z]=min(lse);
```

```

if minlse<minerror
    minerror=minlse;
    minsig=sigma(z);
    minmu=mu;
    minx=minmu-(y/2);
    maxx=minmu+(y/2)-1;
    if minx<1
        minx=1;
    end;
    if maxx>y
        maxx=y;
    end;
    xrange=minx:maxx;
    signalmin=signal(minx:maxx);
    fmin=(1/(minsig*sqrt(2*pi))).*exp((-1*(xrange-minmu).^2)./(2*minsig^2));
    maxf=max(fmin);
    fmin=fmin/maxf;
    fmin=fmin';
end;
end;

%figure,
%plot(xrange,fmin,'r',xrange,signalmin);
%ylabel('Normalized Amplitude');
%xlabel('Data Point');
%title('Gaussian Fit to Signal');

```

**%This is a similar Main Peak Location Program, but it employs sub-sampling
%techniques**

```
%Obtains signal from excel spreadsheet
clear all;
a=xlsread('C:\Documents and Settings\Evangeline\My Documents\Thesis\laser
data\Signals\bragg.xls');
signal=a(:,2);
signal=signal(419:1578);
y=length(signal);
wavelength=1:y;
avg=sum(signal)/y;
signal=signal-avg;
signal=(signal)/max(signal);
orig_signal=signal;
[min imin]=min(signal);
[max imax]=max(signal);
totalsig=abs(max-min);
rmssignal=sqrt(sum(signal.^2)/y);
deviation=[0 0.0002 0.0004 0.0006 0.0008 0.001 0.002 0.004 0.006 0.008 0.01 0.02 0.03
0.04 0.05];
t=length(deviation);
orig_signal=signal;
orig_wavelength=wavelength;

for count=1:t
    stddev=deviation(count);
    sumnoise=0;
    if stddev~=0
        for i=1:y
            noise=sqrt(stddev)*randn(1);
            new_signal(i)=orig_signal(i)+noise;
            sumnoise=sumnoise+(noise)^2;
        end;
    else
        new_signal=orig_signal;
    end;
    if stddev==0
        sumnoise=0;
    end;
    rmsnoise=sqrt((sumnoise)/y);
    %signal=(signal)/max(signal);
    minerror=4e6;
    signal=new_signal;
    format long;
    figure,
```

```

subplot(3,2,1);
plot(wavelength,signal);
ylabel('Normalized Amplitude');
%xlabel('Data Point');
title(['Original Signal with Noise standard deviation ',num2str(stddev)]);

signal=new_signal;
wi=1:0.0625:length(signal);
si=interp1(orig_wavelength,signal,wi);

signal=si;
wavelength=wi;

%Method 1
%Threshold and Middle Value
peak1=middlevalue(signal,wavelength);

%Method 2
%Highest point/Lowest Point
peak2=highlow(signal,wavelength);

%Method 3
%Fitting a polynomial
[peak3,xvalues,ysignal,polysignal]=polynomial2(signal,wavelength);
subplot(3,2,2);
plot(xvalues,ysignal,'o',xvalues,polysignal,'-');
ylabel('Normalized Amplitude');
%xlabel('Data Point');
title('Polynomial Fit to Signal');

%Method 4
%Take the Derivative and find the Zero Crossing
[peak4,filtersig,derivsig,xderiv]=derivative(signal,wavelength);
subplot(3,2,3);
plot(wavelength,filtersig);
ylabel('Normalized Amplitude');
%xlabel('Data Point');
title('Filtered Signal');
subplot(3,2,4);
plot(xderiv,derivsig);
ylabel('Normalized Amplitude');
%xlabel('Data Point');
title('Derivative of Filtered Signal');

%Method 5
%Fitting a Lorentzian Curve

```

```

[peak5,lorentz,newsig,xrange]=lorentzian(signal,wavelength,minerror,y);
subplot(3,2,5);
plot(xrange,lorentz,'r',xrange,newsig);
ylabel('Normalized Amplitude');
xlabel('Data Point');
title('Lorentzian Fit to Signal');

%Method 6
%Fitting a Gaussian Curve
[peak6,gauss,newsignal,xaxis]=gaussian(signal,wavelength,minerror,y);
subplot(3,2,6)
plot(xaxis,gauss,'r',xaxis,newsignal);
ylabel('Normalized Amplitude');
xlabel('Data Point');
title('Gaussian Fit to Signal');

%Peaks from Different Methods
peak(count,:)= [peak1 peak2 peak3 peak4 peak5 peak6];
ideal=peak(1,6);
difference(count,:)=abs(peak(count,:)-ideal);

%Noise to Signal Ratio
noisesig(count,:)=rmsnoise/rmssignal;
logofnoisesig(count,:)=log(rmsnoise/rmssignal);
noisedev(count,:)=stddev;
noisetosigratio(count,:)=rmsnoise/totalsig;
logofntosratio(count,:)=log(rmsnoise/totalsig);
end;

%Noise to Signal Ratio
noise=ones(t,3);
noise(:,1)=noisedev;
noise(:,2)=noisetosigratio;
noise(:,3)=logofntosratio;

rmsnoise=ones(t,3);
rmsnoise(:,1)=noisesig;
rmsnoise(:,2)=logofnoisesig;
rmsnoise(:,3)=rmsnoise;

%data
data=zeros(t,21);
data(:,1:3)=noise;
data(:,5:7)=rmsnoise;
format;
data(:,9:14)=peak;

```

```
data(:,16:21)=difference;
```

```
%write to temporary file temp.out in C:\MatlabR12\work  
dlmwrite('temp.out',data,',' );
```

**%This program obtains the etalon, gas cell and Bragg signals using an oscilloscope
%and determines the Bragg peak wavelength in reference to the gas cell and etalon**

```
clear all;
a=xlsread('C:\Documents and Settings\Evangeline\My Documents\Thesis\laser
data\Signals\bragg.xls');
bragg=a(:,2);
bragg=bragg(419:1578);
y=length(bragg);
lengths(1)=y;
datapointb=1:y;
avg=sum(bragg)/y;
bragg=bragg-avg;
bragg=(bragg)/max(bragg);
[min imin]=min(bragg);
[max imax]=max(bragg);
totalsig=abs(max-min);
rmsbragg=sqrt(sum(bragg.^2)/y);
```

```
b=xlsread('C:\Documents and Settings\Evangeline\My Documents\Thesis\laser
data\Signals\etalon.xls');
etalon=b(:,2);
etalon=etalon(248:1754);
y=length(etalon);
lengths(2)=y;
datapointe=1:y;
avg=sum(etalon)/y;
etalon=etalon-avg;
maxetalon=etalon(1);
for i=1:length(etalon)
    if etalon(i)>maxetalon
        maxetalon=etalon(i);
    end;
end;
etalon=(etalon)/maxetalon;
[min imin]=min(etalon);
[max imax]=max(etalon);
totalsig=abs(max-min);
rmsetalon=sqrt(sum(etalon.^2)/y);
```

```
a=xlsread('C:\Documents and Settings\Evangeline\My Documents\Thesis\laser
data\Signals\gascell.xls');
gascell=a(:,2);
gascell=gascell(216:1734);
```

```

y=length(gascell);
lengths(3)=y;
datapointg=1:y;
avg=sum(gascell)/y;
gascell=gascell-avg;
maxgascell=gascell(1);
for i=1:length(gascell)
    if gascell(i)>maxgascell
        maxgascell=gascell(i);
    end;
end;
gascell=(gascell)/maxgascell;
[imin imin]=min(gascell);
[imax imax]=max(gascell);
totalsig=abs(max-min);
rmsgascell=sqrt(sum(gascell.^2)/y);

[max_length,m]=max(lengths);

for p=1:m
    if p~=m
        t=1:lengths(p)/max_length:lengths(p)+lengths(p)/max_length;
        q=length(t);
        %y=ones(p,q);
        y(p,1:q)=t;
    else
        t=1:lengths(p)/max_length:lengths(p);
        q=length(t);
        %y=ones(p,q);
        y(p,1:q)=t;
    end;
end;

newbragg=interp1(datapointb,bragg,y(1,:));
newetalon=interp1(datapointe,etalon,y(2,:));
newgascell=interp1(datapointg,gascell,y(3,:));

datapoint=1:max_length;

figure
plot(datapoint,newbragg,'b',datapoint,newetalon,'r',datapoint,newgascell,'g');
axis([0 max_length -4.0 1]);
grid on;
xlabel('Data Point');
ylabel('Normalized Amplitude');
title('Etalon, Gas Cell and Bragg Signals');

```



```
bragg=newbragg';  
etalon=newetalon';  
gascell=newgascell';
```

```
[data,waveperdiv]=peakdetection2(bragg,etalon,gascell,datapoint);
```

```
gascell_points=data(1:3,1);  
gascell_peaks=data(1:3,2);  
etalon_points=data(:,3);  
etalon_peaks=data(:,4);  
bragg_point=data(1,5);  
bragg_peak=data(1,6);
```

**%This function is the main peak location program which uses polynomial curve
 %fitting to find the peak positions and uses interpolation from the etalon and gas
 %cell to find the Bragg wavelength**

function [data,waveperdiv]=peakdetection2(bragg,etalon,gascell,datapoint)

%%
 %Gas Cell Peak Detection%%
 %%%

```

flag=0;
lindex=1;
start=1;
loopindex=1;
gas=-1*gascell;
maxgas=gas(1);
for i=start:length(gas)
    if gas(i)>maxgas
        maxgas=gas(i);
    end;
end;
threshold=0.4*maxgas;
while loopindex~=0

    i=start+2;
    if flag==0
        while (gas(i)<threshold)&(i~=length(datapoint))&(gas(i-1)<threshold)&(gas(i+1)<threshold)
            i=i+1;
        end;
    else
        i=i+3;
        while (gas(i)<threshold)&(i~=length(datapoint))&(gas(i-1)<threshold)&(gas(i+1)<threshold)
            i=i+1;
        end;
    end;

    point1=gas(i);
    %[maxsig n]=max(gas);
    j=i+2;
    if j<length(datapoint)
        while (gas(j)>threshold)&(gas(j-1)>threshold)&(gas(j+1)>threshold)
            j=j+1;
        end;
    end;
end;

```

```

w=j;
if (gas(w+1)<threshold)&(gas(w+2)>threshold)&(gas(w+3)<threshold)
    flag=1;
else
    flag=0;
end;

point2=gas(j);
stop=j;
x=datapoint(i:j);
y=gas(i:j);
p=polyfit(x,y',2);
f=polyval(p,x);
[maxpol,z]=max(f);
peak=x(z);

gascell_peaks(loopindex,:)=peak;
%xvalues(loopindex,:)=x;
%ysignal(loopindex,:)=y';
%polysignal(loopindex,:)=f;

%figure
%plot(x,y,'o',x,f,'-');
start=stop;
end;

if j>=length(datapoint)
    start=length(datapoint);
end;

if start>=length(datapoint)
    loopindex=0;
else
    loopindex=loopindex+1;
end;

end;

%%%%%%%%%%%%%%%%%%%%%%%%%%%%%%%%%%%%%%%%%%%%%%%%%%%%%%%%%%%%%%%%%%%%%%%%
%Etalon Peak Detection%%%%%%%%%%%%%%%%%%%%%%%%%%%%%%%%%%%%%%%%%%%%%%%%%%%%%%%%%%%%%%%%%%%%%%%%
%%%%%%%%%%%%%%%%%%%%%%%%%%%%%%%%%%%%%%%%%%%%%%%%%%%%%%%%%%%%%%%%%%%%%%%%

start=1;
loopindex=1;
peakindex=1;
maxetalon=etalon(1);

```

```

for i=1:length(etalon)
    if etalon(i)>maxetalon
        maxetalon=etalon(i);
    end;
end;
%threshold=0.35*maxetalon;
%threshold=median(etalon);
threshold=0;
while loopindex~=0

    i=start;
    while (etalon(i)<threshold)&(i~=length(datapoint))&(etalon(i+1)<threshold)
        i=i+1;
    end;
    w=i;
    if w+10>=length(datapoint)
        last=length(datapoint)-2;
    else
        last=w+10;
    end;
    new_i=last;
    for t=last:-1:w
        if (etalon(t)>threshold)&(etalon(t+2)>threshold)&(etalon(t+1)>threshold)
            new_i=t;
        end;
    end;
    if new_i==last
        new_i=last;
    end;
    i=new_i;
    point1=etalon(i);

    j=i+2;
    if j<=length(datapoint)
        while (j~=length(datapoint))&(etalon(j)>threshold)&(etalon(j-1)>threshold)&(etalon(j+1)>threshold)
            j=j+1;
        end;

        w=j;
        point2=etalon(j);

        if w+10>=length(datapoint)
            last=length(datapoint);
            stop=last;
        else

```

```

        last=w+10;
        for t=w:last
            if etalon(t)<threshold
                new_j=t;
            end;
        end;
        stop=new_j;
    end;

    x=datapoint(i:j);
    y=etalon(i:j);

    if length(x)>5
        p=polyfit(x,y',2);
        f=polyval(p,x);
        [maxpol,z]=max(f);
        peak=x(z);
        etalon_peaks(peakindex,:)=peak;
        peakindex=peakindex+1;
        %figure
        %plot(x,y,'o',x,f,'-');
    end;

    start=stop;
end;

if j>=length(datapoint)
    start=length(datapoint);
end;

if start>=length(datapoint)
    loopindex=0;
else
    loopindex=loopindex+1;
end;

end;

%%%%%%%%%%%%%%%%%%%%%%%%%%%%%%%%%%%%%%%%%%%%%%%%%%%%%%%%%%%%%%%%%%%%%%%%
%Bragg Peak Detection%%%%%%%%%%%%%%%%%%%%%%%%%%%%%%%%%%%%%%%%%%%%%%%%%%%%%%%%%%%%%%%%%%%%%%%%
%%%%%%%%%%%%%%%%%%%%%%%%%%%%%%%%%%%%%%%%%%%%%%%%%%%%%%%%%%%%%%%%%%%%%%%%

maxbragg=bragg(1);
for i=1:length(bragg)

```

```

        if bragg(i)>maxbragg
            maxbragg=bragg(i);
        end;
    end;
    threshold=0.4*maxbragg;
    i=1;
    while bragg(i)<threshold
        i=i+1;
    end;
    point1=bragg(i);
    [maxsig n]=max(bragg);
    j=n;
    while bragg(j)>threshold
        j=j+1;
    end;
    point2=bragg(j);

```

```

x=datapoint(i:j);
y=bragg(i:j);
p=polyfit(x,y',2);
f=polyval(p,x);
[maxpol,z]=max(f);
bragg_peak=x(z);
%figure
%plot(x,y,'o',x,f,'-');

```

```

%%%%%%%%%%%%%%%%%%%%%%%%%%%%%%%%%%%%%%%%%%%%%%%%%%%%%%%%%%%%%%%%%%%%%%%%
%Peak Assignment%%%%%%%%%%%%%%%%%%%%%%%%%%%%%%%%%%%%%%%%%%%%%%%%%%%%%%%%%%%%%%%%%%%%%%%%
%%%%%%%%%%%%%%%%%%%%%%%%%%%%%%%%%%%%%%%%%%%%%%%%%%%%%%%%%%%%%%%%%%%%%%%%

```

```

%laser swept from 1535 to 1537nm
%from the gas cell data sheet, absorption lines occur at 1535.5401, 1536.1170,
1536.7034
%wavelengths per data point= 2nm/length(datapoint)
format long;
theoretical(1)=1535e-9;
for i=2:y
    theoretical(i)=theoretical(i-1)+(2e-9/length(datapoint));
end;
theoretical=theoretical*1e9;
%waveperdiv=(2/length(datapoint));

gaspeak1=gascell_peaks(1);
gaspeak2=gascell_peaks(2);

```

```
gaspeak3=gascell_peaks(3);
```

```
gcpeak1=1535.5401;
```

```
gcpeak2=1536.1170;
```

```
gcpeak3=1536.7034;
```

```
gcpeaks=[gcpeak1;gcpeak2;gcpeak3];
```

```
waveperdiv1=(gcpeak2-gcpeak1)/(gascell_peaks(2)-gascell_peaks(1));
```

```
waveperdiv2=(gcpeak3-gcpeak2)/(gascell_peaks(3)-gascell_peaks(2));
```

```
waveperdiv=[waveperdiv1;waveperdiv2];
```

```
pindex=1;
```

```
for z=1:length(etalon_peaks)
```

```
    if (etalon_peaks(z)>=gaspeak1)&(etalon_peaks(z)<gaspeak2)  
        etapeak(pindex)=gcpeak1+((etalon_peaks(z)-gaspeak1)*waveperdiv1);
```

```
        newepeak(pindex)=etalon_peaks(z);
```

```
        pindex=pindex+1;
```

```
    elseif (etalon_peaks(z)>=gaspeak2)&(etalon_peaks(z)<gaspeak3)  
        etapeak(pindex)=gcpeak2+((etalon_peaks(z)-gaspeak2)*waveperdiv2);
```

```
        newepeak(pindex)=etalon_peaks(z);
```

```
        pindex=pindex+1;
```

```
    end;
```

```
end;
```

```
braggpeak=bragg_peak;
```

```
for z=1:length(etapeak)-1
```

```
    if (braggpeak>newepeak(z))&(braggpeak<newepeak(z+1))
```

```
        if (braggpeak>gaspeak1)&(braggpeak<gaspeak2)
```

```
            bpeak=etapeak(z)+((braggpeak-newepeak(z))*waveperdiv1);
```

```
        else
```

```
            bpeak=etapeak(z)+((braggpeak-newepeak(z))*waveperdiv2);
```

```
        end;
```

```
    end;
```

```
end;
```

```
data=ones(length(newepeak),6);
```

```
data(1:length(gascell_peaks),1)=gascell_peaks;
```

```
data(1:length(gcpeaks),2)=gcpeaks;
```

```
data(1:length(newepeak),3)=newepeak';
```

```
data(1:length(etapeak),4)=etapeak';
```

```
data(1,5)=braggpeak;
```

```
data(1,6)=bpeak;
```

```
dlmwrite('temp.out',data);
```

**%This program simulates the etalon transmission lines with varying constants of
%refractive index and temperature**

%Assuming constant n and T

%Finding Etalon Constants

n=1.76;
r=((n-1)^2)/((n+1)^2);
nl=8.707821e-3; %assumed refl=0 @ 1550.4nm by observation of data plot provided by
supplier

%Wavelength Range

xmin=1549e-9;
xmax=1551e-9;
lambda=xmin:1e-12:xmax;

%Solving for Etalon Transmission

delta=(4*pi*nl)/lambda;
t=((1-r)^2)/((1-r)^2+4*r*(0.5-0.5*cos(delta)));

figure

plot(lambda*1e9,10*log10(1-t),'r');
title('Simulated Etalon Spectrum');
xlabel('Wavelength (nm)');
ylabel('Intensity (dB)');
%axis([xmin*1e9 xmax*1e9 -30 -5]);
grid on;

figure

plot(lambda*1e9,(1-t),'r');
axis([xmin*1e9 xmax*1e9 0 0.3]);
title('Simulated Etalon Spectrum');
xlabel('Wavelength (nm)');
ylabel('Intensity');
grid on;

%%
%%

%Assuming n varies with wavelength
%Applying Sellmeier dispersion formula

%n=1.76;
%r=((n-1)^2)/((n+1)^2);

%Sellmeier Coefficients


```

b1=1.78922056;
b2=3.28427448e-1;
b3=2.01639441;
c1=1.35163537e-2;
c2=6.22729599e-2;
c3=1.68014713e2;

%Wavelength Range
min=1549e-9;
max=1551e-9;
lamda=min:1e-12:max;

%Find n using Sellmeier Formula
term1=(b1*(lamda.*1e6).^2)./((lamda.*1e6).^2-c1);
term2=(b2*(lamda.*1e6).^2)./((lamda.*1e6).^2-c2);
term3=(b3*(lamda.*1e6).^2)./((lamda.*1e6).^2-c3);
n=sqrt(term1+term2+term3+1);

%Solving for Etalon Transmission
l=0.00493994967724; %l=nl/n @ 1550.4nm l=8.707821e-3/1.76273475823312
delta=(4*pi*n*l)/lamda;
r=((n-1).^2)/((n+1).^2);
t=((1-r).^2)/((1-r).^2+4*r.*(0.5-0.5*cos(delta)));

figure
plot(lamda*1e9,10*log10(1-t),'r');
title('Simulated Etalon Spectrum using Sellmeier Dispersion Formula');
xlabel('Wavelength (nm)');
ylabel('Intensity (dB)');
grid on;
figure
plot(lamda*1e9,(1-t),'r');
axis([min*1e9 max*1e9 0 0.3]);
title('Simulated Etalon Spectrum using Sellmeier Dispersion Formula');
xlabel('Wavelength (nm)');
ylabel('Intensity');
grid on;

%%%%%%%%%%%%%%%%%%%%%%%%%%%%%%%%%%%%%%%%%%%%%%%%%%%%%%%%%%%%%%%%%%%%%%%%
%%%%%%%%%%%%%%%%%%%%%%%%%%%%%%%%%%%%%%%%%%%%%%%%%%%%%%%%%%%%%%%%%%%%%%%%

%Assuming n varies with temperature

%Applying Schott Formula
format long;

```

%Schott constants

d0=-5.26e-6;

d1=7.41e-9;

d2=-1.89e-11;

e0=1.02e-9;

e1=1.62e-9;

lamdatk=0.288e-6;

%Sellmeier constants

b1=1.78922056;

b2=3.28427448e-1;

b3=2.01639441;

c1=1.35163537e-2;

c2=6.22729599e-2;

c3=1.68014713e2;

%Wavelength range

min=1549e-9;

max=1551e-9;

%Nominal Temperature

t0=25; %degrees celsius

%Temperature range

mint=-40;

maxt=80;

delt=40;

iter=(abs(mint)+abs(maxt))/delt +1;

lamda=min:1e-12:max;

%Initializing transmission array

t=ones(length(lamda),iter);

%Initializing temperature

temp=mint;

%Main loop

for i=1:iter

 deltatemp=temp-t0;

%find n @ t0=25 celsius with varying wavelength using sellmeier formula

term1=(b1*(lamda.*1e6).^2)/((lamda.*1e6).^2-c1);

term2=(b2*(lamda.*1e6).^2)/((lamda.*1e6).^2-c2);

term3=(b3*(lamda.*1e6).^2)/((lamda.*1e6).^2-c3);

n=sqrt(term1+term2+term3+1);

```

%find dn/dT using Schott formula
termone=(n.^2-1)./(2*n);
termtwo=(d0*deltatemp)+(d1*deltatemp.^2)+(d2*deltatemp.^3);
termthree=((e0*deltatemp)+(e1*deltatemp.^2))./((lamda*1e9).^2-(lamdatk*1e9)^2);

dn=termone.*(termtwo+termthree);

%find new n
nrev=n+dn;
n=nrev;

%calculate etalon transmission
%l=4.947626e-3;
l=0.00493994967724;
delta=(4*pi*n*l)/lamda;
r=((n-1).^2)./((n+1).^2);
t(:,i)=(((1-r).^2)./((1-r).^2+4*r.*(0.5-0.5*cos(delta))))';

%iterate temperature
temp=temp+delt;

end; %main for loop

%Initializing Plot Settings
%set(gcf,'DefaultAxesColorOrder',[1 0 0;0 1 0;0 0 1;1 1 0;0 0 0],
'DefaultAxesLineStyleOrder','-|-.');

figure
plot(lamda*1e9,10*log10(1-t));
title('Simulated Etalon Spectrum');
xlabel('Wavelength (nm)');
ylabel('Intensity (dB)');
grid on;

figure
plot(lamda*1e9,(1-t));
title('Simulated Etalon Spectrum');
xlabel('Wavelength (nm)');
ylabel('Intensity');
grid on;

```

APPENDIX B

ETALON SIMULATION EQUATIONS

Etalon Simulation

$$\text{Reflectivity} = R = \frac{(n-1)^2}{(n+1)^2}$$

$$\text{Trans} = T = \frac{(1-R)^2}{(1-R)^2 + 4R\sin^2(\delta/2)} \quad \text{Refl} = 1 - \text{Trans} \quad \delta = \frac{4\pi nl}{\lambda} \quad \sin^2(x) = \frac{1 - \cos(2x)}{2}$$

$$\text{Refl} = 1 \text{ @ } T = 0$$

$$\text{Refl} = 0 \text{ @ } T = 1$$

Using etalon signal in manual: max reflection @ 1550.0nm
min reflection @ 1549.862nm

Assuming nominal comb spacing = 138pm, $\lambda_m = 1550.0\text{nm}$ $\lambda_{m-1} = 1549.862\text{nm}$
 $\lambda_{m+1} = 1550.138\text{nm}$

$$\begin{aligned} \text{For } \text{Refl} = 0 \quad T = 1 &= \frac{(1-R)^2}{(1-R)^2 + 4R\sin^2(\delta/2)} \\ (1-R)^2 + 4R\sin^2(\delta/2) &= (1-R)^2 \\ 4R\sin^2(\delta/2) &= 0 \\ \sin^2(\delta/2) &= 0 \\ \frac{1 - \cos(\delta)}{2} &= 0 \end{aligned}$$

$$\begin{aligned} \cos(\delta) &= 1 \\ \cos(4\pi nl/\lambda) &= 1 \\ \frac{4\pi nl}{\lambda} &= 2m\pi \quad m = 0, 1, 2, \dots \end{aligned}$$

$$nl = \frac{m\lambda}{2} \quad nl = \text{length of cavity}$$

$$nl = \frac{m\lambda}{2} = (m-1)(1549.862/2) = m(1550.0/2) = (m+1)(1550.138/2)$$

$$\text{Using } (m-1)(1549.862/2) = m(1550.0/2)$$

$$m = 11230.884058$$

$$m = 11231$$

$$nl = (m\lambda)/2 = (11231 \cdot 1550.0)/2 = 8.704025 \text{ mm}$$

Assuming constant n and temp

$$T = \frac{(1-R)^2}{(1-R)^2 + 4R\sin^2(\delta/2)} = \frac{(1-R)^2}{(1-R)^2 + 4R\sin^2(4\pi nl/\lambda)}$$

$$nl = 8.704025\text{mm}$$

$$n = 1.76$$

Assuming n varies with wavelength

n varies using Sellmeier dispersion formula

$$n^2(\lambda) - 1 = \frac{B_1\lambda^2}{\lambda^2 - C_1} + \frac{B_2\lambda^2}{\lambda^2 - C_2} + \frac{B_3\lambda^2}{\lambda^2 - C_3}$$

$$n = \sqrt{\frac{B_1\lambda^2}{\lambda^2 - C_1} + \frac{B_2\lambda^2}{\lambda^2 - C_2} + \frac{B_3\lambda^2}{\lambda^2 - C_3} + 1}$$

Using data sheet: $B_1 = 1.78922056$
 $B_2 = 3.28427448 \times 10^{-1}$
 $B_3 = 2.01639441$
 $C_1 = 1.35163537 \times 10^{-2}$
 $C_2 = 6.22729599 \times 10^{-2}$
 $C_3 = 1.68014713 \times 10^2$

Using Sellmeier equation, $n @ 1550.0\text{nm} = 1.76274190612355$

$$\text{Therefore, } I = n_i/n = \frac{8.704025 \times 10^{-3}}{1.76274190612355} = 0.00493777618254$$

- find n using Sellmeier equation
- find $R = (n-1)^2 / (n+1)^2$
- $T = \frac{(1-R)^2}{(1-R)^2 + 4R\sin^2(4\pi n l / \lambda)}$

Assuming n varies with wavelength and temperature

- find n_{T_0} using Sellmeier formula
- find Δn using Schott formula

$$\Delta n(\lambda, T) = \frac{n_{T_0}^2 - 1}{2n_{T_0}} (D_0 \Delta T + D_1 \Delta T^2 + D_2 \Delta T^3 + \frac{E_0 \Delta T + E_1 \Delta T^2}{\lambda^2 - \lambda_{Tk}^2})$$

From data sheet:

$$\begin{aligned} D_0 &= -4.93 \times 10^{-6} \\ D_1 &= 7.94 \times 10^{-9} \\ D_2 &= -6.32 \times 10^{-11} \\ E_0 &= 9.79 \times 10^{-7} \\ E_1 &= 14.7 \times 10^{-10} \\ \lambda_{Tk} &= 0.296 \times 10^{-6} \end{aligned}$$

$$\text{new } n = n_{T_0} + \Delta n$$

- find $R = (n-1)^2 / (n+1)^2$
- $T = \frac{(1-R)^2}{(1-R)^2 + 4R \sin^2(4\pi n l / \lambda)}$

Determining the etalon constants using two peak wavelengths

λ_1 and λ_2 are found from interpolation from a gas cell line

$$m = \frac{\lambda_1}{\lambda_2 - \lambda_1} \quad m \text{ is rounded off to get an integer}$$

$$nl = \frac{m\lambda_2}{2}$$

$$\lambda = \lambda_2 * 1e-3$$

$$n = \sqrt{\frac{B_1\lambda^2}{\lambda^2 - C_1} + \frac{B_2\lambda^2}{\lambda^2 - C_2} + \frac{B_3\lambda^2}{\lambda^2 - C_3} + 1}$$

$$l = nl/n * 1e-9$$

The constants n and l can now be used to find the other etalon peaks.